Modeling and Robust Control of Integrated Ride and Handling of Passenger Cars

by

Ali Fellah Jahromi

A thesis

in the Department

of Mechanical and Industrial Engineering

Presented in Partial Fulfilment of the Requirements
for the Degree of Doctorate of Philosophy in Mechanical Engineering at
Concordia University
Montreal, Quebec, Canada

April 2015

CONCORDIA UNIVERSITY

School of Graduate Studies

This is to certify that the thesis prepared

By: Ali Fellah Jahromi

Entitled: Modeling and Robust Control of Integrated Ride and Handling of Passenger Cars

and submitted in partial fulfillment of the requirements for the degree of

Doctor of Philosophy

complies with the regulations of the University and meets the accepted standards with respect to originality and quality.

Signed by the final Examining Committee:

Dr. Rachida Dssouli	Chair
Dr. Zhaoheng Liu	External Examiner
Dr. Zhi Chen	External to Program
Dr. Ramin Sedaghati	Examiner
Dr. Youmin Zhang	Examiner
Dr. Wen Fang Xie	Co-supervisor
Dr. Rama B. Bhat	Co-supervisor

Approved by:

_____
Chair of Department or Graduate Program Director

_____
Dean of Faculty

April 2015

Abstract

Modeling and Robust Control of Integrated Ride and Handling of Passenger Cars

Ali Fellah Jahromi,

Concordia University, 2015

Vehicle industries in the last decade have focused on improving ride quality and safety of passenger cars. To achieve this goal, modeling and simulation of dynamic behaviour of vehicles have been widely studied to design model based and robust control strategies. This PhD work presents a new integrated vehicle model and a nonlinear robust controller. The thesis is divided into two main sections: dynamic modeling and controller design.

A new fourteen Degrees of Freedom integrated ride and handling vehicle model is proposed using Lagrangian method in terms of quasi-coordinates. The governing equations are derived considering the interaction between the ride and handling systems, Euler motion of the frames attached to the wheels and body, the load transfer among the wheels, acceleration and braking. A non-dimensional factor called coupling factor is introduced to study the coupling among different DOFs of the dynamic system for a defined vehicle maneuver. The coupling factor is considered as an indicator parameter to demonstrate the advantages of the developed model over the existing dynamic models. The improved model is validated using ADAMS/Car for different manoeuvres. The simulation results confirm the accuracy of the improved dynamic model in comparison with the ADAMS/Car simulations and the models available in the literature.

Considering the proposed nonlinear integrated ride and handling vehicle model, a nonlinear robust controller is designed for an intermediate passenger car. The H∞ robust control strategy is designed based on the Hamiltonian-Jacobi-Isaacs (HJI) function, Linear Matrix Inequality and State Feedback techniques. In order to improve the ride and handling quality of the vehicle, a Magnetorheological (MR) damper and a differential braking system are used as control devices.

A frequency dependent MR damper model is proposed based on the Spencer MR damper model. The parameters of the model are identified using a combination of Genetic algorithms and Sequential Quadratic Programming approaches based on the experimental data. A mathematical model is validated using the experimental results which confirm the improvement in the accuracy of the model and consistency in the variation of damping with frequency. Based on the proposed MR damper model, an inverse model for the MR damper is designed. A differential braking system is designed to assign desired braking action. The dynamic behavior of the controlled vehicle is simulated for single lane change and bump input, considering three different road conditions: dry, rainy and snowy. The robustness of the designed controller is investigated when the vehicle is under these road conditions. The simulation results confirm the interactive nature of the ride and handling systems and the robustness of the designed control strategy.

Acknowledgement

Last, but not least, my sincere heartfelt thanks goes out to my wife Ms. Zahra Rostamkhani, my mother Dr. Shohreh Khaefi, my father Dr. Mahmoud Fellah Jahromi, my mother-in-law Ms. Vahideh Mirmohammadrezaei, my father-in-law Mr. Mohammad Rostamkhani and my brother Mr. Arash Fellah Jahromi. They have been with me in all the way; I could not graduate without their encouragement and constant support.

To

My wife Zahra

Table of Contents

List of Figures

List of Tables

Nomenclature

Symbol	Description
DOF	Degree of Freedom
GA	Genetic Algorithms
HJI	Hamiltonian-Jacobi-Isaacs
LHS	Left Hand Side
LMI	Linear Matrix Inequality
MR	Magnetorheological
SQP	Sequential Quadratic Programming
A	Hysteresis loop size
a	Acceleration of MR damper rod
a_{c0}	Viscous damping coefficient at large velocities and zero voltage
a_{c1}	Viscous damping coefficient at small velocities and zero voltage
a_{α}	MR fluid yield stress coefficient in zero voltage
B	Coordinate system attached to the car body center
B_1	Coordinate system attached to the center of the front right wheel
B_2	Coordinate system attached to the center of the front left wheel
B_3	Coordinate system attached to the center of the rear right wheel
B_4	Coordinate system attached to the center of the rear left wheel
b_{c0}	Viscous damping voltage coefficient at large velocities
b_{c1}	Viscous damping voltage coefficient at small velocities
b_{α}	MR fluid yield stress voltage coefficient
C_1	Vehicle viscous damping coefficient on the front right side
C_2	Vehicle viscous damping coefficient on the front left side
C_3	Vehicle viscous damping coefficient on the rear right side
C_4	Vehicle viscous damping coefficient on the rear left side
C_{t1}	Viscous damping coefficient of front right tire
C_{t2}	Viscous damping coefficient of front left tire
C_{t3}	Viscous damping coefficient of rear right tire
C_{t4}	Viscous damping coefficient of rear left tire
$C_{\theta f}$	Equivalent viscous damping of front anti roll bar

$C_{\theta r}$	Equivalent viscous damping of rear anti roll bar
d	Displacement of MR damper rod
E_B	Transformation matrix of rotational motion for frame attached to the vehicle body
E_{t1}	Transformation matrix of rotational motion for frame attached to the front right wheel
E_{t2}	Transformation matrix of rotational motion for frame attached to the front left wheel
E_{t3}	Transformation matrix of rotational motion for frame attached to the rear right wheel
E_{t4}	Transformation matrix of rotational motion for frame attached to the rear left wheel
F_{c1}	Active control force acting on front right side
F_{c2}	Active control force acting on front left side
F_{c3}	Active control force acting on rear right side
F_{c4}	Active control force acting on rear left side
F_{MR1}	MR damper force acting on front right side
F_{MR2}	MR damper force acting on front left side
F_{MR3}	MR damper force acting on rear right side
F_{MR4}	MR damper force acting on rear left side
F_{MR_E}	Measured MR damper force based on experiment
F_{b1}	Braking force acting on front right side
F_{b2}	Braking force acting on front left side
F_{b3}	Braking force acting on rear right side
F_{b4}	Braking force acting on rear left side
G	Stationary coordinate system
h_f	Distance between pitch center and body center of gravity
h_s	Distance between roll center and body center of gravity
h_r	Half of track base, right side
h_l	Half of track base, left side
K	Kinetic energy
K_1	Suspension spring stiffness coefficient of front right side
K_2	Suspension spring stiffness coefficient of front left side
K_3	Suspension spring stiffness coefficient of rear right side
K_4	Suspension spring stiffness coefficient of rear left side
K_{t1}	Stiffness coefficient of front right tire
K_{t2}	Stiffness coefficient of front left tire

K_{t3}	Stiffness coefficient of rear right tire
K_{t4}	Stiffness coefficient of rear left tire
K_{mr0}	MR damper accumulator stiffness for large velocities
K_{mr1}	MR damper accumulator stiffness for small velocities
K_{x1}	Cornering stiffness of front right tire in longitudinal axis
K_{x2}	Cornering stiffness of front left tire in longitudinal axis
K_{x3}	Cornering stiffness of rear right tire in longitudinal axis
K_{x4}	Cornering stiffness of rear left tire in longitudinal axis
K_{y1}	Cornering stiffness of front right tire in lateral axis
K_{y2}	Cornering stiffness of front left tire in lateral axis
K_{y3}	Cornering stiffness of rear right tire in lateral axis
K_{y4}	Cornering stiffness of rear left tire in lateral axis
$K_{\theta f}$	Stiffness coefficient of front anti roll bar
$K_{\theta r}$	Stiffness coefficient of rear anti roll bar
L	Lagrangian function
l_f	Distance between front wheels and vehicle center of gravity
l_r	Distance between rear wheels and vehicle center of gravity
m_1	Mass of the front right wheel
m_2	Mass of the front left wheel
m_3	Mass of the rear right wheel
m_4	Mass of the rear left wheel
m_5	Mass of car body
n	Smoothness of transition coefficient of MR fluid from elastic to plastic
I	Vehicle body mass moment of inertia
I_1	Front right wheel mass moment of inertia
I_2	Front left wheel mass moment of inertia
I_3	Rear right wheel mass moment of inertia
I_4	Rear left wheel mass moment of inertia
R	Wheel radius
R_b	Brake disc radius
T_B	Translational transformation matrix for attached frame to vehicle body
T_{t1}	Transformation matrix of translational motion for attached frame to the front right

	wheel
T_{t2}	Transformation matrix of translational motion for attached frame to the front left wheel
T_{t3}	Transformation matrix of translational motion for attached frame to the rear right wheel
T_{t4}	Transformation matrix of translational motion for attached frame to the rear left wheel
U	Potential energy
V	Applied MR damper voltage
$\tilde{V}_B$	Skew-symmetric matrix of translational quasi- velocity in vehicle body frame
$\tilde{V}_{t1}$	Skew-symmetric matrix of translational quasi- velocity in front right wheel frame
$\tilde{V}_{t2}$	Skew-symmetric matrix of translational quasi- velocity in front left wheel frame
$\tilde{V}_{t3}$	Skew-symmetric matrix of translational quasi- velocity in rear right wheel frame
$\tilde{V}_{t4}$	Skew-symmetric matrix of translational quasi- velocity in rear left wheel frame
V_x	Longitudinal quasi-velocity in vehicle body frame
V_{x1}	Longitudinal quasi-velocity in front right wheel frame
V_{x2}	Longitudinal quasi-velocity in front left wheel frame
V_{x3}	Longitudinal quasi-velocity in rear right wheel frame
V_{x4}	Longitudinal quasi-velocity in rear left wheel frame
V_y	Lateral quasi-velocity in vehicle body frame
V_{y1}	Lateral quasi-velocity in front right wheel frame
V_{y2}	Lateral quasi-velocity in front left wheel frame
V_{y3}	Lateral quasi-velocity in rear right wheel frame
V_{y4}	Lateral quasi-velocity in rear left wheel frame
V_z	Vertical quasi-velocity in vehicle body frame
V_{z1}	Vertical quasi-velocity in front right wheel frame
V_{z2}	Vertical quasi-velocity in front left wheel frame
V_{z3}	Vertical quasi-velocity in rear right wheel frame
V_{z4}	Vertical quasi-velocity in rear left wheel frame
x	Longitudinal motion in vehicle body frame
x_1	Longitudinal motion in front right wheel frame
x_2	Longitudinal motion in front left wheel frame

x_3	Longitudinal motion in rear right wheel frame
x_4	Longitudinal motion in rear left wheel frame
y	Lateral motion in vehicle body frame
y_1	Lateral motion in front right wheel frame
y_2	Lateral motion in front left wheel frame
y_3	Lateral motion in rear right wheel frame
y_4	Lateral motion in rear left wheel frame
Z	Vertical motion in vehicle body frame
z_1	Vertical motion in front right wheel frame
z_2	Vertical motion in front left wheel frame
z_3	Vertical motion in rear right wheel frame
z_4	Vertical motion in rear left wheel frame
Z_0	Initial displacement associated with spring K_{mr1}
Z_{i1}	Road disturbance on front right wheel
Z_{i2}	Road disturbance on front left wheel
Z_{i3}	Road disturbance on rear right wheel
Z_{i4}	Road disturbance on rear left wheel
Z_s	Displacement of sprung mass
Z_u	Displacement of un-sprung mass
α_1	Rotations of front right wheel about wheel axis
α_2	Rotations of front left wheel about wheel axis
α_3	Rotations of rear right wheel about wheel axis
α_4	Rotations of rear left wheel about wheel axis
β	Non-dimensional coefficient of hysteretic loop of MR damper
δ	Steering angle
φ	Vehicle body pitch motion
Γ	Non-dimensional coefficient of hysteretic loop of MR damper
θ	Vehicle body roll motion
μ	Road friction factor
μ_1	Friction coefficient between braking pad and disc on front right wheel
μ_2	Friction coefficient between braking pad and disc on front left wheel
μ_3	Friction coefficient between braking pad and disc on rear right wheel

μ_4	Friction coefficient between braking pad and disc on rear left wheel
υ	Constant magnetic field of MR damper
$\tilde{\omega}_B$	Skew-symmetric matrix of rotational quasi-velocity in vehicle body frame
$\tilde{\omega}_{t1}$	Skew-symmetric matrix of rotational quasi-velocity in front right wheel frame
$\tilde{\omega}_{t2}$	Skew-symmetric matrix of rotational quasi-velocity in front left wheel frame
$\tilde{\omega}_{t3}$	Skew-symmetric matrix of rotational quasi-velocity in rear right wheel frame
$\tilde{\omega}_{t4}$	Skew-symmetric matrix of rotational quasi-velocity in rear left wheel frame
ω_x	Rotational quasi-velocity about x-axis in vehicle body frame
ω_{x1}	Rotational quasi-velocity about x-axis in front right wheel frame
ω_{x2}	Rotational quasi-velocity about x-axis in front left wheel frame
ω_{x3}	Rotational quasi-velocity about x-axis in rear right wheel frame
ω_{x4}	Rotational quasi-velocity about x-axis in rear left wheel frame
ω_y	Rotational quasi-velocity about y-axis in vehicle body frame
ω_{y1}	Rotational quasi-velocity about y-axis in front right wheel frame
ω_{y2}	Rotational quasi-velocity about y-axis in front left wheel frame
ω_{y3}	Rotational quasi-velocity about y-axis in rear right wheel frame
ω_{y4}	Rotational quasi-velocity about y-axis in rear left wheel frame
ω_z	Rotational quasi-velocity about z-axis in vehicle body frame
ω_{z1}	Rotational quasi-velocity about z-axis in front right wheel frame
ω_{z2}	Rotational quasi-velocity about z-axis in front left wheel frame
ω_{z3}	Rotational quasi-velocity about z-axis in rear right wheel frame
ω_{z4}	Rotational quasi-velocity about z-axis in rear left wheel frame
ψ	Yaw motion in vehicle body frame
ψ_1	Yaw motion in front right wheel frame
ψ_2	Yaw motion in front left wheel frame
ψ_3	Yaw motion in rear right wheel frame
ψ_4	Yaw motion in rear left wheel frame

CHAPTER 1 Introduction and Literature Review

1.1. Introduction

Research on vehicle industries is geared towards application of new technologies in order to increase the ride quality, the stability of the vehicle and to compensate for the human error in driving. It is reported that one person is killed in a car crash approximately every minute in the world [1], [2]. According to the United States Department of Transportation (DOT) report, over 90 percent of the accidents are due to human errors [2], [3].

One of the main reasons of car crash in highways is braking in curves and consequently losing the control of vehicle caused by the problems in the handling system [2], [3]. In addition, the road condition and asphalt quality have a direct effect on ride and handling systems. For instance, uneven road conditions such as those due to potholes can cause serious problems for the stability of vehicles when the driver executes a single or double lane change [4].

The handling model found in the literature [2] does not consider the dynamics of the ride input. However, there exists coupling between the ride and handling systems, and it is important to model the coupling effect in the stability analysis. Therefore, the vehicle should be modeled considering the dynamics of the ride and handling models together. The studies show that the coupling in the dynamic equations of the ride and handling system should be considered to accurately simulate the dynamic behavior of vehicles [5].

The study on the effect of ride quality on handling system shows that improving the ride quality may have negative effects on the handling level [5], since there exist coupling effect between the ride and handling systems. However, in most studies on the ride and handling control systems, the coupling effect is neglected to simplify the dynamic equations of the model. Nevertheless, the studies show that the effect of coupling in dynamic equations cannot be neglected [6], [7], [8].

The objectives of the present study are to propose a new vehicle model which is able to simulate all vehicle manoeuvrings, and to improve ride quality and stability of the vehicle using a semi-active suspension system and direct yaw moment strategy based on the proposed model. In this model, all possible Degrees of Freedom (DOFs) of the dynamic model of the vehicle, coupling between the DOFs, kinematic constraints and load transfer effect among all wheels are considered. Moreover, a robust control strategy is proposed based on the new model for improving the ride quality and handling level.

1.2. Literature Review and Research Background

There have been many studies on the ride and handling systems of vehicles and implementing advanced technology in dynamic and control systems in order to improve passenger comfort and safety. In this section, the studies on the modeling of ride and handling, and related control strategies are reviewed; furthermore, the advantages and disadvantages of these studies are discussed.

1.2.1. Modeling of Suspension and Steering Systems

The DOFs of the suspension and steering systems in the vehicle are coupled. However, in view of the complexity of governing equations, the suspension and handling systems have been studied separately by decoupling them. A considerable number of the literature in this area have been devoted to the linearized and decoupled form of suspension and handling models. The literature review shows that the vehicle modeling falls in three sub-categories: ride, handling and integrated model of ride and handling.

1.2.1.1. Ride Modeling

Ride modeling is the study of the suspensions system to analyze the dynamics of the vehicle. It can be classified into three categories: Quarter Car, Half Car and Full Car models. The Quarter Car model is the simplest model to simulate the response of the vehicle to road disturbance which is shown in Figure 1.1. The main assumption of the Quarter Car model is that all wheels can be moved independently; therefore, the suspension system is modeled using two DOFs: one for the body motion and the other for the tire. The dynamics of the Quarter Car model can be presented as linear or nonlinear equations based on the elements of the model. The linear model consists of a linear spring that corresponds to the tire stiffness and car spring, and a viscous damping to account for the tire damping and car damper [9], [10], [11], [12], [13], [14]. The nonlinear Quarter Car model considers a nonlinear stiffness for the car spring to increase the accuracy of the model (the real car spring is nonlinear) [15]. As the simplest model to study new control approaches for semi-active and active suspension systems, the Quarter Car model has its own drawbacks. Mainly, the modeling of the suspension system using Quarter Car model causes

3

over estimation in the simulation due to considering independency of wheels. In other words, only one shock absorber is responsible for absorbing all disturbance energy.
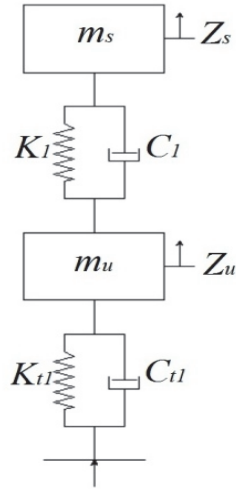
Figure 1. 1 Schematic of Quarter Car model

The Half Car model is a suspension model considering the dependency of wheels located in the front and rear axles or the left and right of the body which is shown in Figure 1.2. The Half Car model has four DOFs to present bounce and pitch of the body and wheels, motion in the perpendicular axis of vehicle planar motion [16], [17], [18], [19]. Using the Half Car model for the suspension system and considering the coupling dynamics between the wheels located in the front and rear axles would improve the accuracy of the simulation of the suspension travel. However, in the Half Car model, the effect of the coupling between the wheels located on the same axle (roll motion), which is a significant DOF of the body in dynamic simulation of vehicle roll over, is not considered.
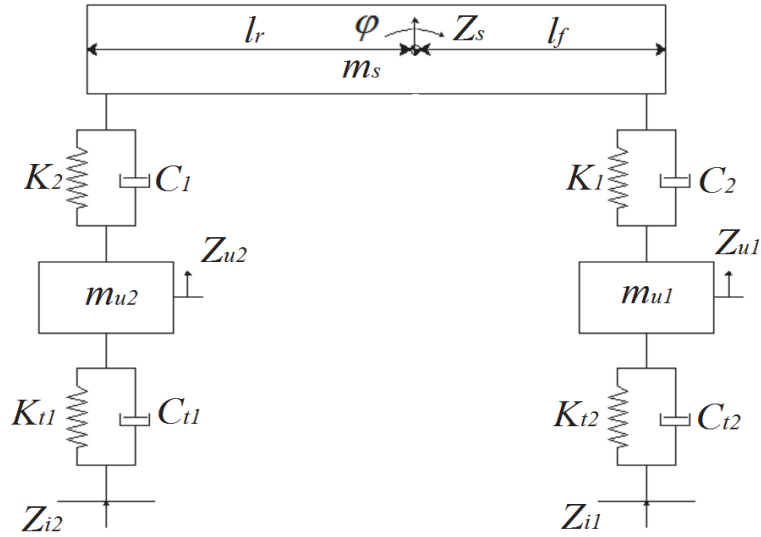
Figure 1. 2 Schematic of Half Car model

The Full Car model studies the dynamics of the suspension system considering the dependency of all wheels on road disturbance which is shown in Figure 1.3. There are seven DOFs in the Full Car model: bounce, roll and pitch are the three DOFs of the body, and the motions of the four wheels are defined by four DOFs. The dynamic equations of the Full Car model can be either linear [20], [21], [22] or nonlinear [23] depending on the properties of suspension system elements, such as nonlinear car spring. The Full Car model has the best precision to simulate the dynamics of suspension system if the vehicle has a constant speed with no steering angle. However, these assumptions are not valid in most cases of vehicle manoeuvrings.
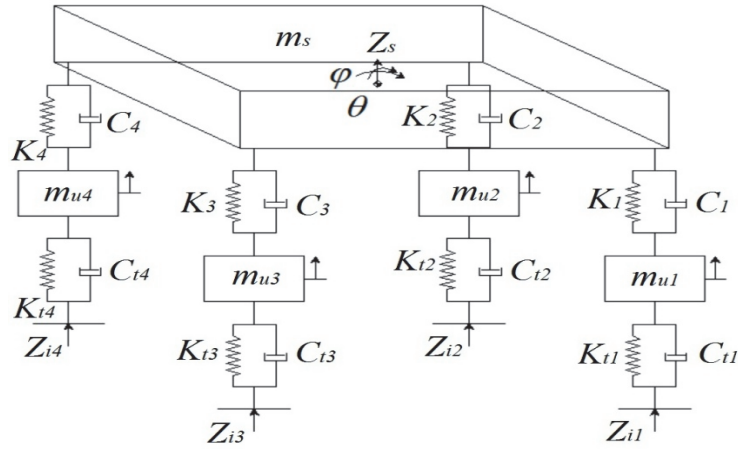
Figure 1. 3 Schematic of Full Car model

1.2.1.2. Handling Model

Handling model is used to study the planar motion of the vehicle. Based on the objectives of the study, the handling models can be categorized as: two DOFs, three DOFs, and eight DOFs. The linear model of the handling system, which is utilized as a model for lane keeping and yaw rate control, has two DOFs including yaw rate and lateral motion of the vehicle [24], [25]. The schematic model of handling bicycle model is shown in Figure 1.4. In the 2-DOF model, it is assumed that the vehicle has a constant speed. Moreover, the effect of the roll motion in vehicle handling, which is the common DOF between ride and handling, is neglected.
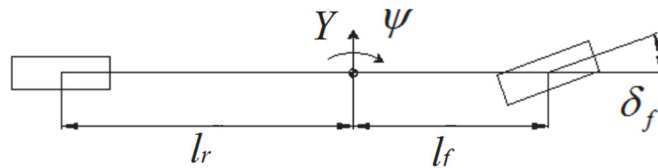
Figure 1. 4 Schematic of bicycle handling model

In the 3-DOF model, the lateral motion, yaw rate and roll motion are considered as the DOFs of the handling system which is presented in Figure 1.5. The roll motion has a significant effect on the vehicle dynamics, especially in cornering. The roll motion is studied in the control system using an anti roll bar as the actuation system [26]. In the study of vehicle motion, one needs to consider the effect of traction and braking, because in actual maneuvering the speed is not constant.
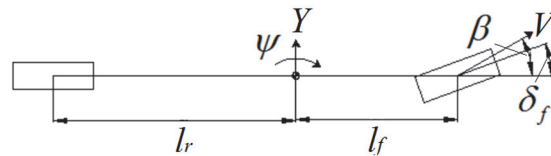
Figure 1. 5 Schematic of three DOFs handling model

The handing model with eight DOFs consists of lateral, longitudinal, roll and yaw motions, and four DOFs for wheel motions as shown in Figure 1.6 [6]. The handling model with 8-DOF is an accurate nonlinear model which is used to study the differential braking system. However, in this model, the effect of the coupling between the ride and handling systems is neglected.
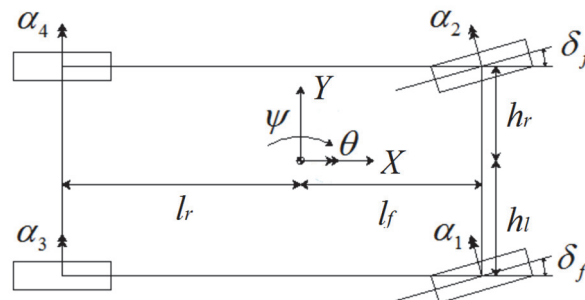
Figure 1. 6 Schematic of eight DOFs handling model

1.2.1.3.   Integrated Ride and Handling Model

The Integrated Ride and Handling model is a dynamic model including the DOFs of the Full Car and the handling model. The studies on the integrated model of ride and handling have shown that the coupling dynamics between the suspension and handling systems has a significant effect on the dynamic simulation of the vehicle [27]. Mashadi and Crolla [5] studied the effect of road excitation on the stability of handling system. Their research shows that a sinusoidal excitation, similar to that experienced in minor roads, with amplitude and frequency of 25 mm and 5 Hz, respectively, can change the understeer-oversteer behavior of the vehicle during cornering. Using the integrated ride and handling vehicle model improves the performance of dynamic simulation as presented in Figure 1.7. The diameter of the sphere represents the coordination of the system, which is improved in vertical, longitudinal and lateral directions [28].
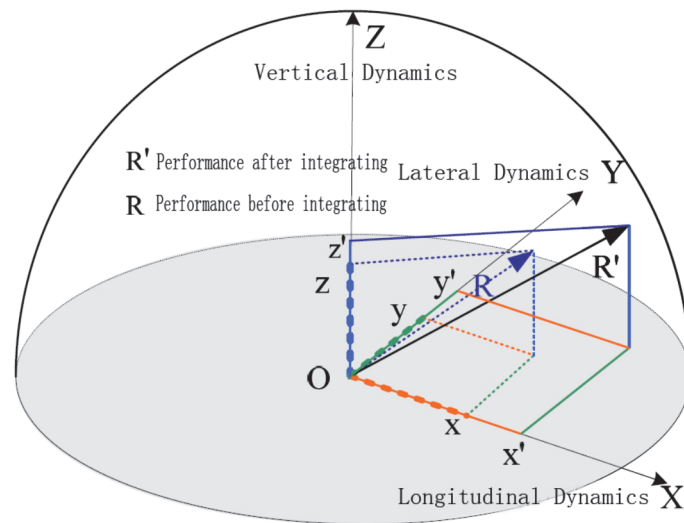
Figure 1. 7 Potential benefits of using integrated ride and handling model [28]

The integrated models of ride and handling have been classified in two categories: using multi-body dynamic simulation software [27] or a mathematical model [7], [8], [27], [29], [31]. It should be noted that in most of the studies on integrated ride and handling model, the effect of traction and braking is neglected, since it is assumed that the velocity of vehicle on longitudinal direction is constant [7], [8], [27], [29], [30].

The studies on the Integrated Ride and Handling model often use a local coordinate system to present the governing equations of the system, and assume the same angular motion in the local coordinate system for the wheels and body of the vehicle [7], [8], [27], [29], [30]. However, depending on the kinematic constraints of the suspension system, wheels and body have different angular motions on different coordinate systems. In addition, the effect of Euler angle is neglected in the dynamic modeling of the vehicle [7], [8], [27], [29], [30]. However, based on the ride and handling assumptions of the integrated model, the roll, pitch and yaw are components of the Euler transformation matrix. Therefore, these motions cannot be neglected in the dynamic model of vehicle.

Bera *et al.* [31] studied the effect of the braking system (variable vehicle speed) in the integrated model of vehicle dynamics using bond graphs. The coupling of the handling and ride systems, the Euler angles and a variable speed in longitudinal direction were used in this study. However, the effect of load transfer between wheels and the different transformation matrices for Euler angles of wheel and body were neglected. Therefore, the same angular motion for body and wheels were used; however, in a physical vehicle the wheels do not have the same rotation as the body.

1.2.2. Semi-active Suspension System

Suspension systems can be categorized as: passive, active and semi-active. Passive suspension systems consist of traditional dampers and springs (without actuating system) which have been used by most of car manufactures in passenger cars. The active suspension system consists of an actuator (electromagnetic motor or hydraulic actuator), which can apply an independent force on the suspension system to improve ride quality [9], [14], [15]. In the semi-active suspension system, a controllable damper makes the dissipation energy rate variable [10], [11], [12], [32]. In order to improve the ride quality, both active and semi-active suspension systems have been studied in literature. However, in view of the high cost of active suspension system, the semi-active suspension system has been studied more often for industrial applications [33].

The studies on the semi-active suspension system can be categorized in two groups: using (i) hydraulic valves [11] and (ii) Magnetorheological (MR) damper systems [10], [11], [12], [32]. The system using hydraulic valves can produce two damping modes, hard and soft, depending on the road condition. However, the complexity of the mechanical system, high power requirement, and narrow force range in suspension systems using hydraulic valves, make the MR damper more appealing in industrial applications.

1.2.2.1. Mathematical Model of Magnetorheological Damper

The semi-active control system provides both features of passive and active devices in terms of reliability and adaptability. Using semi-active system, the rate of energy dissipation becomes controllable, while in active control devices, the energy can be added to the system to control the dynamic response. Magneto-rheological (MR) damper is a semi-active control device which is

10

commonly used in vehicle industries and structural applications. The MR damper contains MR fluid instead of regular oil. The MR fluid is a smart material which contains micron sized magnetic polarized metal particles which provide variable viscous damping with changing magnetic field [34].

The application of MR fluid is dependent on three different operational modes: flow, squeeze-flow and shear [35]. For instance, MR dampers and servo valves are designed based on flow mode of MR fluid [36]. The squeeze-flow mode of MR fluid is utilized in the application of impact control dampers for large forces [36]. The shear mode can be used for brakes, clutches, and damping layer of sandwich structures [36]. In order to describe the dynamic behavior of the MR damper, different mathematical models have been proposed in both discrete and continuous time domain.

Modeling of MR damper by using black box nonlinear models is carried out in discrete time domain [37] where MR damper hysteresis, function of displacement and velocity are modeled by Neural Network (NN). In this model, three parameters are indicated based on the collected experimental input and output data. However, the non-model based parameter identification is only valid for the system operation range during which the experimental data are collected and used for training the NN model. Therefore the accuracy of model cannot be guaranteed for extrapolating the range of operation.

The Bingham visco-plastic MR damper model [38] is built in continuous time domain and it describes the dynamic behavior of MR damper based on the measured shear stress and the shear strain rate. The Bingham model consists of a Coulomb friction element parallel with viscous

damping. Using Bingham model, the storage energy in the MR damper cannot be modeled. Moreover, the difference between the simulated force and the real force increase when the velocity is near zero.

The modified Bingham MR damper model proposed by Gamota and Filsko [39] is a viscoelastic-plastic model. The so-called Gamota and Filsko model is a Bingham model which is in series with a parallel set of spring and viscous damper. The Gamota and Filsko MR damper model improves the accuracy of the model in describing the hysteresis loop and storage energy of the MR damper. However, the simulation of this modified Bingham model needs step size in the order of 10^{-6} which is the main drawback of this model [34].

The Bouc-Wen model [40] is a continuous, visco-elastic-plastic model which can describe a wide range of hysteresis behavior [34]. The hysteresis behavior of Bouc-Wen model is described by an evolutionary variable with three coefficients of velocity which results in smoothness of transition from the pre-yield to the post-yield region. The roll-off effect cannot be simulated using Bouc-Wen model in the region of the small magnitude of the velocity where the velocity and acceleration have opposite directions [34].

In the Spencer MR damper model [34], a spring and a viscous damping element are added to the Bouc-Wen model to simulate the roll-off effect at small velocities. Therefore, the other pair of damping and stiffness elements can be adjusted for small velocities or high frequency region. The Spencer model is capable of simulating the roll-off effect in all velocity and acceleration regions. In the Spencer model, the assigned damping coefficients only depend on the changing current. However, the MR damper viscosity depends on the frequency of excitation [41] and

temperature of MR fluid [42]. And in the literature, MR damper models cannot describe such frequency dependent behavior.

1.2.2.2. Semi-active Suspension Systems Using Magnetorheological Damper

There are many theoretical and experimental studies on the application of MR dampers [10], [11], [12], [32] for instance, Du *et al.* [12] studied the application of MR damper as an actuator in the quarter-car models both theoretically and experimentally. Based on their experimental results, they suggested a polynomial mathematical model for the MR damper force as a function of current. This research shows the margin of desired force for a medium size passenger car (weight: 2000 kilogram, wheelbase: 4.6 meter, and track: 1.8 meter) is around 2000 (N) for a current around 1 (A).

1.2.3. Direct Yaw-moment Control System

Vehicle handling control is the study of vehicle stability during cornering and straight motions. Direct Yaw-moment Control (DYC) is a control strategy to improve the stability of the vehicle which can be applied by three mechanisms: controlling the steering angle (Steer-by-Wire), controlling the drive torque (due to the traction) of the wheels independently (Active Torque Distribution), and using different braking forces in the wheels (Differential Braking) [2].

The steer-by-wire is a control strategy to make a yaw moment against the moment produced due to the centrifugal force. In this control strategy an electric motor (handwheel feedback motor) is coupled with the steering wheel to modify the steering angle which is applied by the driver [43], [44], [45], [46], [47]. Therefore, the control input signal is the steering angle, and the output is

the lateral force due to tire friction on the road. The steer-by-wire method is highly sensitive to the tire model [43], [44], [45], [46], [47]. Therefore, when the road condition (frequency and amplitude of the road) is changed, the tire model may not be valid or accurate. Consequently, the steer-by-wire system cannot insure an accurate result due to the sensitivity of the system to the tire model.

The active torque distribution is a robust method to improve the handling of the vehicle by applying yaw moment. The input of the active torque distribution method is the independent torque on each wheel, and the output is the yaw moment produced by various lateral forces on tires [48], [49], [50], [51]. This method is not sensitive to the tire model. However, the main drawbacks of this control strategy are its high cost and limitations in power sources of the vehicle.

The differential braking system applies asymmetrical braking on wheels to improve the stability of the vehicle [2], [52], [53], [54], [55], [56] which is shown in Figure 1.8. This actuating system is not sensitive to the tire model and road condition. The actuating system of the differential braking system can be implemented using a control kit on an existing Anti Block System (ABS) in the vehicle. Since this control strategy needs less power sources and can be easily installed, it has been used to improve the handling level of passenger cars [2], [52], [53], [54], [55], [56].

14
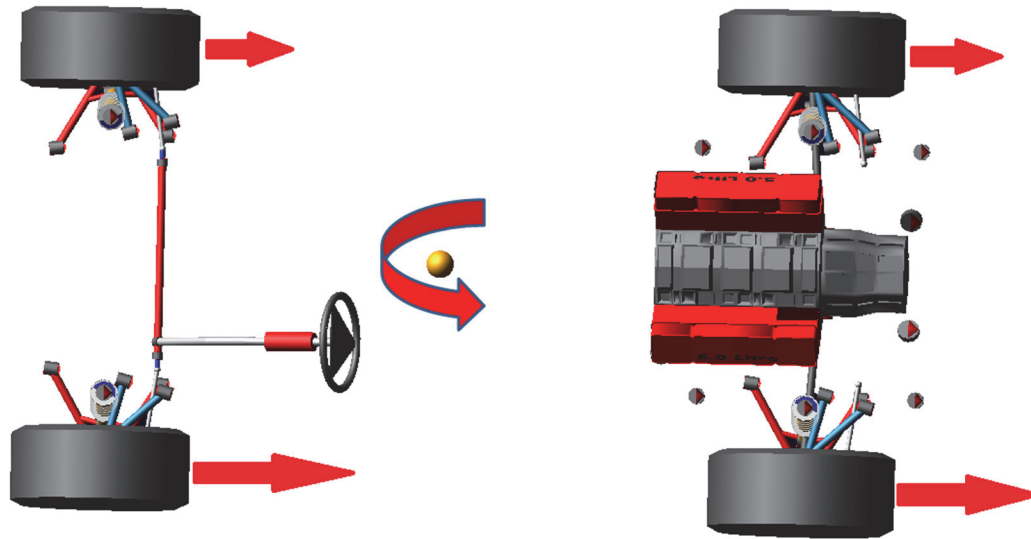
Figure 1. 8 Differential braking system

1.2.4. Control

The ride comfort and stability of the vehicle cannot be guaranteed just by optimizing the passive elements of suspension and handling systems. Therefore, the semi-active suspension system and direct yaw moment strategies are studied to improve the comfort and safety of the vehicle. The control strategies of the semi-active and DYC actuators are studied by researchers based on industry needs and feasibility of the control in practical sense. Two engineering approaches are reviewed for control strategies: non-model based for simplicity in design and model based for performance and stability analysis.

1.2.4.1. Non-model Based Control Strategies

Non-model based control strategies are designed based on the desired response of the system by using intelligent control approaches for instance, Neural Networks [57], [58], [59]. Therefore, the complexity of mathematical equations and linearization error could be avoided. Mainly, four kinds of non-model based strategies have been studied in the ride and handling control of passenger cars: PID [11], [23], [60], [61], [62], [63], [64], Fuzzy-Skyhook [65], [66], [67], [68], Online Tuning-Skyhook [69], [70] and Neural Networks [57], [58], [59].

The PID controller is a well-known industrial controller whose parameters can be tuned online in a control loop to minimize the system error. This controller is utilized in semi-active [11], [60], [61] and active [23], [62], [63], [64] nonlinear suspension systems. The Fuzzy-Skyhook controller has been used as an intelligent controller for the nonlinear systems. One of the applications of the Fuzzy-Skyhook is the tuning of the skyhook control gains in ride control [65], [66], [67], [68]. However, the stability of the system highly depends on the range of the data used in tuning Fuzzy-Skyhook controller.

When the physical model of the system and experimental facility are available, and the controller is designed using a non-model based technique, the control gains can be directly selected by online tuning. In experimental studies the online tuning method could be used to assign the skyhook control gains [69], [70]. The Neural Network is used to design a controller for the system with complicated dynamic equations, such as the vehicle dynamic model, or when the dynamic equations of the model are not available [57], [58], [59]. The most important issue in tuning procedure of the Neural Network-based controller is the number of samples for training

the system. However, it should be noted that the sample data is not available for most cases of vehicle maneuvering.

All of the non-model based control approaches can be easily implemented in experimental set-ups without using mathematical model. However, the stability and robustness of these methods cannot be guaranteed, and the performance of the controllers is not optimal.

1.2.4.2.   Model Based Strategies

Most of the model based control strategies for suspension and handling systems reviewed here are linear or linearized without considering the nonlinearity of the actuator and the coupling between the ride and handling systems. Although some researchers have defined nonlinear models, they have designed the controller based on a simplified linear system and evaluated the response of the controller in closed-loop of the nonlinear system [6]. Therefore, optimal linear and robust control strategies have been used in most studies in the ride or handling control problems. The feedback linearization is another nonlinear control technique utilized in some studies [71], [72], [73], [74]. The feedback linearization technique introduces linear dynamics of nonlinear systems without simplification assumptions. Therefore, using this technique, linear control strategies can be established based on a linearized model.

Linear Quadratic Regulator (LQR) and Linear Quadratic Gaussian (LQG) [15] methods are optimal control strategies which can be used in the linear Multi-Input Multi-Output (MIMO) control systems. The suspension systems in most abovementioned studies have been modeled

using a linear formulation. Therefore, LQR controller as a state feedback control strategy was utilized to improve the ride quality of the passenger car [14] [15], [21], [22], [24]. The LQR control gain is an optimal pole placement gain which is obtained by minimizing the actuation energy, and guarantees the stability of the system. The mathematical procedure to find the LQR gain mainly depends on two positive semi definite "Q" and "R" matrices whose size is related to the number of inputs and state variables. Therefore, the matrices can have any elements to satisfy the positive semi definite condition [14] [15], [21], [22], [24]. Since the matrices "Q" and "R" are important in improving the efficiency of the controller, a hybrid optimization method based on Genetic Algorithm and Sequential Quadratic Programming has been proposed to select the optimal gains for "Q" and "R" matrices [22].

The H-infinity (H∞) control strategy is another robust and optimal control method that has been implemented in ride and handling models [6], [12], [32], [75], [76], [77], [78]. The H∞ algorithm is an optimization procedure based on the infinity norm for MIMO systems considering the coupling of the dynamic equations, which guarantees the stability of the system. Using the body acceleration and tire deflection as controller input variables, some researchers have employed the H∞ control method for ride control [12], [32], [77], [78]. They utilized the Genetic Algorithm (GA) as the optimization method to find the static gain in H∞ controller, and found that this control strategy is efficient and robust to model uncertainty in random excitation for ride control. Therefore, H-infinity controller is efficient if the model is built based on the real dynamics and kinematics of the system.

The feedback linearization technique is used to linearize the nonlinearities of the vehicle model due to the dynamics of the actuator [71], [72] or tire model [73]. The main advantage of this method is to define new state variables and a linear model with the same behavior of the nonlinear model. The study on the handling control using anti-lock braking system and state feedback linearization as the control strategy shows that the state feedback linearization technique is able to introduce a linear model of handling system including the nonlinearity of the tire model [73]. The feedback linearization method has also been used in studying the ride control of semi-active suspension systems [72].

Using model based control strategies the stability and the robustness of the system can be guaranteed. However, most of model based control approaches in literature are presented based on linear control plant. The integrated ride and handling dynamic model considering Euler motion is a nonlinear plant. Using nonlinear H∞ control strategy, a coupled ride and handling control approach can be designed considering nonlinearities of the dynamic plant which is studied in this thesis.

1.3. Thesis Objectives and Scope

In the previous section, various modeling and control strategies to improve the ride and handling quality of the vehicle were reviewed. In most studies, some effective parameters in the ride and handling control systems of vehicle were either simplified or neglected. Therefore, an elaborate study is required in the ride and handling control. The important points of this study are summarized as follows:

19

I. The coupling in the dynamics of the ride and handling has significant effects in cornering, acceleration and deceleration of the vehicle. Therefore, by defining variable speed in longitudinal direction, the effect of variation of the vehicle speed is considered.

II. The rotation frames of the body and wheels are different which leads to modelling the vehicle using multi-body dynamics approaches. Therefore, the dynamic equations of the vehicle are derived using local inertia frames considering Euler motion.

III. A new integrated vehicle model is proposed which is capable of simulating all vehicle manoeuvres and investigating the coupling among the handling and ride motion. In this model, all possible DOFs of the dynamic model of the vehicle, coupling among the DOFs, kinematic constraints and load transfer effect among all wheels are considered.

IV. The governing equations of the proposed integrated ride and handling model are highly nonlinear. Therefore, the numerical results of the proposed model are validated by ADAMS/Car, as a commercial vehicle simulation software.

V. A semi-active full car model using MR damper and differential braking for handling system makes a multi-input multi-output system. As a result, a multi-objective control algorithm considering the coupling dynamics and the nonlinearity of the system should be designed to improve ride and handling of the vehicle.

VI. The mathematical model of MR damper and braking system is considered in the dynamic equations of the integrated ride and handling model. Spencer MR damper model is

characterized by the experimental data, and a mathematical model based on Spencer equations is proposed to make the MR damper model frequency dependent.

VII. Vehicle safety in handling the manoeuvres considering uncertainties of road conditions is one of the essential goals in the handling control system design which can be guaranteed using robust control strategies. Therefore, a nonlinear H∞ control approach is designed based on the proposed integrated ride and handling system to be robust against the road input and variation in road conditions.

The main objective of this research is to model the ride and handling system of a passenger car considering all nonlinearities, the coupling dynamic effect of the ride and handling systems and the effect of braking and traction. This model can be used to design a multi-objective control strategy for ride and handling system. The control devices for the suspension and handling systems are variable damping coefficient (MR damper) and variable braking force, respectively. Based on the proposed integrated ride and handling model, a nonlinear H∞ control approach is designed for an intermediate passenger car.

1.4. Thesis Organization

A new integrated ride and handling model using Boltzmann Hamel equations is derived in Chapter 2. The accuracy of the proposed model has been validated by ADAMS/car. A factor to indicate the necessity of using the integrated ride and handling model over exiting decoupled model is proposed in this chapter.

In Chapter 3, the design procedure of a nonlinear H∞ controller using LMI technique is presented. Subsequently, the linearization approach and simplification assumptions have been explained. Finally, the mathematical proof of the designed controller is given.

The characterization of MR damper and differential braking system is explained in Chapter 4. Based on Spencer mathematical model of MR damper, a new frequency dependent MR damper model is proposed using experimental data. The controller reference signals for improving ride and handling quality are defined in this chapter. Finally, the differential braking system control logic is presented.

The simulation of the proposed vehicle model and controller are presented in Chapter 5. The performance of the designed controller is evaluated in single lane change maneuver considering the road bump input. The robustness of the control system has been studied for different road and weather conditions.

The comprehensive conclusions of all chapters, the original contributions of thesis and recommendations for future works are presented in Chapter 6.

CHAPTER 2   Integrated Ride and Handling

Modeling and Validation

2.1. Introduction

In this chapter a new integrated ride and handling vehicle model based on Boltzmann Hamel equations is proposed to simulate vehicle maneuvering in traction, braking, cornering and passing bump speed or potholes. The dynamic behaviour of the vehicle is simulated by fourteen DOF considering Euler motion. The proposed model is validated using ADAMS/Car software and is compared with the existing decoupled models in [6], [22]. A coupling factor is proposed to represent the coupling among different DOF of the dynamic system. The proposed coupling factor is an indicator parameter that underlines the significance of the integrated model for any vehicle maneuver over the decoupled ride or the handling models.

2.2. Dynamic Equations of Integrated Ride and Handling Model

The vehicle model in the present study includes an integrated model of ride and handling systems. The ride model is a full car with seven DOF, and handling is defined using seven DOF, considering the effect of acceleration and braking (longitudinal acceleration), wheel rotations, lateral, yaw and roll motions in the dynamics of the handling system. The vehicle model is presented in Figures (2.1) to (2.3).
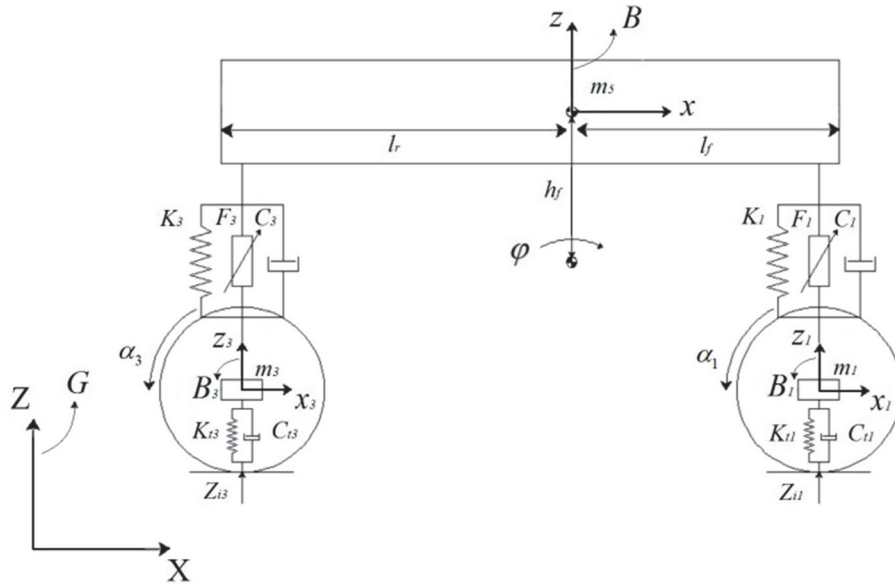
Figure 2. 1 Side view (right) of the suspension system model
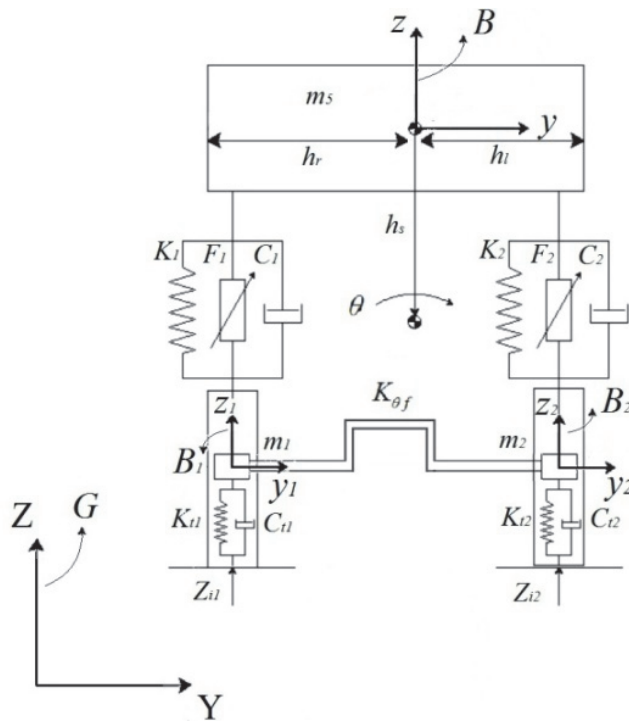
Figure 2. 2 Front view of the suspension system model
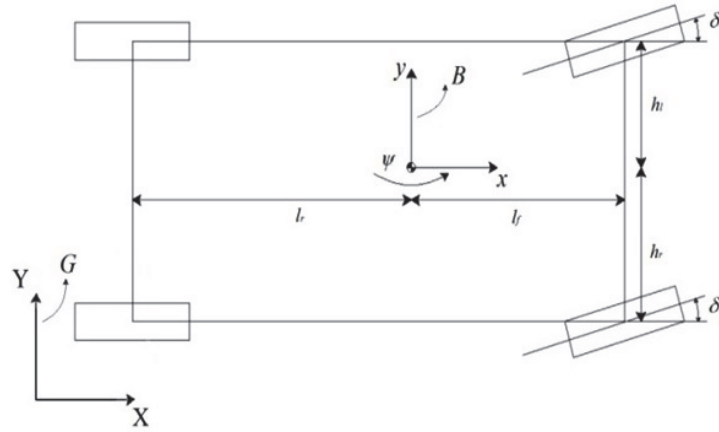
Figure 2. 3 Top view of the handling system model

The motion of the body is defined by six DOF which are x, y, z, θ, φ, ψ in B coordinates system attached to the car body centre. Motions of the wheels are defined in B_{1-4} coordinates attached to the center of the wheels and are designated x_{1-4}, y_{1-4}, z_{1-4}, α_{1-4}, ψ_{1-4}. The kinematic constraints in the actual vehicle dictate that the x_{1-4}, y_{1-4} and ψ_{1-4} are equal to x, y and ψ, respectively, which means that the body and wheels cannot have independent motions along longitudinal and lateral axes and rotation about z axis. Therefore, the number DOF of the model are limited to fourteen where six DOF related to car body and two DOF for each wheel.

2.3. Assumptions

I. The MacPherson suspension system is assumed as the kinematic linkage of the suspension system mechanism. The roll center and pitch center are calculated based on this assumption.

25

II.   The front wheel steering system is assumed with the same steering angles for both wheels. Moreover, the lateral, longitudinal and yaw motions are assumed the same for the wheels on the front and rear axles.

III.   The motion of body and wheels are defined in five local coordinate systems. The B coordinate system in Figures (2.1) to (2.3) is attached to the center of gravity of the body and the B1-4 coordinate systems show the coordinates of the rolling joints of the wheels.

IV.   The mass moment of inertia of tires about the vertical axis (z) is much smaller than that of the body, and, therefore, it is neglected in modeling.

V.   The inertia frames attached to the wheels can rotate only about z axis.

2.4. Lagrangian Dynamics

The integrated vehicle model has fourteen DOF considering the 3D motion of the body and wheels with kinematic constraints shown in Figures (2.1) to (2.3). The governing equations of the vehicle model are derived using the Lagrangian method from kinetic and potential energies of the system. Consequently, using the conservative energy of the system, the dynamic equation for 3D motion of the body can be derived considering the coupling effect of the suspension and handling systems. The Lagrangian equation is presented as follows:

$$\frac{d}{dt}\left(\frac{\partial L}{\partial \dot{q}_i}\right) - \frac{\partial L}{\partial q_i} = Q_i \quad {}_{i=1-14} \tag{2.1}$$

26

where L is the Lagrangian of the system, and q_i and $\dot{q}_i$ are the independent generalized coordinates corresponding to the system DOFs. L, q_i and $\dot{q}_i$ are defined as follows:

$$L = K - U \tag{2.2}$$

$$q_i = [x, y, z, \theta, \varphi, \psi, z_1, z_2, z_3, z_4, \alpha_2, \alpha_1, \alpha_3, \alpha_4] \tag{2.3}$$

where x, y, z, θ, φ and ψ, respectively, represent the longitudinal, lateral, bounce, roll, pitch and yaw motions of vehicle body in attached body coordinate system B. Also, z_{1-4} are wheel bounces in the local coordinate systems B_1, B_2, B_3 and B_4, respectively, which are shown in Figures 2.1 and 2.2. Further, α_{1-4} are rotations of wheels about wheel axis for front right, front left, rear right and rear left wheels in attached body coordinate systems B_1, B_2, B_3 and B_4 , respectively, out of which α_1 (front right) and α_3 (rear right) are shown in Figure 2.1. The dot operator ($\cdot$) is the time derivative of the variables.

Strictly, the generalized coordinates should be linearly independent of each other [79], [80], [81], [82]. However, due to the rotation of the coordinate systems and the nature of the nonholonomic constraints, the attached body coordinates B, B_1, B_2, B_3 and B_4 for the body and the wheels are dependent on each other [80]. Therefore, the effect of Euler rotation angles for translational and rotational motion should be considered. For example, the x axis in B frame has a projection on the y and z axis due to the rotation of the body about roll center.

The Boltzmann-Hamel (BH) equations present a dynamic modeling strategy for the nonholonomic constraints [80]. Using BH equations, a type of Lagrange's equations are defined

27

in terms of the quasi-coordinates based on the literature [80]. The Lagrangian method using the quasi-coordinates is one of the strategies to derive the dynamic equations of an aircraft [79], [82] which has a motion similar to the 3D motion of vehicle body. The quasi-coordinates form is defined in order to have independent observations of the mentioned reference frames and considering the coordinate rotations [79], [81]. In other words, the quasi-coordinates form is a transformation matrix method for local coordinate system. The Lagrangian equations using quasi-coordinates are defined in equations (2.4) and (2.5) [79], [83].

$$\frac{d}{dt}(\frac{\partial L}{\partial \dot{Q}_{li}}) + \tilde{\omega}_p \frac{\partial L}{\partial \dot{Q}_{li}} - T_p \frac{\partial L}{\partial Q_{li}} = T_p F \tag{2.4}$$

$$\frac{d}{dt}(\frac{\partial L}{\partial \dot{Q}_{ri}}) + \tilde{\omega}_p \frac{\partial L}{\partial \dot{Q}_{ri}} + \tilde{V}_p \frac{\partial L}{\partial \dot{Q}_{li}} - (E_p^{-1})^T \frac{\partial L}{\partial Q_{ri}} = (E_p^{-1})^T M \tag{2.5}$$

where the p subscript represents B, t_1, t_2, t_3 and t_4 with respect to the vehicle body and tires. Based on the definition of the Lagrange's equation in terms of quasi-coordinates (BH equations), Q_{li} and Q_{ri} represent the position vectors and the Euler angles of the attached body coordinate systems, B, B_1, B_2, B_3 and B_4 are relative to the stationary frame G. The translational and the angular quasi-velocities are defined as $\dot{Q}_{li}$ and $\dot{Q}_{ri}$ in equations (2.8) and (2.9), respectively [83].

$$Q_{li} = [x, y, z, x_1, y_1, z_1, x_2, y_2, z_2, x_3, y_3, z_3, x_4, y_4, z_4] \tag{2.6}$$

$$\dot{Q}_{li} = [V_x, V_y, V_z, V_{x1}, V_{y1}, V_{z1}, V_{x2}, V_{y2}, V_{z2}, V_{x3}, V_{y3}, V_{z3}, V_{x4}, V_{y4}, V_{z4}] \tag{2.7}$$

$$Q_{ri} = [\theta, \varphi, \psi, \alpha_1, \psi_1, \alpha_2, \psi_2, \alpha_3, \psi_3, \alpha_4, \psi_4] \qquad (2.8)$$

$$\dot{Q}_{ri} = [\omega_x, \omega_y, \omega_z, \omega_{x1}, \omega_{y1}, \omega_{z1}, \omega_{x2}, \omega_{y2}, \omega_{z2}, \omega_{x3}, \omega_{y3}, \omega_{z3}, \omega_{x4}, \omega_{y4}, \omega_{z4}] \qquad (2.9)$$

2.4.1. Rotation Matrices

The vehicle body rotation is not about the centroidal axis of the body, because of the suspension system joints (MacPherson). The roll motion (rotation around x-axis) and pitch motion (rotation around y-axis) are defined for the body rotation. The transformation matrix is assumed by the sequence xyz rotation (Appendix I). The longitudinal, lateral and bounce of the vehicle body frame B can be represented in quasi-coordinates by the transformation matrix shown in equations (10) and (11). The rotation DOFs of body, i.e. roll, pitch and yaw, should be multiplied by the matrix E in equation (2.13) to be represented in the quasi-coordinates format (equation 2.13). The equations (2.12) and (2.13) are defined based on the images of rotational velocities.

$$T_B = \begin{bmatrix} 1 & 0 & 0 \\ 0 & \cos(\theta) & -\sin(\theta) \\ 0 & \sin(\theta) & \cos(\theta) \end{bmatrix} \begin{bmatrix} \cos(\varphi) & 0 & \sin(\varphi) \\ 0 & 1 & 0 \\ -\sin(\varphi) & 0 & \cos(\varphi) \end{bmatrix} \begin{bmatrix} \cos(\psi) & -\sin(\psi) & 0 \\ \sin(\psi) & \cos(\psi) & 0 \\ 0 & 0 & 1 \end{bmatrix} \qquad (2.10)$$

$$\begin{bmatrix} V_x \\ V_y \\ V_z \end{bmatrix} = T_B \begin{bmatrix} \dot{X} + h_f \dot{\varphi} \sin \varphi \\ \dot{Y} - h_s \dot{\theta} \sin \theta \\ \dot{Z} - h_s \dot{\theta} \sin \theta + \dot{\varphi} \sin(\varphi)\left(h_f + h_s(\cos(\theta) - 1)\right) \\ + \dot{\theta} h_s \sin(\theta)(\cos(\varphi) - 1) \end{bmatrix} \qquad (2.11)$$

$$E_B = \begin{bmatrix} 1 & 0 & \sin(\varphi) \\ 0 & \cos(\theta) & -\sin(\varphi)\cos(\theta) \\ 0 & -\sin(\theta) & \cos(\varphi)\cos(\theta) \end{bmatrix} \tag{2.12}$$

$$\begin{bmatrix} \omega_x & \omega_y & \omega_z \end{bmatrix}^T = E_B \begin{bmatrix} \dot{\theta} & \dot{\varphi} & \dot{\psi} \end{bmatrix}^T \tag{2.13}$$

where h_s and h_f are the distance of the roll center and pitch center of the vehicle body from the center of gravity, respectively.

The frames relative to the tires (B_{1-4}) have different transformation matrices based on the kinematic constraints and positions of the coordinate systems. The linear and angular velocities of the tires in the quasi-coordinates are presented in equations (2.14) to (2.18). As mentioned in the fifth assumption, the attached frames on tires only rotate around z-axis.

$$T_{tj} = \begin{bmatrix} \cos(\psi + \delta) & -\sin(\psi + \delta) & 0 \\ \sin(\psi + \delta) & \cos(\psi + \varphi) & 0 \\ 0 & 0 & 1 \end{bmatrix}_{j=1-2} \tag{2.14}$$

$$T_{tj} = \begin{bmatrix} \cos(\psi) & -\sin(\psi) & 0 \\ \sin(\psi) & \cos(\psi) & 0 \\ 0 & 0 & 1 \end{bmatrix}_{j=3-4} \tag{2.15}$$

$$\begin{bmatrix} V_{xj} & V_{yj} & V_{zj} \end{bmatrix}^T = T_{tj} \begin{bmatrix} \dot{X} & \dot{Y} & \dot{Z}_j \end{bmatrix}^T_{j=1-4} \tag{2.16}$$

$$E_j = I_{3\times3} \quad _{j=1-4} \tag{2.17}$$

$$\begin{bmatrix} 0 & \omega_{yj} & \omega_{zj} \end{bmatrix}^T = I_{3\times3} \begin{bmatrix} 0 & \dot\varphi_j & \dot\psi \end{bmatrix}^T \quad _{j=1-4} \tag{2.18}$$

The terms $\tilde{V}_p$ and $\tilde{\omega}_p$ in equations (2.4) and (2.5) are the skew-symmetric matrices of translational and rotational quasi- velocity vectors in time derivative process, which are presented in equations (2.19) to (2.22). The $\tilde{\omega}_{tl-4}$ (equation 2.22) are used to present the effect of rotation coordinate system located on wheels in time derivative procedure. Based on the kinematic constraints of the system, (wheels only rotate about z axis) only the rotation about z axis is presented.

$$\tilde{V}_B = \begin{bmatrix} 0 & -V_z & V_y \\ V_z & 0 & -V_x \\ -V_y & V_x & 0 \end{bmatrix} \tag{2.19}$$

$$\tilde{\omega}_B = \begin{bmatrix} 0 & -\omega_z & \omega_y \\ \omega_z & 0 & -\omega_x \\ -\omega_y & \omega_x & 0 \end{bmatrix} \tag{2.20}$$

$$\tilde{V}_{tj} = \begin{bmatrix} 0 & -V_{zj} & V_{yj} \\ V_{zj} & 0 & -V_{xj} \\ -V_{yj} & V_{xj} & 0 \end{bmatrix}_{j=1-4} \tag{2.21}$$

31

$$\tilde{\omega}_{tj} = \begin{bmatrix} 0 & -\omega_{zj} & 0 \\ \omega_{zj} & 0 & 0 \\ 0 & 0 & 0 \end{bmatrix}_{j=1-4} \qquad (2.22)$$

2.4.2. Kinetic and Potential Energy

$\dot{Q}_{li}$ and $\dot{Q}_{ri}$ present the translational and angular quasi-velocities of the system. Using the quasi-coordinates and considering the kinematic constraints of the system, the kinetic and potential energy of the vehicle can be represented as:

$$K = \frac{1}{2}V_B m_5 V_B^T + \frac{1}{2}\omega_B I \omega_B^T + \frac{1}{2}\sum_{j=1}^{4} V_{tj} m_j V_{tj}^T + \frac{1}{2}\sum_{j=1}^{4}\omega_{tj} I_j \omega_{tj}^T \quad _{j=1-4} \qquad (2.23)$$

$$U = \frac{1}{2}\sum_{j=1}^{4} K_j v_j^2 + \frac{1}{2}K_{\theta f}(\gamma_1^2 + \gamma_2^2) + \frac{1}{2}K_{\theta r}(\gamma_3^2 + \gamma_4^2) + \frac{1}{2}\sum_{j=1}^{4} K_{tj}(z_j - z_{ij})^2$$
$$+ m_5 g h_f (1 - \cos(\varphi)) + m_5 g h_s (1 - \cos(\theta)) \quad _{j=1-4} \qquad (2.24)$$

where z_{i1-4} are road inputs due to the bumpy surface, and m_{1-4} and m_5 are the mass of wheels and body, respectively. The terms V_B, V_{tj}, ω_B and ω_{tj} are the linear and angular velocity vectors of body and wheels, respectively, which are defined in equations (25) to (28).

$$V_B = \begin{bmatrix} V_x & V_y & V_z \end{bmatrix}^T \qquad (2.25)$$

$$V_{tj} = \begin{bmatrix} V_{xj} & V_{yj} & V_{zj} \end{bmatrix}^T_{j=1-4} \qquad (2.26)$$

$$\omega_B = \begin{bmatrix} \omega_x & \omega_y & \omega_z \end{bmatrix}^T \tag{2.27}$$

$$\omega_{tj} = \begin{bmatrix} \omega_{xj} & \omega_{yj} & \omega_{zj} \end{bmatrix}^T_{j=1-4} \tag{2.28}$$

The I and I_{1-4} matrices, used in equation (2.23), represent the body and wheels mass moment of inertia based on the assumption of the modeling as:

$$I = diag([I_x, I_y, I_z]) \tag{2.29}$$

$$I_j = diag([0, I_{\omega j}, 0])_{j=1-4} \tag{2.30}$$

where I_x, I_y and I_z are the mass moments of inertia of body around longitudinal, lateral and vertical axes corresponding to the center of gravity of the body (B coordinate system). $I_{\omega 1-4}$ are the mass moments of inertia of tire around the lateral axis of the B_{1-4} coordinate systems corresponding to the center of gravity of the wheels.

Further, v_{1-4}, in equations (2.31) to (2.34), are motions with respect to the four edges of the vehicle given by:

$$v_1 = z_1 - z - l_f \sin(\varphi) - h_r \sin(\theta) \tag{2.31}$$

$$v_2 = z_2 - z - l_f \sin(\varphi) + h_l \sin(\theta) \tag{2.32}$$

$$v_3 = z_3 - z + l_r \sin(\varphi) - h_r \sin(\theta) \tag{2.33}$$

$$v_4 = z_4 - z + l_r \sin(\varphi) + h_l \sin(\theta) \tag{2.34}$$

where h_r and h_l are the distances between the wheels and the center of gravity, while $h_r + h_l$ is the track base. Further, l_f and l_r are the distances between the axles and the center of gravity of vehicle, and the $l_f + l_r$ is called wheel base.

In modeling the suspension system, the anti-roll bar is considered as the stabilizer part to absorb the roll motion. The anti-roll bar can be modeled by two rotational bars in the front and rear axles ($K_{\theta f}$ and $K_{\theta r}$), and the value of structural damping is chosen from previous studies (Lee, 1999). The $\gamma_{1,2}$ and $\gamma_{3,4}$, in equations (2.35) and (2.36), are the motion of two ends of anti-roll bars in the front and rear axles, respectively.

$$\gamma_{1,2} = \frac{\sin(\theta) - \left(\dfrac{z_1 - z_2}{h_r + h_l} \right)}{h_r + h_l} \tag{2.35}$$

$$\gamma_{3,4} = \frac{\sin(\theta) - \left(\dfrac{z_3 - z_4}{h_r + h_l} \right)}{h_r + h_l} \tag{2.36}$$

34

2.4.3. Non-conservative Equations

The *F* and *M* terms in equations (2.4) and (2.5) are the external forces and moments applied to the system, which are presented in equations (2.37) and (2.38). Based on the definition of the BH equations [79], [80], [82], the non-conservative forces and moments should be defined in the local coordinate systems and the effect of Euler motions is applied by the transformation matrices, T_p (equations 10 and 14) and E_p (equations 2.12 and 2.16). These parameters consist of three kinds of non-conservative forces and moments: dissipation (dampers), friction (tire forces) and actuating forces.

$$F = F_p - \frac{\partial D}{\partial \dot{q}_{li}} \tag{2.37}$$

$$M = M_p - \frac{\partial D}{\partial \dot{q}_{ri}} \tag{2.38}$$

where $\dot{q}_{li}$ and $\dot{q}_{ri}$ are the state vectors of linear and angular velocities in the coordinate systems *B*, B_1, B_2, B_3 and B_4, which are attached to the body and the tires. In order to define the *F* and *M* vectors in the attached body coordinate system, these must be multiplied by *T* and $(E^{-1})^T$. The $\dot{q}_{li}$ and $\dot{q}_{ri}$ vectors are represented as follows:

$$\dot{q}_{li} = [\dot{x}, \dot{y}, \dot{z}, \dot{x}_1, \dot{y}_1, \dot{z}_1, \dot{x}_2, \dot{y}_2, \dot{z}_2, \dot{x}_3, \dot{y}_3, \dot{z}_3, \dot{x}_4, \dot{y}_4, \dot{z}_4] \tag{2.39}$$

$$\dot{q}_{ri} = [\dot{\theta}, \dot{\varphi}, \dot{\psi}, \dot{\alpha}_1, \dot{\psi}_1, \dot{\alpha}_2, \dot{\psi}_2, \dot{\alpha}_3, \dot{\psi}_3, \dot{\alpha}_4, \dot{\psi}_4] \tag{2.40}$$

The damping function for the model due to the car dampers, tire dampers and anti-roll bar structural damping is presented in the following equation.

$$D = \frac{1}{2}\sum\nolimits_{j=1}^{4} C_j \dot{v}_j^2 + \frac{1}{2}\sum\nolimits_{j=1}^{4} C_{ij}(\dot{z}_j - \dot{z}_{ij})^2 + \frac{1}{2}C_{\theta f}(\dot{\gamma}_1^2 + \dot{\gamma}_2^2) + \frac{1}{2}C_{\theta r}(\dot{\gamma}_3^2 + \dot{\gamma}_4^2)$$

(2.41)

where C_{1-4}, C_{t1-4}, $C_{\theta f}$ and $C_{\theta r}$ are the damping coefficients of the car shock absorbers, tires damping and anti-roll bar structural damping of front and rear axles, respectively.

The tire friction forces affect the lateral and longitudinal motions. Moreover, these forces produce moments in yaw motion and rotations of tires about wheel axes. The other non conservative forces and moments are the control forces due to the MR damper and braking system. However, it should be noted that the MR damper only changes the dissipation rate of the energy. The tire friction and actuating forces and moments (F_p and M_p) are presented by the following equations:

$$F_B = T_B \begin{bmatrix} F_x & F_y & F_z \end{bmatrix}^T$$

(2.42)

$$F_{tj} = T_{tj} \begin{bmatrix} 0 & 0 & -F_j \end{bmatrix}^T_{j=1-4}$$

(2.43)

$$M_B = (E_B)^{-1} \begin{bmatrix} M_\theta & M_\varphi & M_\psi \end{bmatrix}^T$$

(2.44)

$$M_{tj} = (E_{tj}^{-1})^T \begin{bmatrix} 0 & M_{bj} & 0 \end{bmatrix}^T_{j=1-4}$$

(2.45)

where F_x and F_y are the tire forces in lateral and longitudinal directions (equations 2.46 and 2.47), F_z is the vertical force which can act on the body (equation 2.48) and, F_{C1-4} are control forces on the front right, front left, rear right and rear left wheels, respectively, given by:

$$F_x = (F_{x1} + F_{b1} + F_{x2} + F_{b2})\cos(\delta) - (F_{y1} + F_{y2})\sin(\delta) + F_{x3} + F_{x4} \tag{2.46}$$

$$F_y = (F_{y1} + F_{y2})\cos(\delta) + F_{y3} + F_{y4} + (F_{x1} + F_{b1} + F_{x2} + F_{b2})\sin(\delta) \tag{2.47}$$

$$F_z = F_{C1} + F_{C2} + F_{C3} + F_{C4} \tag{2.48}$$

In equations (2.46) to (2.48) F_{x1-4} and F_{y1-4} are the forces of each tire in longitudinal and lateral directions which are computed using the Dugoff tire model [2]. The tire forces based on Dugoff tire model for each tire are presented as follows:

$$F_{xj} = K_{xj} \frac{\Delta_j}{1 + \Delta_j} f(\lambda_j) \quad {}_{j=1-4} \tag{2.49}$$

$$F_{yj} = K_{yj} \frac{\tan(s_j)}{1 + \Delta_j} f(\lambda_j) \quad {}_{j=1-4} \tag{2.50}$$

$$\lambda_j = \frac{\mu F_{Vj}(1 - \Delta_j)}{2\sqrt{(K_{xj}\Delta)^2 + (K_{yj}\tan(s_j))^2}} \quad {}_{j=1-4} \tag{2.51}$$

$$\begin{cases} f(\lambda) = \lambda(2-\lambda) & if \ \ \lambda < 1 \\ f(\lambda) = 1 & if \ \ \lambda \geq 1 \end{cases} \qquad (2.52)$$

$$s_1 = \delta - \tan^{-1}(\frac{\dot{y} + l_f \dot{\psi}}{\dot{x} + h_r \dot{\psi}}) \qquad (2.53)$$

$$s_2 = \delta - \tan^{-1}(\frac{\dot{y} + l_f \dot{\psi}}{\dot{x} - h_l \dot{\psi}}) \qquad (2.54)$$

$$s_3 = \tan^{-1}(\frac{-\dot{y} + l_r \dot{\psi}}{\dot{x} + h_r \dot{\psi}}) \qquad (2.55)$$

$$s_4 = \tan^{-1}(\frac{-\dot{y} + l_r \dot{\psi}}{\dot{x} - h_r \dot{\psi}}) \qquad (2.56)$$

$$\Delta_{Tj} = \frac{R\dot{\alpha}_j - \dot{x}}{R\dot{\alpha}_j} \quad {}_{j=1-4} \qquad (2.57)$$

$$\Delta_{Bj} = \frac{R\dot{\alpha}_j - \dot{x}}{\dot{x}} \quad {}_{j=1-4} \qquad (2.58)$$

where δ and R are the steering angle and wheel radius, respectively. K_{x1-4} and K_{y1-4} are the lateral

and longitudinal stiffness of each tires.

Equations (57) and (58) present the tire slip ratio regarding the traction and braking modes of the

vehicle. Thus, based on the assumption for the modeling of the vehicle motion, only one of Δ_{B1-4}

or Δ_{T1-4} should be used.

F_{V1-4} are the vertical loads acting on the tires, which consist of static load due to the body and wheel weight, and dynamic load due to the tire motions and load transfer. The load transfers due to the acceleration, braking and bouncing of tires as the dynamic part of the vertical load have significant effects on calculating the tire forces; these effects have been neglected in most of the studies due to the simplification of the model. The vertical loads are presented as follows:

$$F_{V1} = \frac{m_t g l_r}{2(l_f + l_r)} + m_1 \ddot{z}_1 - m_t \ddot{x} \frac{h_f}{2(l_f + l_r)} + m_t \ddot{y} \frac{h_s l_r}{(l_f + l_r) \times (h_r + h_l)} - \frac{K_{\theta f} \theta + C_{\theta f} \dot{\theta}}{(h_r + h_l)} \qquad (2.59)$$

$$F_{V2} = \frac{m_t g l_r}{2(l_f + l_r)} + m_2 \ddot{z}_2 - m_t \ddot{x} \frac{h_f}{2(l_f + l_r)} - m_t \ddot{y} \frac{h_s l_r}{(l_f + l_r) \times (h_r + h_l)} + \frac{K_{\theta f} \theta + C_{\theta f} \dot{\theta}}{(h_r + h_l)} \qquad (2.60)$$

$$F_{V3} = \frac{m_t g l_f}{2(l_f + l_r)} + m_3 \ddot{z}_3 + m_t \ddot{x} \frac{h_f}{2(l_f + l_r)} + m_t \ddot{y} \frac{h_s l_f}{(l_f + l_r) \times (h_r + h_l)} - \frac{K_{\theta r} \theta + C_{\theta r} \dot{\theta}}{(h_r + h_l)} \qquad (2.61)$$

$$F_{V4} = \frac{m_t g l_f}{2(l_f + l_r)} + m_4 \ddot{z}_4 + m_t \ddot{x} \frac{h_f}{2(l_f + l_r)} - m_t \ddot{y} \frac{h_s l_f}{(l_f + l_r) \times (h_r + h_l)} + \frac{K_{\theta r} \theta + C_{\theta r} \dot{\theta}}{(h_r + h_l)} \qquad (2.62)$$

where m_t is the total mass of body and wheels.

M_θ, M_φ and M_ψ are the moments about lateral, longitudinal and vertical axes of the vehicle, respectively, due to the tire forces and steering moment in front axle. These moments are shown as follows:

$$M_\theta = h_l(F_2 + F_4) - h_r(F_1 + F_3) \tag{2.63}$$

$$M_\varphi = l_f(F_1 + F_2) - l_r(F_3 + F_4) \tag{2.64}$$

$$M_\psi = l_f(F_{y1} + F_{y2})\cos\delta - l_r(F_{y3} + F_{y4}) + (h_r(F_{x1} + F_{b1}) - h_l(F_{x2} + F_{b2}))\cos\delta$$
$$+ l_f(F_{x1} + F_{b1} + F_{x2} + F_{b2})\sin\delta \tag{2.65}$$

M_{b1-4} in equation (2.66) are the moments due to the braking and friction around the lateral axis of the wheels given by:

$$M_{bj} = -F_{bj}R_b - F_{xj}R \quad {}_{j=1-4} \tag{2.66}$$

where F_{b1-4} are braking forces which act on the braking pads of the wheels, and R_b is the distance of braking pads from the geometric center of the wheels.

In the modeling of the system, five frames are defined to derive the dynamic equations of wheels and body. These coordinate frames have vertical, lateral and longitudinal motions. The body frame rotates about three axes (*xyz*), while the attached wheel frames only rotate about vertical axis based on the wheel kinematic constraints and assumptions. Although the model has fourteen DOF, twenty six different local coordinates are defined in the model. In order to avoid the complexity of the local coordinate systems, the dynamic equations are represented in a global coordinate system. In the global coordinate system *G,* shown in Figures (2.1) to (2.3), the coordinates are same as the corresponding motions of the longitudinal, lateral and yaw motions

of body wheels in viewing the kinematic constraints. Therefore, fourteen equations present the dynamic behavior of the model with respect to the fourteen DOFs (Appendix).

2.5. Model Validation

In order to validate the presented governing equations and evaluate the precision of the method, the full vehicle model is created in ADAMS/Car software (Figure 2.4). The numerical parameters for both models are identical, and are presented in Appendix (Table 3). The results of the developed model for double lane-change ISO 3888-1:1999 [84] and ramp steer maneuvering are presented and compared with the ADAMS/Car simulation. It should be noted that the presented model has several nonlinear terms involving sines and cosines due to the Euler motion. However, roll, pitch and yaw in the vehicle model are very small. Since small motion approximation is carried out, all of sine terms with respect to roll, pitch and yaw angles are substituted with the angle of roll, pitch and yaw, and the cosine terms are assumed to be identities.
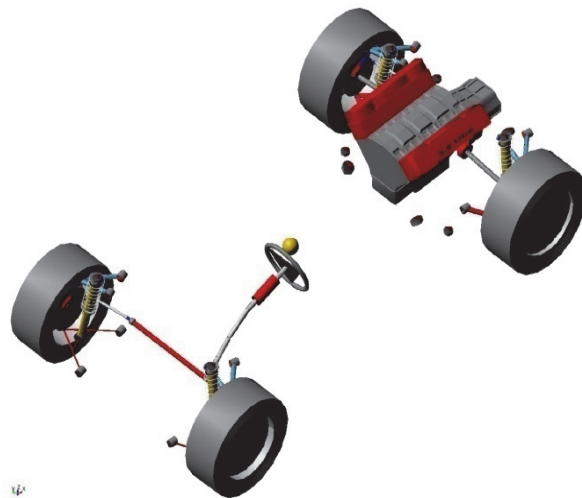
Figure 2. 4 Vehicle model simulated in ADAMS software

2.5.1. Input Signals

The input signals for the model are the road disturbance and steering angle of the vehicle. In this study, three different input signals, shown in Figure (2.5), are applied to the system. These signals are chosen to validate the model using ADAMS/Car simulation and to compare the proposed model with the existing model in previous studies.
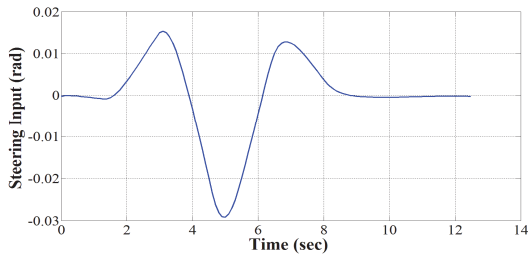
(a)
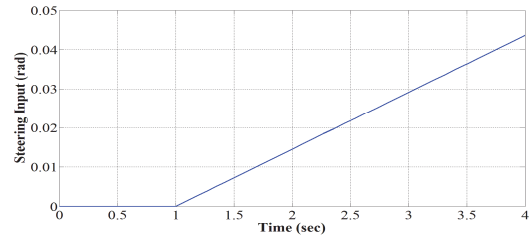
(b)
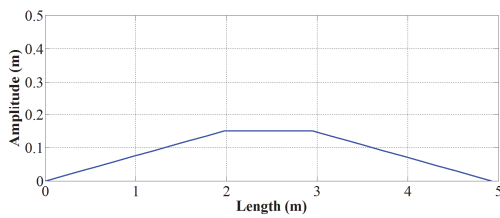
(c)
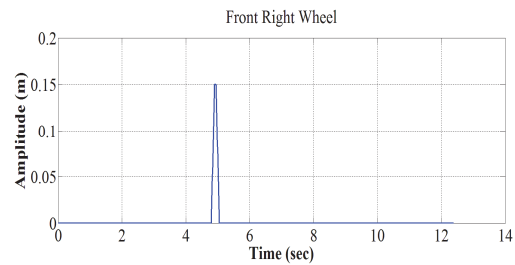
Figure 2. 5 (a) Steering angle for double lane-change based on ISO, (b) steering angle with amplitude of 3.5 (degree) and duration of 3 (sec), (c) bump speed with 5 (m) length and 0.15 (m) amplitude

In order to compare the responses of the proposed model and ADAMS/Car simulation, both models are excited by the ISO double lane changing steering input and ramp steering presented in Figures 2.5(a) and (b), respectively. In addition, the third bump road input signal, shown in Figure 2.5(c), is introduced to study the coupling factor and the effect of ride excitation on handling stability.

2.5.2. Simulation Results

In order to check the validity of the dynamic model, it is excited using an input signal (Figure 2.5a), which is generated by ADAMS/Car to simulate the drive behavior, with 20 (m/s) speed controlled by a PID controller. Figure (2.6) shows the responses of the ADAMS/Car simulation and the developed model which is numerically solved using Matlab/Simulink. In addition, a handling model with seven DOFs [6] (Lateral, Longitudinal, Yaw motion and wheels rotation) is excited by the same input signal in order to study the effect of coupling in vehicle motion simulation.
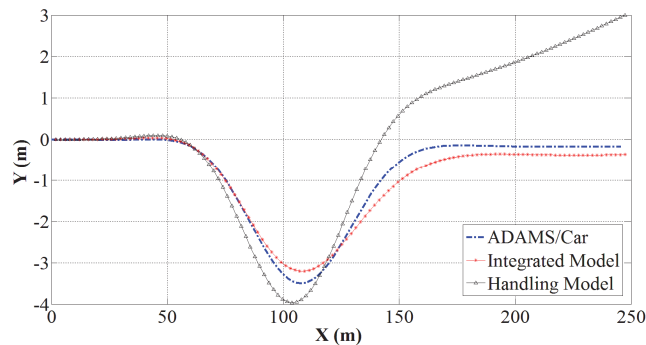
Figure 2. 6 Planar motion of vehicle in the double lane change maneuvering using ADAMS/Car, integrated and handling model (7-DOF)

43

The response of the developed model is validated using a ramp steering angle as the second validation test. The ramp steering angle input signal (Figure 2.5b) is applied to all three models considering a constant longitudinal speed 15 (m/s) using a cruise control system. The results of the ramp steering input are presented in Figure (2.7).
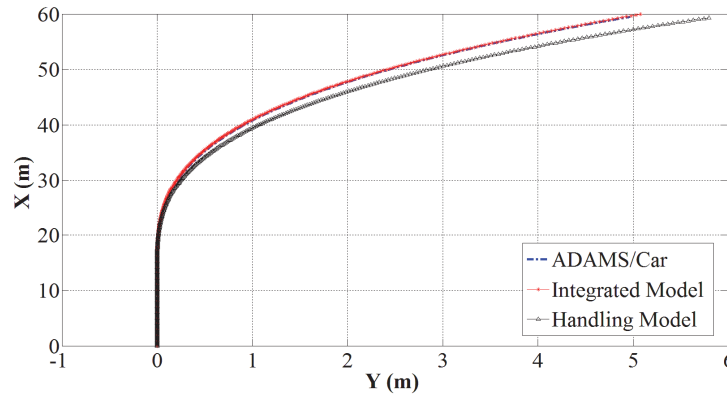
Figure 2. 7 Comparison of ADAMS/Car, integrated model and handling model in planar motion for ramp steering

Figures (2.6) and (2.7) show that the results of the developed dynamic model are close to ADAMS/Car simulation in both manoeuvring cases. Moreover, the results show that the handling model without considering the effect of the ride system in [6], neglects the energy absorbed in the suspension system. Therefore, the elimination of the coupling effect of the ride handling system causes over-estimation in the response of the model. As shown in Figures (6) and (7), due to the effect of energy absorption in ride handling system, the integrated model is less sensitive to the steering input compared to the handling model. Table 2.1 presents the quantitative comparison of the Normalized Root Mean Square Error (NRMSE) of lateral motion

of both the integrated ride and handling, and the handling models with respect to the ADAMS/Car simulation.

Table 2.1.   NRSME of validation tests

Maneuvering	Integrated Model	Handling Model
Double Lane Change	2.96%	16.17%
Ramp Steer	0.53%	4.76%

Table 1 confirms that the integrated ride and handling dynamic model can be used for model based control strategies with high accuracy. The saturation criterion of the tire model is responsible for the difference between the errors of the integrated model and ADAMS/Car simulation for different manoeuvres. It should be noted that the reason for the small error between the ADAMS/Car simulation and integrated ride and handling dynamic model is due to the variable roll center in ADAMS/Car model.

2.6. Coupling Factor

The coupling among DOFs of the ride and handling systems is the main reason for using the integrated ride and handling system with nonlinear dynamic equations. In order to study the significance of using an integrated ride and handling model, a non-dimensional factor is introduced as a coupling factor for the DOFs of the integrated ride and handling model. The coupling factor is defined as:

$$CF = 1 - \frac{\min\left(\left\|\bar{Q}_i\right\|_\infty, \left\|\bar{Q}_{ci}\right\|_\infty\right)}{\max\left(\left\|\bar{Q}_i\right\|_\infty, \left\|\bar{Q}_{ci}\right\|_\infty\right)} \qquad (2.67)$$

where $\bar{Q}_{ci}$ are the velocity and displacement vectors of body and wheel DOFs of the integrated ride and handling model for double lane change maneuver and bump speed inputs. $\bar{Q}_i$ are velocity and displacement vectors of decoupled ride [22] and handling [6] models: x, y, ψ and their time derivatives come from the decoupled handling model, and z, θ, φ, z_1, z_2, z_3, z_4 and their time derivatives are from the decoupled ride model. The infinity norm of vectors for displacement DOFs are calculated based on absolute the value of the vectors. It must be noted that angular velocity and angle of wheels are not studied as a coupling factor since they are affected by the engine input and exist in a limited range determined by the engine coupling.

The coupling factor is a value between zero and one where the "zero" value for the initial DOF indicates no coupling and the value "one" represents the maximum coupling between the ride and the handling model. For example, the longitudinal motion (x) has minimum coupling factor which implies that the handling model and the integrated model have similar results in simulating the longitudinal motion.
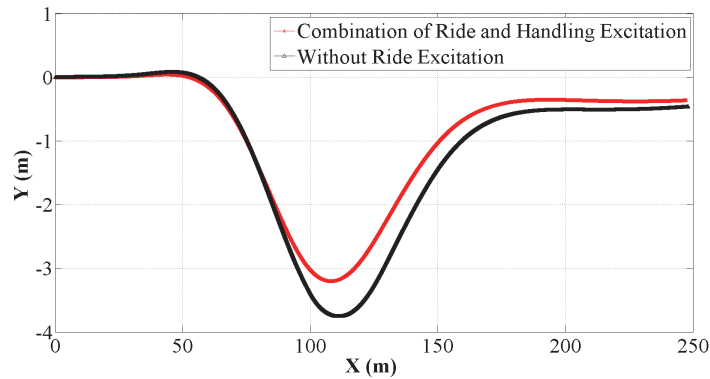
Figure 2. 8 Simulation of the double lane change motion of vehicle with and without ride excitation using integrated model

The planar motion of the vehicle is shown in Figure (2.8). It shows that the ride excitation can induce the unwanted steering and thus can increase the lateral motion which poses more danger at higher speeds. Therefore, it is necessary to define the integrated ride and handling model for the purpose of designing model based control strategies. The coupling factor is studied for ISO double lane change maneuvering considering bump input (Figure 2.5c) for front and rear right wheels. This maneuver consists of a turning scenario for the handling system and the bump speed for the ride system. The simulated maneuvering scenario can excite the integrated model. Therefore, using the ISO double lane change maneuvering, the results of the integrated model and the decoupled ride and handling model can be utilized for studying the coupling factor. Table 2 shows the coupling factor based on the planar motion.

Table 2.2.   Quantitative study for coupling factors

DOF	Maximum amplitude of decoupled ride model	Maximum amplitude of handling model	Maximum amplitude of integrated model	Coupling factor
x	-	247.8 (m)	244.8 (m)	0.0121
y	-	5.5944 (m)	3.8831 (m)	0.3059
ψ	-	0.3459 (rad)	0.2420 (rad)	0.3003
dx/dt	-	20.00 (m/s)	20.07 (m/s)	0.0036
dy/dt	-	3.3046 (m/s)	2.3767 (m/s)	0.3351
$d\psi/dt$	-	0.2420 (rad/s)	0.3459 (rad/s)	0.2966
z	0.0516 (m)	-	0.1415 (m)	0.6354
φ	0.0380 (rad)	-	0.0354 (rad)	0.0372
θ	0.0534 (rad)	-	0.0672 (rad)	0.2053
z_1	0.0123 (m)	-	0.0355 (m)	0.6535
z_2	0.1589 (m)	-	0.1395 (m)	0.1219
z_3	0.0250 (m)	-	0.0563 (m)	0.5566
z_4	0.1622 (m)	-	0.1784 (m)	0.0907
dz/dt	0.3351 (m/s)	-	1.6311 (m/s)	0.8144
$d\varphi/dt$	0.7552 (rad/s)	-	0.7525 (rad/s)	0.0476
$d\theta/dt$	0.4922 (rad/s)	-	0.3956 (rad/s)	0.4224
dz_1/dt	0.3041 (m/s)	-	0.5876 (m/s)	0.3701
dz_2/dt	1.7363 (m/s)	-	1.5521 (m/s)	0.0647
dz_3/dt	0.4149 (m/s)	-	0.8066 (m/s)	0.4656
dz_4/dt	1.8293 (m/s)	-	2.1199 (m/s)	0.1855

Based on the data presented in Table 2.2, the significant DOFs in the coupling of the ride and the handling systems are classified as follows:

i.   The bounce rate of the body and the front left wheel, are the most important coupling factors. In Table 2.2, the numerical values related to coupling factors of the body and front left wheel are 0.7580 and 0.8350, respectively. The coupling in the governing equations (Appendix II) confirms that the bounce motion of the vehicle body with respect to the ride system is affected by the steering input, indirectly, as shown in the equation (II.3) in Appendix II. The dampers in the integrated model are responsible for absorbing the two sources of energy due to the bump speed and steering input whereas, the damper in the decoupled ride model are only responsible for absorbing the energy of the bump speed. Therefore, the bounce rate in the integrated model is greater than that of the decoupled ride model as presented in Table 2.2.

ii.   The second significant coupling factor is the roll rate which is 0.6438 as presented in Table 2. In the decoupled model of the ride system, the dampers are responsible for the absorption of vibration due to the ride excitation only. On the other hand, in the integrated model, as the steering and the ride input also make roll angle, the dampers are responsible for attenuating the vibrations encountered due to the both sources.

iii. The lateral motion is the third significant DOF based on the defined maneuver with value of 0.3351. Figure (2.8) shows that when the vehicle passes the speed bump, the lateral motion increases due to the ride excitation. Therefore, the handling model has a limitation while simulating the lateral motion, which significantly affects the stability of the vehicle.

iv.   The fourth coupling factor is the yaw motion with value 0.2966. Based on the defined dynamic equations, the yaw motion is affected by the components of the vertical motion of the body due to bump speed. The effect due to the vertical motion of the body is neglected in the decoupled handling model which poses some limitations on its applicability.

The coupling factor is an indicator to present the significance of using the integrated model for any vehicle manoeuvre instead of the decoupled ride or the handling model. In other words, for small coupling factor, the decoupled models, which are simpler than the integrated model, can be used for practical application. But when the coupling factors are significant the decoupled model will give erroneous results.
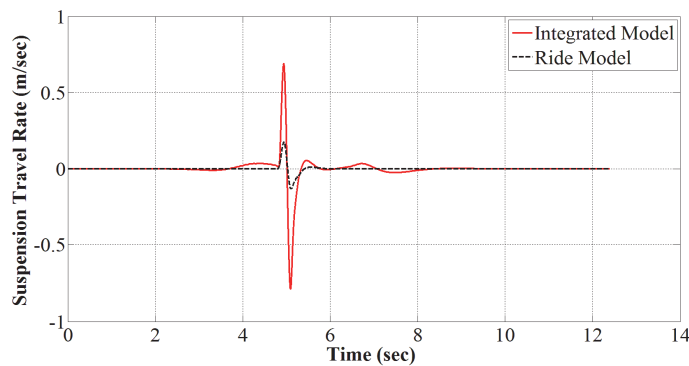
Figure 2. 9 Suspension travel rate of front left wheel

The large values of coupling factors of wheel (z_2) and body bounce (z) prove the significant effect of handling system and steering input in ride quality of the vehicle. Figure (2.10) shows that ride quality is affected by handling motion, and the vibration transferred to the passengers of vehicle has large amplitude. The main reason for this result is that the integrated model is

50

affected by two sources of input causing the vibration in the system (bump and steering inputs). Consequently, neglecting the effect of handling system can introduce large errors in the simulation of vehicle dynamic behavior.
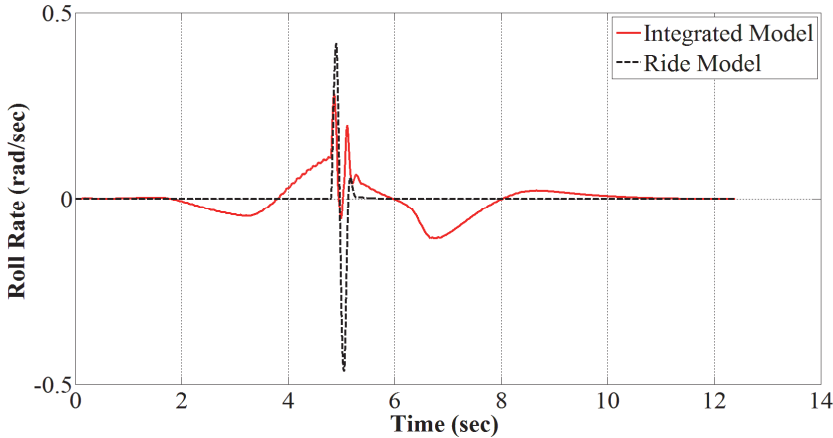
Figure 2. 10 Roll rate of integrated and the ride model
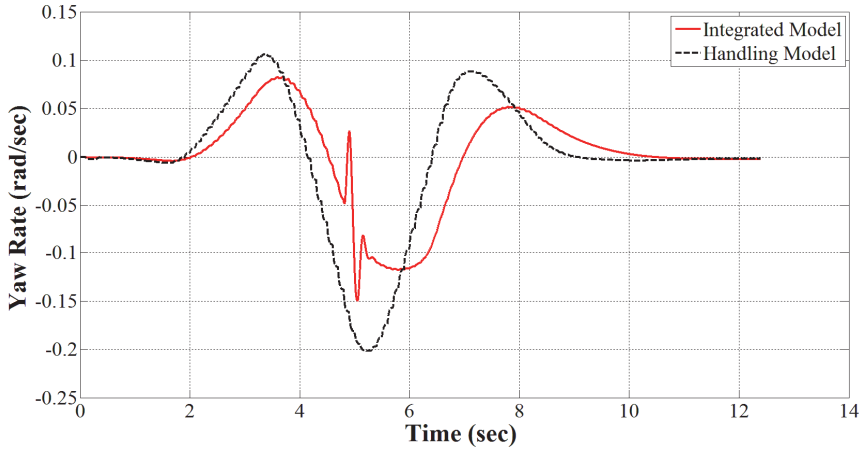
Figure 2. 11 Yaw rate of integrated and the handling model
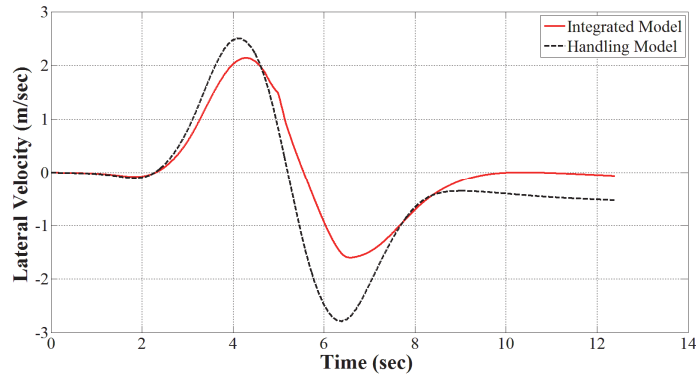
Figure 2. 12 Lateral velocity of integrated and the ride model

The roll rate, yaw rate and lateral velocity depicted in Figures (2.10) to (2.12), increase largely due to the steering input. The integrated model has a peak value when the bump speed is applied under the front right wheel, which affects the yaw motion (Figure 2.11). During cornering, the vehicle has a steady state error on roll motion which cannot be simulated when the effect of handling is not considered. Figures (2.10) to (2.12) confirm that the errors due to the yaw and roll motions are not negligible in the design procedure of the control algorithm. The coupling factor of roll rate and yaw rate have significant values, since these two factors are two main parameters of the Euler motion (equations 9 and 11) and the Euler motion is not negligible in dynamic modeling of the vehicle.

2.7. Summary

A new integrated ride and handling model using the Lagrangian method in quasi-coordinates (BH equations) system is introduced. The developed governing equations could be used for the

model based control strategies. The dynamic model is derived considering the Euler motions of the frames attached to the body and wheels. In addition, the dynamic vertical load, the load transfer, and the acceleration and braking capability of the vehicle are considered in modeling the dynamic behavior of the system. The numerical results of the developed model are validated based on the ISO standards and the ramp steering using ADAMS/Car simulation. The results of ADAMS/Car simulation and the developed model are compared in Table 1. The comparison validates the accuracy of the developed model as the percentage error between the results of the developed model and the ADAMS/Car simulation is approximately 3%.

Based on the numerical solution of the developed model and comparison between the decoupled ride and handling models, a quantitative non-dimensional parameter is introduced as the coupling factor to study the impact of using the integrated model for different vehicle manoeuvres. The results show that the rate of suspension travel is the most significant DOF amongst all. The quantitative study of the coupling factor identified the advantage of the proposed model in the application of the roll stability. Moreover, the coupling factors for the yaw and the lateral motions are significant, which explains the importance of the proposed model in using the direct yaw moment approaches.

CHAPTER 3 Robust Control Synthesis

3.1. Introduction

The robust control approach guarantees the stability and performance of a linear system against the disturbance input when designing a controller. However, the dynamic behaviour of the vehicle is nonlinear as presented in the proposed integrated vehicle model. In this chapter, based on the integrated ride and handling model, a nonlinear H∞ controller is designed for an intermediate passenger car and the linearization assumptions are discussed. The controller plant is partially linearized using Jacobian technique. The controller is designed to be robust against the road input under different weather conditions. The design procedures of the robust controller based on Linear Matrix Inequality (LMI) approach are presented in this chapter. Finally, the stability proof of the presented control system is provided.

3.2. Control Model

The H∞ control approach was introduced by Zames in 1979 according to which the infinity norm of a sensitivity function was minimized for a single-input-single-output feedback system [85]. The H∞ control theory is based on the minimization of peak value of a closed loop response function in frequency domain [86]. The design of H∞ control algorithm using state space representation of a system is established by Green in 1989 [87] based on the liner control system

theory. However, the nonlinear H∞ problems require finding the Hamilton-Jacob Inequalities which is one of the most challenging topics in nonlinear robust control strategies [88].

In the present study, the H∞ controller is designed to minimize the effects of the road disturbance and provide robust stability in the conditions involving severe vehicle maneuvering. The H∞ control scheme is utilized to provide robust ride quality and handling stability against the road disturbances and uncertainties due to the variation of the friction factor between the tire and road under different weather conditions. The proposed integrated ride and handling vehicle model, which is described in Chapter 2 is represented mathematically in equation (3.1).

$$\dot{\eta} = \Gamma(\eta) + B(\eta)u + G(\eta)w$$
$$Q = h_1\eta \tag{3.1}$$
$$D = h_2\eta$$

where $\eta \in R^{28 \times 1}$ is state vector as shown in equation (3.2), $u \in R^{1 \times 8}$ is the input vector which is defined in equation (3.3) as suspension system control forces and braking forces, $w \in R^{1 \times 16}$ is disturbance vector as presented in equation (3.4) which defines the bump input and tire forces to provide robustness against the variations in those terms. Therefore, by choosing these terms as disturbance inputs, the nonlinearities of the tire model are excluded from plant.

The $\Gamma(\eta)$ in equation (3.1) is the dynamics of the system and consists of 28 equations based on the governing equations in chapter 2 which is presented in (3.5). The $\Gamma(\eta)$ has two parts: the first part is $\Gamma_1(\eta)$ which is presented in equation (3.6), and the second part is $\Gamma_2(\eta)$ which is presented in equations (II.1) to (II.11) in appendix II. It should be noted that the $\Gamma_2(\eta)$ is the dynamics of the system considering the acceleration of each DOF (equations II.1 to II.11), and is independent

55

of the disturbance input, system input and acceleration of the other DOF. For instance, the longitudinal acceleration of the vehicle in equation (II.1) is coupled with bounce, lateral, roll and pitch accelerations and it should be decoupled from those terms. An algorithm is designed to decouple the inertia terms in governing equations defined in Appendix II.

The matrices $B(\eta) \in \mathrm{R}^{28 \times 8}$ and $G(\eta) \in \mathrm{R}^{28 \times 16}$, in equation (3.1) are the input matrices and disturbance matrices, respectively. Q and D are function of the state variables, where Q is used as feedback and D is used as measure of the output. The h_1 is derived based on control objectives which are explained in details on Chapter 4. The robust controller gets feedback from $z, \theta, \varphi, z_1, z_2, z_3, z_4, \dot{x}, \dot{y}, \dot{z}, \dot{\theta}, \dot{\varphi}, \dot{\psi}, \dot{z}_1, \dot{z}_2, \dot{z}_3$ and $\dot{z}_4$ as presented in matrix h_1.

$$\eta = [x, y, z, \theta, \varphi, \psi, z_1, z_2, z_3, z_4, \alpha_1, \alpha_2, \alpha_3, \alpha_4,$$
$$\dot{x}, \dot{y}, \dot{z}, \dot{\theta}, \dot{\varphi}, \dot{\psi}, \dot{z}_1, \dot{z}_2, \dot{z}_3, \dot{z}_4, \omega_1, \omega_2, \omega_3, \omega_4]^T \tag{3.2}$$

$$u = [F_{C1}, F_{C2}, F_{C3}, F_{C4}, F_{b1}, F_{b2}, F_{b3}, F_{b4}] \tag{3.3}$$

$$w = [F_{x1}, F_{y1}, F_{x2}, F_{y2}, F_{x3}, F_{y3}, F_{x4}, F_{y4}, Z_{i1}, Z_{i2}, Z_{i3}, Z_{i4}, \dot{Z}_{i1}, \dot{Z}_{i2}, \dot{Z}_{i3}, \dot{Z}_{i4}] \tag{3.4}$$

$$\Gamma(\eta) = \begin{bmatrix} \Gamma_1(\eta) \\ \Gamma_2(\eta) \end{bmatrix} \tag{3.5}$$

$$\Gamma_1(\eta) = [\dot{x}, \dot{y}, \dot{z}, \dot{\theta}, \dot{\varphi}, \dot{\psi}, \dot{z}_1, \dot{z}_2, \dot{z}_3, \dot{z}_4, \omega_1, \omega_2, \omega_3, \omega_4]^T \tag{3.6}$$

$$h_1 = \begin{bmatrix} 0_{3\times2} & I_3 & 0_{3\times23} \\ 0_{4\times6} & I_4 & 0_{4\times18} \\ 0_{10\times15} & I_{10} & 0_{10\times4} \end{bmatrix}_{17\times28} \tag{3.7}$$

$$h_2 = I_{28} \tag{3.8}$$

The displacement and velocity from bumpy road, the variations of the lateral and longitudinal tire forces due to the friction coefficient between road and tires, cornering stiffnesses (K_{y1-4}) and the rolling resistances of the tire (K_{x1-4}) are defined as source of disturbance in vehicle control scheme. As a result, the controller provides robustness against the bumpy road condition and variation of tire forces due to road conditions during snow and rain.

3.3.   Partially Linearized Plant Using Jacobian Method

In order to simplify the control plant and to reduce computational time, the equations are linearized using Jacobian approach. However, the nonlinear terms where the state variables do not have convergence values are considered in nonlinear format. Based on the presented nonlinear controller plant in equation (3.1), an equilibrium point can be defined. The system states can converge to this point from any initial point using the equilibrium value for system input u^* and disturbance w^*.

The Jacobian linearization technique about the equilibrium point of the system is used to obtain a linear equation which makes the exact relation between the deviations of $\Delta\eta$, Δu and Δw as presented in the following equations [90].

$$\Delta\dot{\eta} = \left.\frac{\partial\xi(\eta,u,w)}{\partial\eta}\right|_{\eta^*,u^*,w^*} + \left.\frac{\partial\xi(\eta,u,w)}{\partial u}\right|_{\eta^*,u^*,w^*} + \left.\frac{\partial\xi(\eta,u,w)}{\partial w}\right|_{\eta^*,u^*,w^*} \tag{3.9}$$

$$\xi(\eta,u,w) = \begin{bmatrix} \xi_1(\eta) \\ \xi_2(\eta,u,w) \end{bmatrix} \tag{3.10}$$

where $\xi(\eta,u,w)$ are governing equations of the vehicle model considering control inputs and disturbances. The $\xi_1(\eta)$ is same as $\Gamma_1(\eta)$ which is presented in equation (3.6). The term $\xi_2(\eta,u,w)$ is the dynamics of the system, which contains the disturbances and control inputs and is presented in equations (II.1) to (II.11) in Appendix II, and is decoupled from the accelerations of all DOFs.

The vehicle model with fourteen DOFs is highly nonlinear. Moreover, the DOFs of handling system cannot be linearized about a specific operating point. In other words, the DOFs which define the planar motion of the vehicle in stationary frame do not converge to a specific value. In order to simplify the vehicle model considering the coupling in dynamic equations, the DOFs related to the ride dynamics are linearized about their respective operating points using Jacobian method:

$$\Delta \dot{\eta} = \Delta \Gamma(\eta) + \Delta Bu + \Delta Gw$$
$$Q = h_1 \eta \tag{3.11}$$
$$D = h_2 \eta$$

$$\Delta \Gamma(\eta) = \left[\frac{\partial \xi(\eta, u, w)_i}{\partial \eta_j} \right]_{ij \ \eta^* \ i=1-28, j=1-28} \tag{3.12}$$

$$\Delta B = \left[\frac{\partial \xi(\eta, u, w)_{i1}}{\partial u_{1j}} \right]_{ij \ \eta^*, u^*, w^*, \ i=1-28, j=1-8} \tag{3.13}$$

$$\Delta G = \left[\frac{\partial \xi(\eta, u, w)_{i1}}{\partial w_{1j}} \right]_{ij \ \eta^* \ i=1-28, j=1-16} \tag{3.14}$$

Using Jacobian method, the system is linearized around defined operating point in η^*, u^*, w^* (equations 3.17-19). The η^* is defined as the state variable which has an equilibrium point. The yaw motion does not have an equilibrium point. However, the yaw motion is assumed to be 0.1 (rad) as an average value. This point represents the equilibrium point for this DOF in order to simplify the governing equations of the vehicle model. The roll and pitch motions appear as Euler angles in the denominator of the equations of motion. Therefore, in order to avoid singularity in Jacobian linearization, those variables are assumed to be 0.01 (rad), a small value in the neighborhood of zero.

$$\eta^* = [X, Y, 0, 0.01, 0.01, 0.1, 0, 0, 0, 0, 0, \alpha_1, \alpha_2, \alpha_3, \alpha_4,$$
$$\dot{X}, \dot{Y}, 0, 0, 0, \dot{\psi}, 0, 0, 0, 0, 0, \omega_1, \omega_2, \omega_3, \omega_4] \qquad (3.15)$$

$$u^* = 0_{1 \times 8} \qquad (3.16)$$

$$w^* = 0_{1 \times 16} \qquad (3.17)$$

3.4. Controller Design

Considering the nonlinearities in the dynamic equations and the necessity of robustness, the nonlinear H∞ approach is used to control the MR damper voltage and braking torque. The block diagram of control algorithm is shown schematically in Figure 3.1.
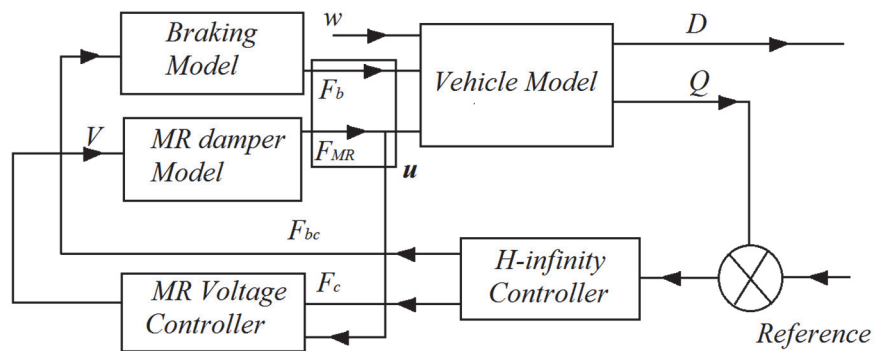
Figure 3. 1 Block diagram of the robust control algorithm.

The inputs of the H∞ controller are the errors in the state variables which should be minimized as shown in Figure 3.1 and equation (3.7). The outputs of the controller are the F_{C1-4} and braking force (F_{bc}). However, the control forces are active and should be converted to semi-active form using MR damper inverse model which is explained in detail in Chapter 4. The outputs of the MR damper model and braking model serve as the input to the vehicle as the semi-active control forces. The control signal can be formulated as shown in equation (3.18).

$$u = K(\eta) \tag{3.18}$$

The closed-loop response of the plant in equation (3.11) is represented using state feedback approach in equation (3.19). It should be noted that ΔB and ΔG are linearized using Jacobian technique about η^*.

$$
\begin{aligned}
\dot{\eta} &= v(\eta) + \Delta Gw \\
Q &= h_1\eta \\
D &= h_2\eta
\end{aligned}
\tag{3.19}
$$

$$v(\eta) = \Delta\Gamma(\eta) + \Delta Bu \tag{3.20}$$

Assuming γ as a positive gain considering the global stability of the system at origin, ($\zeta(0,0) = 0$ and $K(0) = 0$ without disturbance ($w = 0$), the storage energy function can be defined in (3.21) based on the performance criteria of the controller which is shown in (3.22).

$$\int_0^T Q(s)^T Q(s)ds \le \gamma^2 \int_0^T w(s)^T w(s)ds \tag{3.21}$$

$$\dot{V}(\eta) \le \frac{1}{2}\left(\gamma^2\|w\|^2 - \|Q\|^2\right) \tag{3.22}$$

The storage energy function can be achieved by solving the HJI function [91], [92]. The Lyapunov function $V(\eta)$ is a positive semi-definite function which satisfies the inequality in equation (3.23). The HJI function in inequality (3.23) means that if the Lyapunov function satisfies this inequality, the robust performance will be provided for the state variables defined in Q.

$$V(\eta)v(\eta) + \frac{1}{4\gamma^2}V(\eta)\eta^T GG^T \eta V(\eta)^T + \eta^T h_1^T h_1 \eta \le 0 \tag{3.23}$$

3.5. Control Theorem and Proof

Theorem: Consider the following conditions [55], [91], [92], [93] for control system (3.19) and controller (3.18).

I. There exist $N \in \mathrm{R}^{28 \times 28}$ and $M \in \mathrm{R}^{28 \times 28}$ as non-singular and symmetric matrices considering given positive number γ, and the inequality presented in equation (3.23) can be represented by Linear Matrix Inequality (LMI) using Schur complement lemma in (3.24).

62

$$\begin{bmatrix} 2\left(M + \dfrac{1}{2\gamma^2}GG^T\right) & HN \\ HN & -I_{28} \end{bmatrix} \leq 0 \tag{3.24}$$

$$M < 0 \tag{3.25}$$

$$-N < 0 \tag{3.26}$$

where $H \in \mathrm{R}^{28 \times 28}$ is null space of the h_1 which is presented as follows:

$$h_1^T h_1 = H^T H \tag{3.27}$$

II.   Based on the non-singular N matrix calculated by solving LMIs in equations (3.24) to (3.28), there exist a function $v(\eta)$ in equation (3.28) and the control input defined in equation (3.29) which makes the control system satisfy the performance criteria of the H∞ controller in equations (3.23) and (3.24).

$$v(\eta) = MN^{-1}\eta \tag{3.28}$$

$$K(\eta) = \Delta B^T (\Delta B \Delta B^T)^{-1}(v(\eta) - \Delta\Gamma(\eta)) \tag{3.29}$$

It should be noted ΔB is an asymmetric matrix and has full row rank. Therefore the inverse of ΔB is $\Delta B^T (\Delta B \Delta B^T)^{-1}$ in equation (3.29) using right pseudo-inverse technique [94].

Proof: Using Schur complement lemma, the inequality presented in equation (3.24) can be represented as follows:

$$2\left(M+\frac{1}{\gamma^2}GG^T\right)+N^TH^THN\le 0 \tag{3.30}$$

Using pre-and post multiplication, the Left Hand Side (LHS) of the inequality (3.30) by multiplying N^{-1} considering the symmetric matrices N and M, the inequality (3.30) can be represented as:

$$2N^{-1}MN^{-1}+\frac{2}{\gamma^2}N^{-1}GG^TN^{-1}+H^TH\le 0 \tag{3.31}$$

Considering $N \in \mathrm{R}^{28\times28}$ and $M \in \mathrm{R}^{28\times28}$ as non-singular and symmetric matrices, the Lyapunov function can be represented as format of equation (3.32). Therefore, the Lyapunov function is defined by using a linear relation (matrix N) with state variables. When the disturbance effect w is zero, the time derivative of the Lyapunov function can be derived as shown in equation (3.33).

$$V(\eta)=\eta^TN^{-1}\eta \tag{3.32}$$

$$\dot{V}(\eta)=2\eta^TN^{-1}MN^{-1}\eta \tag{3.33}$$

If $N > 0$ and $M < 0$, the derivative of the $\dot{V}(\eta) < 0$ for all $\eta \neq 0$. Following that, $\dot{V}(\eta) = 0$ at $\eta = 0$; as a result, the system is globally asymptotically stable using the defined Lyapunov function.

The inequality (3.23) can be represented in the form of equation (3.34) by substituting $v(\eta)$ and Lyapunov function by (3.32) and (3.33), respectively.

$$\eta^T N^{-1} \eta M N^{-1} \eta + \frac{1}{4\gamma^2} \eta^T N^{-1} \eta \eta^T G G^T \eta \eta^T N^{-1} \eta + \eta^T h_1^T h_1 \eta \leq 0 \tag{3.34}$$

The controller gains are calculated based on state feedback linearization approach and H∞ control strategy. The stability of the controller is proved using Lyapunov method. The control input gains $K(\eta)$ are calculated in equation (3.29) which makes the control system satisfy the performance criteria of the H∞ control presented in equations (3.21) and (3.22).

3.6. Summary

In this chapter, a design methodology of a robust H∞ controller is presented based on the nonlinear integrated ride and handling vehicle model provided in chapter 2. Nonlinear terms in governing equations of the plant due to the state variables for presenting ride system, and ψ and $\dot{\psi}$ for presenting handling system are linearized around their equilibrium points. The solution of HJI function inequality is obtained using LMI and feedback control techniques. Finally, the proof of stability of control system is provided.

CHAPTER 4   Characterization of

Magnetorheological Damper and Differential

Braking System

4.1.   Introduction

In this chapter, the characterization of MR damper and differential braking system has been studied. The MR damper and differential braking system are used as semi-active control device for ride and handling system. In the previous chapter, the designed robust controller does not consider the nonlinearity of control devices. In order to implement the designed robust controller in the real vehicle system, the accurate mathematical model and inverse model of MR damper need to be built. Also, the differential braking system providing variable braking force should be investigated. Hence, this chapter is dedicated to the modeling of control devices: MR damper and differential braking system.

In this chapter, an algorithm is developed to convert the calculated active control force by robust controller to semi-active MR damper force. Based on an experimental study, the relations between frequency variation and viscosity of MR fluid are presented. A model based on Spencer MR damper model is proposed to render MR damper frequency dependent model. The accuracy of the proposed MR damper model is improved in variation of frequency. The differential braking system is used as controller device for the yaw moment control of the vehicle. Also, the

reference signals, anti-lock braking action and braking pressure for handling systems are presented.

4.2. Mathematical Model of Magnetorheological Damper

MR Shock absorber is a damper which contains Magnetorheological fluids. The MR fluid is a smart material whose rheological behavior can be changed by an applied magnetic field. In other words, the MR fluids can produce variable viscosity in the presence of a changing magnetic field. MR damper is used in vehicles as a semi-active control device. The dynamic behavior of MR damper is highly nonlinear which makes it challenging from a control point of view. In this study the dynamic behavior of the MR damper is simulated using the Spencer model [34].

Due to the nonlinearity in dynamic behavior of MR damper, the accuracy and validity of the Spencer MR damper model over wide range of frequencies are not consistent. The schematic of the Spencer MR damper model is shown in Figure 4.1. The governing equations of Spencer MR damper model are presented in equations (4.1) to (4.3), [34].

$$F_{MR} = C_{mr1}(\dot{q} - \dot{Z}_u) + K_{mr1}\left((Z_s - Z_u) - Z_0\right) \tag{4.1}$$

$$\dot{q} = \frac{1}{C_{mr1} + C_{mr0}}\left(\alpha O + C_{mr0}\dot{Z}_s + C_{mr1}Z_u + K_{mr0}(Z_s - q)\right) \tag{4.2}$$

67

$$\dot{O} = -\gamma \left| \dot{Z}_s - \dot{q} \right| \left| O \right|^{n-1} O - \beta (\dot{Z}_s - \dot{q}) \left| O \right|^n + A(\dot{Z}_s - \dot{q}) \tag{4.3}$$

where, K_{mr1} and C_{mr1} are the MR damper accumulator stiffness and viscous damping coefficients for small velocities, respectively. Z_0 is the initial displacement associated with spring K_{mr1}. Further, K_{mr0} and C_{mr0} are accumulator stiffness and viscous damping coefficients for large velocities, respectively.
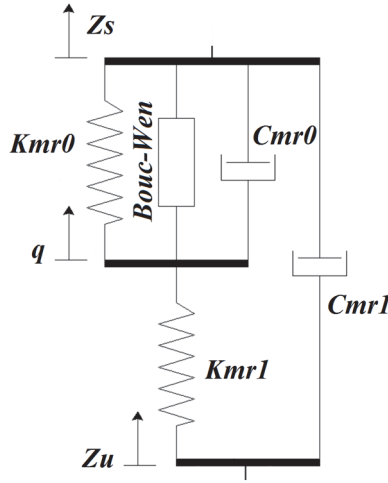
Figure 4. 1 Schematic of Spencer model

Equation (4.2) represents the internal state q which is used to define the roll-off due to the damping coefficient C_{mr1}. The MR damping force in equation (4.1) involves the non-dimensional auxiliary variable O to define the hysteresis. The constants β and γ are the non-dimensional values to present the hysteretic loop in the negative and positive slopes in equation (4.3). Parameter A describes the hysteresis loop size with respect to velocity. The scalar value n is used to represent the smoothness of transition of MR fluid from elastic to plastic [34], [94].

The variable α in equation (4.2) is a polynomial function of voltage to describe the MR fluid yield stress which is defined as a first order polynomial in equation (4.6). The variations of C_{mr1} and C_{mr0} with respect to the frequency of excitation are proposed by $a_{c1}(\Delta Z, \Delta\dot{Z})$ and $a_{c0}(\Delta Z, \Delta\dot{Z})$ in equations (4.4) and (4.5), respectively. The damping coefficients C_{mr1} and C_{mr0} are also functions of voltage as a first order polynomial in equations (4.4) and (4.5), respectively. The equation (4.7) presents a filter to reach rheological equilibrium. Accordingly, one obtains

$$C_{mr1} = a_{C1}(\Delta Z, \Delta\dot{Z}) + b_{C1}u \tag{4.4}$$

$$C_{mr0} = a_{C0}(\Delta Z, \Delta\dot{Z}) + b_{C0}u \tag{4.5}$$

$$\alpha = a_{\alpha} + b_{\alpha}u \tag{4.6}$$

$$\dot{\phi} = -\upsilon(\phi - V) \tag{4.7}$$

where υ is constant for changing rate of magnetic field, V is the applied voltage. The peak value of relative velocity and peak to peak value of relative displacement of MR damper ends are $\Delta\dot{Z}$ and ΔZ are respectively.

4.3.   Characterization of Magnetorheological Damper Based on Experimental Data

The Spencer MR damper model consists of 14 parameters to simulate the hysteresis of MR damper. In order to utilize mathematical Spencer MR damper model and study the behaviour of

MR damper at different frequencies, the parameters of Spencer model are identified using hybrid optimization approach, which is a combination of Genetic Algorithms (GA) and Sequential Quadratic Programming (SQP) based on experimental data. To perform this study, first the parameters of MR damper are identified for constant frequency. In the next step, the trend of variation of MR fluid viscosity with frequency has been studied.

4.3.1. Experimental Setup

In order to gather the experimental force, velocity and displacement data of the MR damper, a MR damper RD 8041 manufactured by Lord Co. is connected to a hydraulic shaker in order to apply harmonic input at one end of MR damper with different frequencies. The experimental set-up consists of MR damper RD 8041, voltage controller kit UI 7000 manufactured by Lord Co., hydraulic pump controller, signal generator, voltmeter, oscilloscope, force sensor and thermometer which are shown in Figures 4.2 and 4.3. The experimental data are gathered in two categories: displacement, velocity and force for variation of frequency in range of 1.5 to 5 Hz in 0.5 (Hz) intervals.
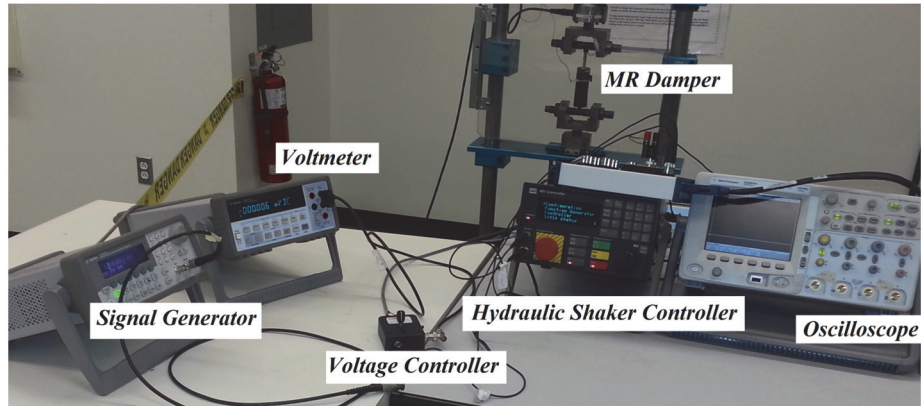
Figure 4. 2 Experimental setup
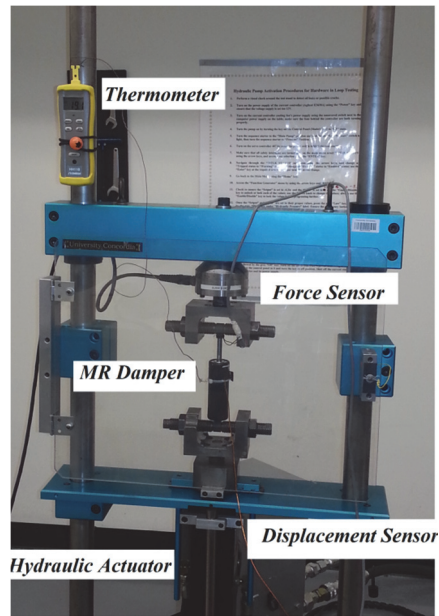
Figure 4. 3 MR damper and hydraulic shaker

The operating range of MR damper RD 8041 is 0 to 2 A and maximum temperature of 71 °C. By increasing the frequency of excitation, the temperature of the MR fluid inside MR damper is increasing which is measured by a digital thermometer attached to the body of the MR damper as

shown in Figure 4.3. Considering this constraint, the maximum frequency which can be applied is 5 Hz. The amplitude of the harmonic excitation is 0.00635 m.

4.3.2.   Hybrid Optimization Approach

In order to identify the parameters of the Spencer model and to study the trend of viscosity versus frequency, the objective function is defined as the error between experimental data and mathematical data calculated by using the Spencer model. The objective function is defined in equation (4.8). The design variables defined in equations (4.1) to (4.7) are presented in (4.9).

$$f = \frac{\sqrt{\dfrac{\sum_{i=1}^{T}(F_{MR}(i) - F_{MR\_E}(i))^2}{T}}}{\max(F_{MR\_E}) - \min(F_{MR\_E})} \tag{4.8}$$

$$\rho = K_{mr0}, K_{mr1}, a_{c0}, a_{c1}, b_{c0}, b_{c1}, a_{\alpha}, b_{\alpha}, A, \beta, \gamma, n, Z_0 \tag{4.9}$$

where the F_{MR} is the MR damper force calculated using the MR damper model. The F_{MR_E} is the measured MR damper force using experiment. The parameter T is the length of measurement.

The constraints are defined to limit the search region. Constrains are defined as lower bounds and upper bounds in both GA and SQP optimization algorithms. The identification of the model parameters is carried out in two steps: (i) identifying ten parameters defined in equations (4.1) to (4.7) using experimental data at frequency of 2.5 Hz and zero volt, (ii) identifying $a_{c1}(\Delta Z, \Delta \dot{Z})$ and $a_{c0}(\Delta Z, \Delta \dot{Z})$ for frequency from 1.5 to 5 (Hz) in 0.5 (Hz) interval at zero current. Therefore,

in the first step, the model has ten design variables and ten lower bounds and upper bounds as linear constraints which are presented in inequalities (4.10) to (4.19).

$$(K_{mr1})_l \leq K_{mr1} \leq (K_{mr1})_u \tag{4.10}$$

$$(K_{mr0})_l \leq K_{mr0} \leq (K_{mr0})_u \tag{4.11}$$

$$(a_{c1})_l \leq a_{c1} \leq (a_{c1})_u \tag{4.12}$$

$$(a_{c0})_l \leq a_{c0} \leq (a_{c0})_u \tag{4.13}$$

$$(a_{\alpha})_l \leq a_{\alpha} \leq (a_{\alpha})_u \tag{4.14}$$

$$(A)_l \leq A \leq (A)_u \tag{4.15}$$

$$(\beta)_l \leq \beta \leq (\beta)_u \tag{4.16}$$

$$(\gamma)_l \leq \gamma \leq (\gamma)_u \tag{4.17}$$

$$(n)_l \leq n \leq (n)_u \tag{4.18}$$

$$(Z_0)_l \leq Z_0 \leq (Z_0)_u \tag{4.19}$$

The lower bound and upper bound of all design variables are given in Table 4.1 based on the indentified parameters for the linear MR damper in the same range of the force as in [96] considering ±50% variation.

Table 4. 1 Parameters of MR damper [96]

Parameter	Quantity	Parameter	Quantity
K_{mr0}	3610 (N/m)	b_α	38430 (N/Vm)
K_{mr1}	840 (N/m)	A	58
a_{c0}	784 (Ns/m)	β	205902 (1/m^2)
a_{c1}	14649 (Ns/m)	γ	136320 (1/m^2)
b_{c0}	1803 (Ns/Vm)	n	2
b_{c1}	34622 (Ns/Vm)	υ	190 (1/s)
a_α	12441 (N/m)	Z_0	0.0245 (m)

In order to identify the design variables $a_{c1}(\Delta Z, \Delta \dot{Z})$ and $a_{c0}(\Delta Z, \Delta \dot{Z})$, eight hybrid optimization algorithms are formulated based on eight experimental data set in the range of 1.5 Hz to 5 Hz in 0.5 (Hz) interval at zero current, respectively. The objective function is defined as the error between the experimental and mathematical model as presented in equation (4.8). The constraints are the lower bounds, upper bounds. The quantities of lower bound and upper bound are assigned based on the sensitivity of the objective function to the design variables. The contour plot of an optimization algorithm in Figure 4.4 presents the sensitivity of objective function to design variables.

The range of design variables in Figure 4.4 are considered to be ±40% from the identified parameters based on 2.5 Hz (first optimization step), in order to identify the viscosity parameters

74

of MR damper at frequency of 1.5 Hz. The lower bound and upper bound for data sets in other frequencies (in the range of 1.5 Hz to 5 Hz) are considered with ±20% variation with respect to the assigned viscosities from previous data set. For example, the lower bound and upper bound of optimized algorithm for 2 Hz are defined based on ±20% from the identified $a_{c1}(\Delta Z, \Delta \dot{Z})$ and $a_{c0}(\Delta Z, \Delta \dot{Z})$ for 1.5 Hz.
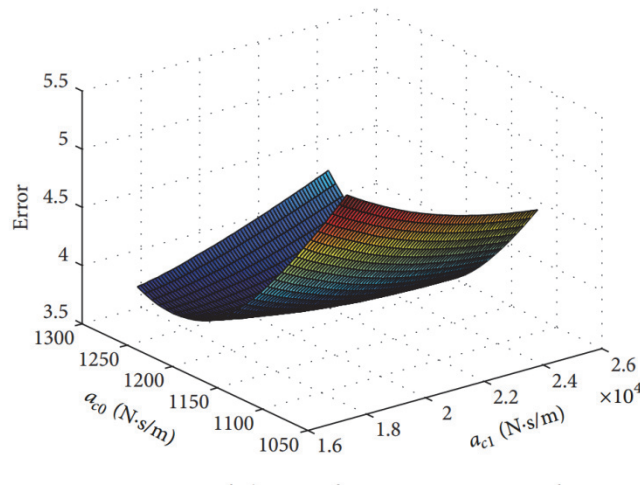
Figure 4. 4 Sensitivity of objective function to variation of viscosity parameters of MR damper in 1.5 Hz

Figure 4.4 shows that the variation of the objective function with respect to the design variable is convex, which guarantees that a global optimum point will be reached in the process of identification. It should be noted that the sensitivity of objective function with respect to viscosity parameters in 20 % variation for all data sets are studied and convexity in the feasible region are checked.

4.3.2.1. Sequential Quadratic Programming Technique

The Sequential Quadratic Programming is a methodology for nonlinear optimization problems considering nonlinear equality and inequality constraints. The SQP is an iterative procedure based on Quadratic Programming (QP) to solve QP sub-problems and to define new iteration [97]. The QP should be solved to satisfy feasibility of problem considering local properties of current iteration. Objective functions, linear and nonlinear constraints of QP sub problems are defined in equations (4.20) to (4.22), [97].

$$f(\rho) \approx \nabla f(\rho^k)^T (\rho - \rho^k) + \frac{1}{2}(\rho - \rho^k)^T Hf(\rho^k)(\rho - \rho^k) \tag{4.20}$$

$$h(\rho^k) + \nabla h(\rho^k)^T (\rho - \rho^k) = 0 \tag{4.21}$$

$$g(\rho^k) + \nabla g(\rho^k)^T (\rho - \rho^k) \le 0 \tag{4.22}$$

where $Hf(\rho)$ is Hessian matrix of objective function.

In nonlinear optimization problems, the SQP method may find one of the extremum points which is near the selected initial point. Therefore, the sensitivity of the initial point with respect to the optimized parameters should be studied. The presented objective function is not robust in variation of initial point. Therefore, the GA is employed to assign the initial point in SQP method which makes the hybrid GA-SQP optimization algorithm.

4.3.2.2. Genetic Algorithm Optimization Technique

The GA is a multi-variable optimization method for solving linear, nonlinear, discrete, continuous, differentiable and non-differentiable constrained problems by using stochastic search algorithms [97],[98],[99]. The Genetic Algorithms is a random search based method which can avoid stopping in local optimum point. However, using GA, the globality of the optimum point cannot be proved and guaranteed. The optimization problem for identifying the MR damper parameters is highly dependent on the initial point. The combination of GA and SQP can solve the problem by using the initial point obtained through GA based on random search in SQP algorithm [22], [100]. The hybrid of GA-SQP approaches can reach global optimum point. But, the globality cannot be proved mathematically. The GA operates based on random point selection in random generation [99]. Therefore, running the same algorithm each time may give different optimal points [99]. As a result, by increasing the number of population and repeating the same algorithm, the relaxation of the obtained initial points is studied. The GA is designed based on the presented objective function (equation 4.8) and constraints (equations 4.10 to 4.19).

4.4. Frequency Dependent Magnetorheological Damper Model

Two optimization approaches are employed to investigate the variation of viscosity of MR fluid with frequency. In the first algorithm the parameters of MR damper are identified for 2.5 Hz and zero current. For the second part the variation a_{c0} and a_{c1} are identified for frequencies in range of 1.5 Hz to 5 Hz in eight sub-optimization algorithms.

4.4.1. Parameter Identification for Constant Frequency

The parameters of Spencer MR damper model are identified using Hybrid optimization of GA-SQP. The identified parameters of Spencer model are presented in Table 4.2 based on experimental data at 2.5 Hz and zero current. The initial values for SQP are assigned using GA. The GA algorithms are used for different number of populations from 80 to 360 in the interval of 80. Moreover, to study the result of relaxation, the algorithms are repeated ten times for each population. The presented results in Table 4.2 are defined based on 240 number of population resulting in minimum error. The identified parameters in this table are used for second step optimization in order to find the viscosity variation of MR damper in different frequencies.

Table 4. 2 Identified parameters of MR damper in 2.5 Hz and zero current

Parameter	Quantity of Hybrid Optimization (GA-SQP)	Parameter	Quantity of Hybrid Optimization (GA-SQP)
K_{mr0}	3361.58 (N/m)	A	87
K_{mr1}	420 (N/m)	β	307269.41 (1/m2)
a_{c0}	1176 (Ns/m)	γ	182842.99 (1/m2)
a_{c1}	21973.50 (Ns/m)	n	2
a_{α}	6515.13 (N/m)	Z_0	0.01225 (m)

Figures 4.5 and 4.6 show the force-velocity and force versus time, respectively. The objective function is defined as the absolute value of the error between the experimental measured data force and generated force in mathematical model. Figure 4.6 confirms that the mathematical model is fitted by experimental data with 2.85 % error. However, since the effect of the velocity

is not considered in the objective function (equation 4.8), the experimental and mathematical

force-velocity curves are not very close for small velocity as can be seen in Figure 4.5.
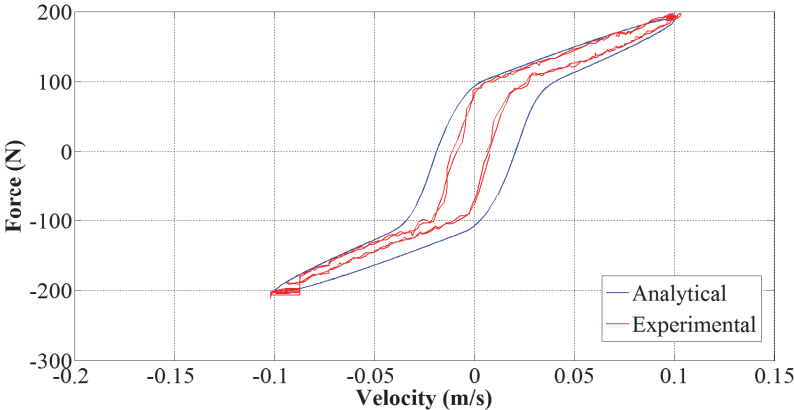
Figure 4. 5 Force velocity hystereis in 2.5 Hz and zero curent
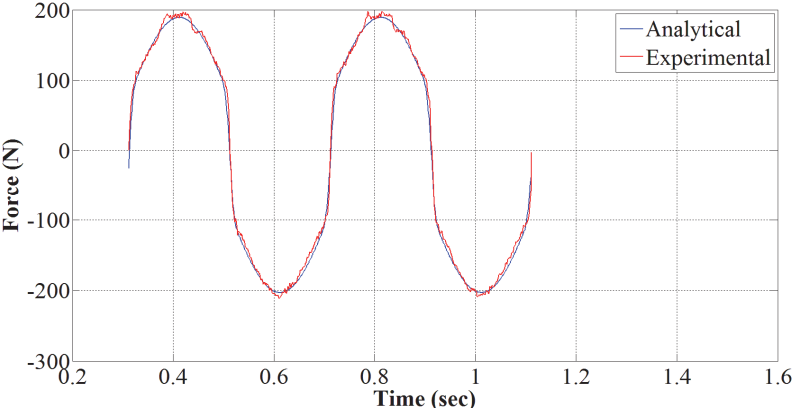
Figure 4. 6 Experimental and mathematical MR damper force in 2.5 Hz and zero current

4.4.2. Parameter Identification for Variable Frequency

The variation of a_{c0} and a_{c1} for the frequencies in the range of 1.5 Hz to 5 Hz in interval 0.5 Hz is

calculated by solving eight sub-optimization problems. The optimization objective is to minimize

the error between the experimental and mathematical data. The constraints are defined in the range of ±40% variation from the optimized values of a_{c0} and a_{c1} for each frequency from the assigned viscosities in 2.5 Hz. The other linear constraints are assigned considering ±20% variation with respect to the assigned viscosities in the previous step. The sensitivity of the objective function to a_{c0} and a_{c1} in the feasible search region is examined to guarantee the convexity of the function in the feasible range defined by lower bound and upper bound. The sub-optimization problems are solved using hybrid optimization technique.
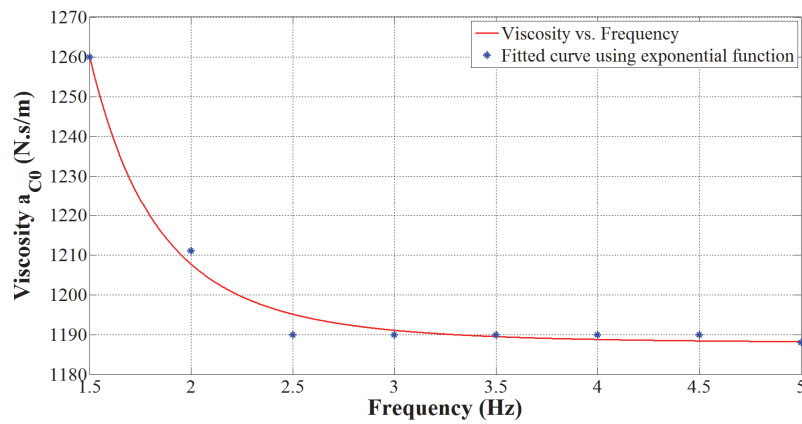

Figure 4. 7 Variation MR damper viscosity a_{c0} versus frequency
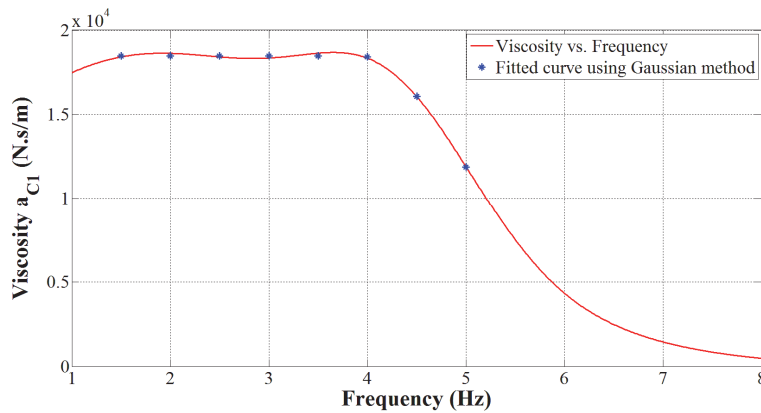
Figure 4. 8 Variation MR damper viscosity a_{c1} versus frequency

Figures 4.7 and 4.8 show the variation of a_{c0} and a_{c1} for different frequencies by star points. The variation of a_{c0} is modeled by an exponential function which can be used for extrapolation. Therefore, the variation of a_{c0} is defined as a function of frequency in equation (4.23). The frequency can be measured by displacement sensor, and the relation between velocity, displacement and frequency are presented in equation (4.25). The variation of a_{c1} with frequency in Figure 4.8 is modeled using the second order Gaussian function in equation (4.24).

$$a_{c0}(\omega) = 1410.71\omega^{-0.102} - 0.6182 \tag{4.23}$$

$$a_{c1}(\omega) = 7087e^{(\frac{4.282-\omega}{1.197})^2} + 18520e^{(\frac{1.783-\omega}{3.25})^2} \tag{4.24}$$

$$\omega(\Delta Z, \Delta \dot{Z}) = \frac{\Delta \dot{Z}}{\pi \Delta Z} \tag{4.25}$$

Figure 4.7 shows that the a_{c0} is sensitive in low frequency region and becomes constant at high frequency, whereas, the a_{c1} in Figure 4.8 is constant at low frequency, and is variable in high frequency region.

In order to compare the effect of using frequency dependent model and frequency independent model (existing model), the error between the experimental and analytical models are presented in Table 4.3 at seven frequencies. The parameters of the frequency independent model are identified at frequency of 2.5 Hz. Therefore, the errors of both frequency independent and frequency dependent models for data samples near 2.5 Hz are close to each other. However, at high frequencies the difference becomes significant. For example, for 5 Hz data sample, the error

is decreased by 1.1. The extrapolation of viscosity variation in Figure 4.8 shows that the difference at high frequencies would be considerable.

Table 4. 3 Comparison between frequency deepened and frequency independent models

Frequency (Hz)	1.5	2	3	3.5	4	4.5	5
Error frequency dependent model	3.13	2.61	2.35	2.57	2.63	3.35	3.75
Error frequency independent model	3.64	2.67	2.36	2.58	2.81	3.95	4.85

Figure 4.9 shows that the existing independent frequency model gives over-estimation in modeling for hysteresis of MR damper in comparison to the proposed frequency dependent model. The main objective in modeling the MR damper is to simulate MR damper force at different frequencies of excitation and current. It shows that the proposed frequency dependent model improves the accuracy of force simulation. Moreover, the proposed model is in agreement with the force simulation in variable frequency and operating conditions of the MR damper.
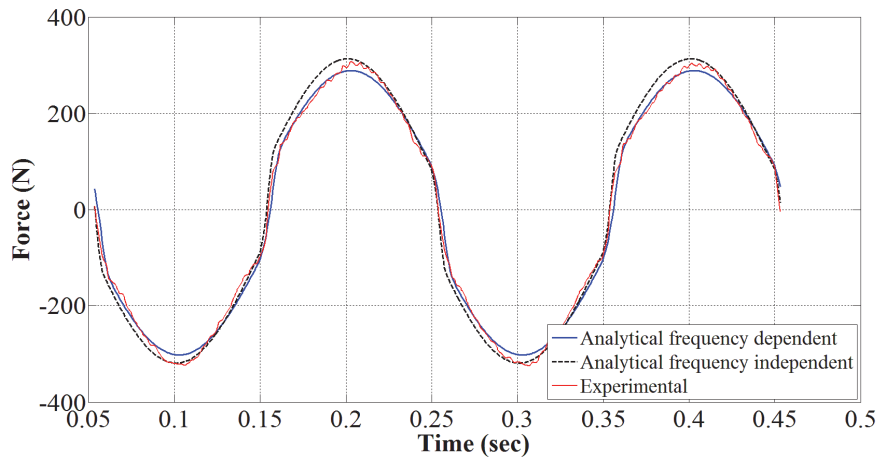
Figure 4. 9 MR damper force in frequency 2.5 Hz and zero current

4.5. Inverse Model Magnetorheological Damper

The mathematical model of MR damper is highly nonlinear. On the other hand, linearizing the MR damper model changes its hysteresis behavior. In order to keep the accuracy of MR damper model and avoid computational cost, the MR damper force is considered as the input of control system. However, the voltage is the input of MR damper model. Therefore, an inverse model of MR damper is utilized to calculate the desired control voltage based on the desired control force which is generated by the robust controller [102]. The inverse model of MR damper is presented in the following flow chart.

Start

Yes

$K_{MR}(F_{Cj} - F_{MRj})\mathrm{sgn}(F_{MRj}) > V_{max\ \ j=1-4}$

No

$V=V_{max}$

End

Yes

$K_{MR}(F_{Cj} - F_{MRj})\mathrm{sgn}(F_{MRj}) < V_{min\ \ j=1-4}$

No

$V=V_{min}$

End

$\phi = K_{MR}(F_{Cj} - F_{MRj})\mathrm{sgn}(F_{MRj})_{\ j=1-4}$

End
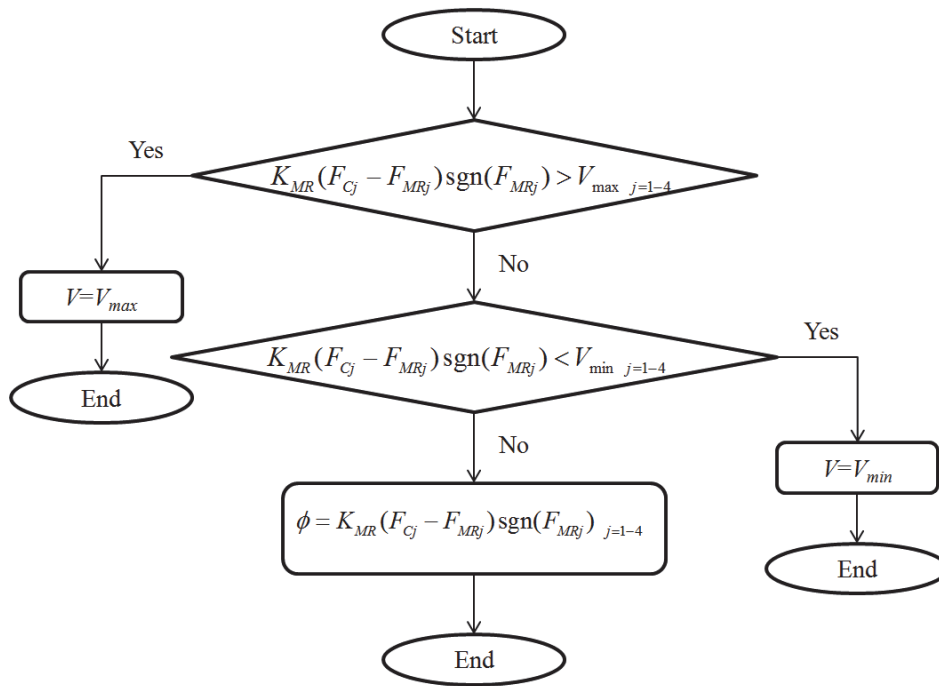
Figure 4. 10 Inverse model of MR damper

where, F_{Cj}, j =1-4 are active control force which should be calculated by controller, V_{max} and V_{min} are maximum and minimum voltage which for the MR damper are 2 and 0 volts, respectively, the K_{MR} is the weighting gain which is chosen as 0.01.

The control objective for the suspension system is to minimize the bounce velocity, roll rate, pitch rate and wheel bounces. Therefore, the reference points for those state variables are selected as zero.

4.6.   Differential Braking System

Differential braking system provides variable braking force (variable oil pressure in hydraulic braking circuit) to produce variable yaw moment. The main purpose of this control device is to make different braking forces on the left and the right side of the vehicle. The differential braking force is designed based on feedback signals of sensors for angular velocity of four wheels, steering angle, lateral velocity and yaw rate [2].

4.6.1.   Controller Reference

In order to design variable braking control system, three criteria should be defined: controller reference, saturation of braking force and braking pressure. Two control references are defined in this study: the desired yaw rate and the desired lateral velocity to keep the vehicle in neutral steering condition. The controller references are presented in equations (4.26) and (4.27), respectively [2]. The desired yaw rate and lateral velocities are defined in G stationary coordinate frame where all DOFs are presented in this frame.

$$\dot{\psi}_d = \frac{V_\beta}{l_f + l_r} \delta \qquad (4.26)$$

$$\dot{Y}_d = \left(\tan\left(\left(1 - \frac{l_f m_t V}{2K_{yr}(l_f + l_r)} \right) \frac{l_r \delta}{l_f + l_r} \right) V_\beta \right) \cos(\psi) + \dot{x}\sin(\psi) \qquad (4.27)$$

where V_β in the velocity of car body considering side slip angle which is presented in equation (4.28), $\dot{x}$ and $\dot{y}$ are the longitudinal and lateral velocities of the vehicle body in the frame B attached to the car body.

$$V_\beta = \frac{\dot{x}}{\cos\left(\tan\left(\frac{\dot{y}}{\dot{x}} \right) \right)} \qquad (4.28)$$

4.6.2. Anti-Lock Braking System

In order to avoid braking lock, the logic of the braking action is formulated relative to slip angle of each wheel [103] which is presented in following flow chart. The range of braking force to decelerate vehicle motion is limited from 0 to 3000 (N) due to limitation of braking circuit.
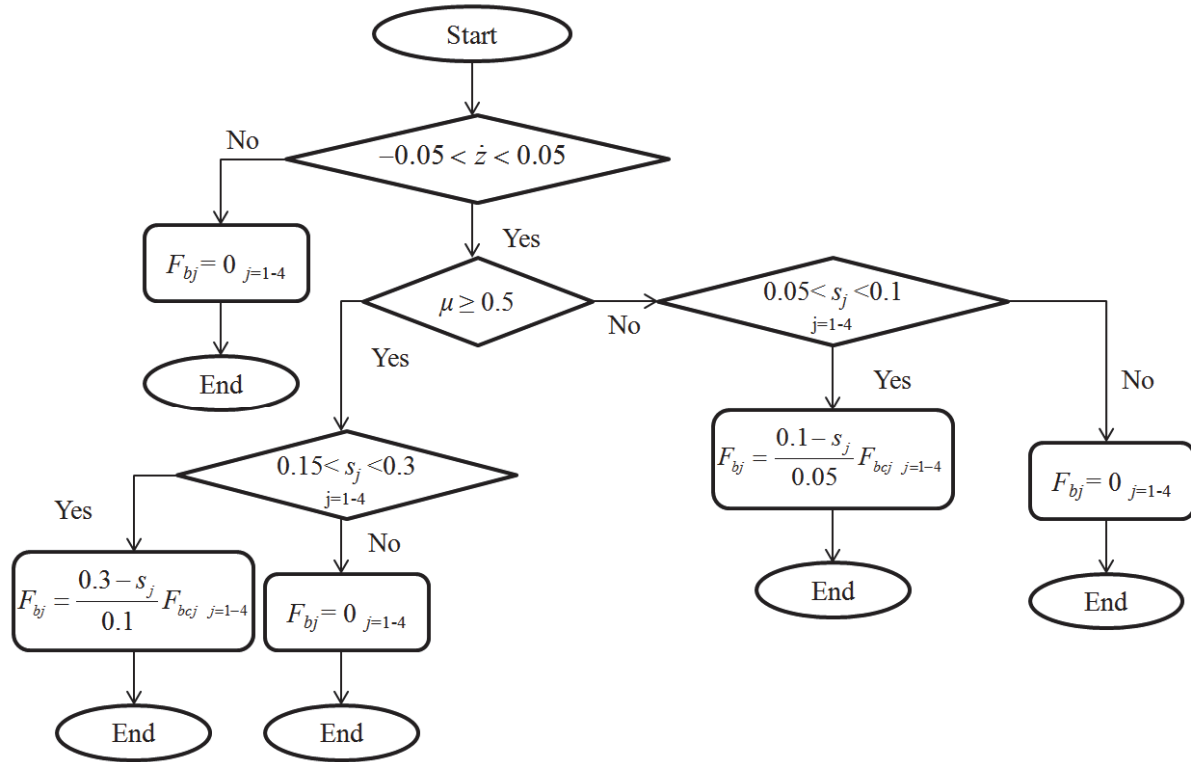
Figure 4. 11 The braking action algorithm

In equation (4.31), the effect of the friction factor under different road conditions: rainy or snowy, are taken into account. In braking action flow chart, the acceptable braking force for rainy and snowy conditions are the function of road friction factor μ. One of the key problems in integrated ride and handling control approach is to avoid conflict and intervention among different control devices [28]. The braking action when the road input is applied makes the vehicle unstable. In order to avoid instability of vehicle, the braking force in the range of body bounce velocity of $\pm0.05\,(\text{m/s})$ would be functional. This control criterion avoids braking if the road input is acting at the same time. The s_j, j=1-4 is the side slip angles of each wheel which is presented in Chapter 2.

86

4.6.3. Braking Pressure

The hydraulic circuit of braking system depends on vehicle brand. Therefore, the required braking pressure is presented in this study. The required pressure to generate braking force can be defined based on the area of the braking pads and friction coefficient between pads and braking disc, where the braking pressure for each wheel is presented in equation (4.28).

$$p_{bj} = \frac{F_{bj}}{A_{pj}\mu_p} \bigg|_{j=1-4}$$

(4.29)

where A_{p1-4} are the area of braking pads, and μ_p is the friction coefficient between braking pad and disc.

4.7. Summary

In this chapter, the variation of MR damper viscosity at different frequencies has been studied using analytical and experimental approaches. The hybrid GA-SQP optimization techniques are used to identify the parameters of the MR damper based on experimental data. The variation of MR damper viscosity with frequency is studied for frequency range from 1.5 HZ to 5 Hz at 0.5 Hz interval using hybrid GA-SQP technique. A mathematical MR frequency dependent model is proposed based on Spencer MR damper model where the viscosity of MR damper is described by exponential and Gaussian functions. The results confirm that the frequency dependent MR

damper model improves the accuracy of the model in force simulation at high frequency region and shows consistency in force simulation as well.

Based on the modified Spencer MR damper model, the MR damper controller is presented. Using the MR damper controller the required voltage to produce semi-active control force is calculated. Moreover, the logic of differential braking approach is presented in this chapter. The control references signal and controller desired target to improve the handling stability of vehicle are discussed.

CHAPTER 5 Simulation of Vehicle Model and Controller

5.1. Introduction

In this chapter the simulation of the proposed vehicle model and control system in MATLAB/ Simulink is explained. In order to study the performance of the designed control approach, a combination of a single lane change maneuver with a bump input is simulated to study the performance of the designed robust controller in tracking the desired path and mitigating the effect of road input. Moreover, using this combination of system inputs, the interaction of ride and handling systems is studied. Finally, the measured performance of the controller in ride and handling quality are presented.

5.2. Simulation of Vehicle Model and Controller in MATLAB

The dynamic behavior of vehicle model and controller is simulated using Matlab/Simulink in order to evaluate the performance of the designed control approach. The components of the vehicle model and control algorithm as explained in Chapters 3 and 4 are implemented using subsystems in Simulink. The feature which is mainly used to implement the dynamic equations of vehicle model, controller etc, is a Matlab embedded function. The Matlab embedded function is an interface between Matlab mfile and Matlab Simulink and a model with this function is compiled by C++ and run by Matlab. Using Matlab embedded function, most of the facilities of

coding in Matlab would be available in Simulink interface. The simulation of the vehicle model and controller is presented in Figure IV.1 in Appendix IV. The parameters of the medium size passenger car are presented in appendix III Table A3.1.

5.3. Single Lane Change Maneuver and Ride Input

The dynamic behavior of the vehicle is simulated for a single lane changing considering a bump input under front right wheel. The traveling speed of the vehicle is assumed as 15 (m/s). The steering input and bump input are shown in Figures 5.1 and 5.2. The passive model simulated in Matlab is defined based on numerical values of the vehicle model in Appendix III Table A3.1. The viscosity of the car dampers (C_{1-4}) are considered as equivalent linear viscous damping coefficient of the MR damper [104] which is 2618 (Ns/m) for the presented MR damper.
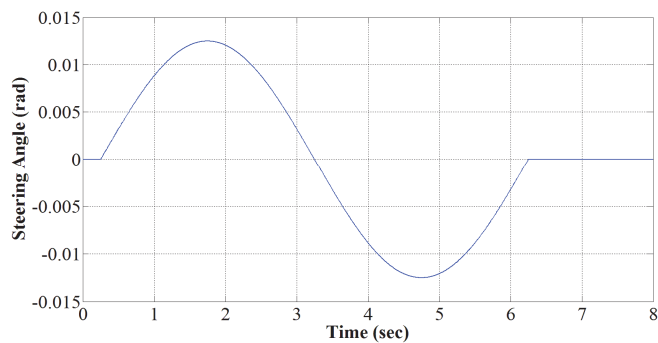

Figure 5. 1 Input steering angle for single lane change maneuver
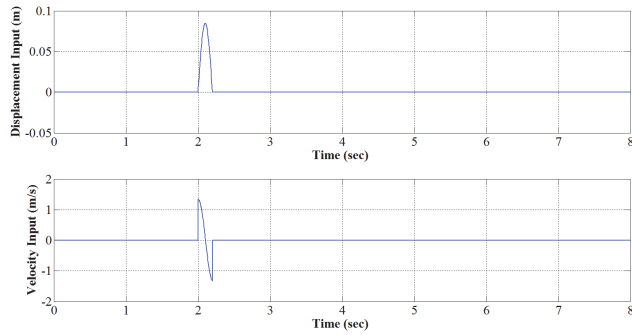
Figure 5. 2 Road input under front right wheel

5.4. Robustness Against Variation of Road Condition

In order to study the robustness of designed control algorithm, the dynamic behavior of the vehicle is simulated for three different road conditions: dry asphalt $\mu = 0.7$, rainy condition $\mu = 0.5$ and snowy condition $\mu = 0.3$. The single lane change maneuver is simulated considering a bump in the road under front right wheel as shown in Figure 5.3. Figures 5.3 to 5.5 show the planar motion of vehicle in stationary frame for single lane change maneuver of the vehicle.
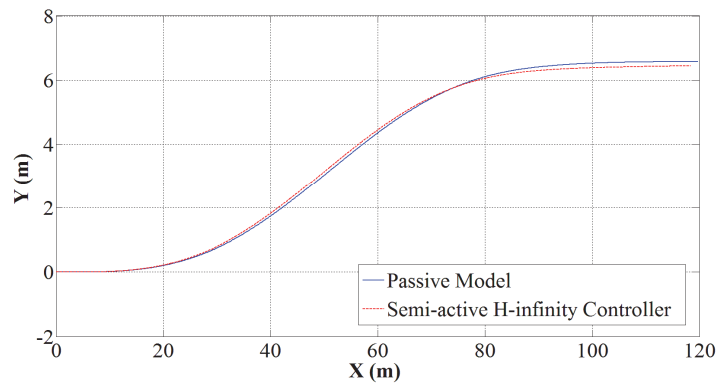
Figure 5. 3 Planar motion of vehicle in dry asphalt condition $\mu = 0.7$ for single lane change maneuver
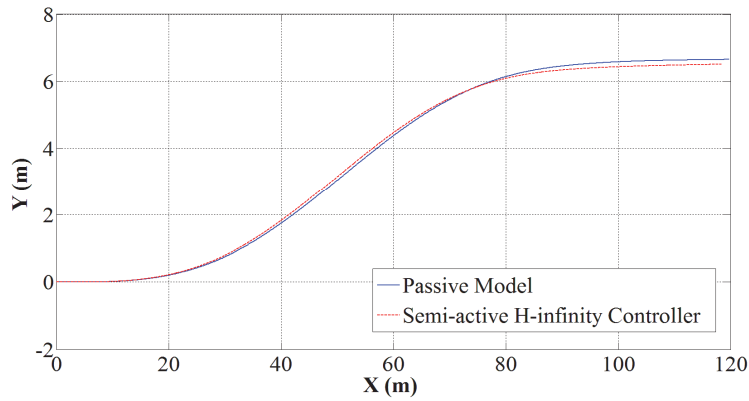
Figure 5. 4 Planar motion of vehicle in rainy asphalt condition $\mu = 0.5$ for single lane change maneuver
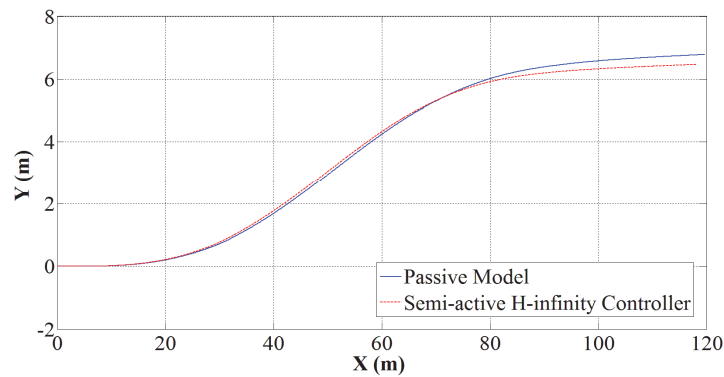
Figure 5. 5 Planar motion of vehicle in snowy asphalt condition $\mu = 0.3$ for single lane change maneuver

Figures 5.3 to 5.5 show that the controller keeps the vehicle stable and reduces the unwanted lateral motion due to the ride input and variation of the road and tire friction factor. The momentum produced due to the variable braking action would be more significant under snowy road condition where the lateral force is smaller than that for rainy and dry asphalt as shown in the planar motion of the vehicle.

5.5. Vehicle Handling Quality for Combination of Ride and Steering Inputs

The performance of controller in improving the handling quality, vehicle stability and the capability of following the control reference signal is studied by comparing the results of robust controller and passive model. Moreover, the differential braking force as part of controller input, which is responsible for handling system, is presented by simulating the differential braking force under different road conditions.

5.5.1.   Simulation Results of Handling System

The controller is designed to follow the desired yaw rate and lateral velocity which are presented in equations (4.26) and (4.27). In order to study the performance of the controller in the following desired reference, the yaw rate and lateral velocity of the vehicle for three different road conditions are presented in Figures 5.6 to 5.11.
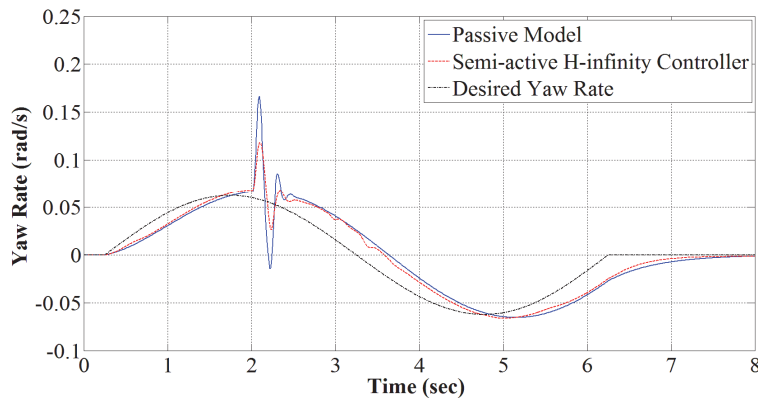

Figure 5. 6 Yaw rate of vehicle in dry asphalt condition $\mu = 0.7$ for single lane change maneuver

93
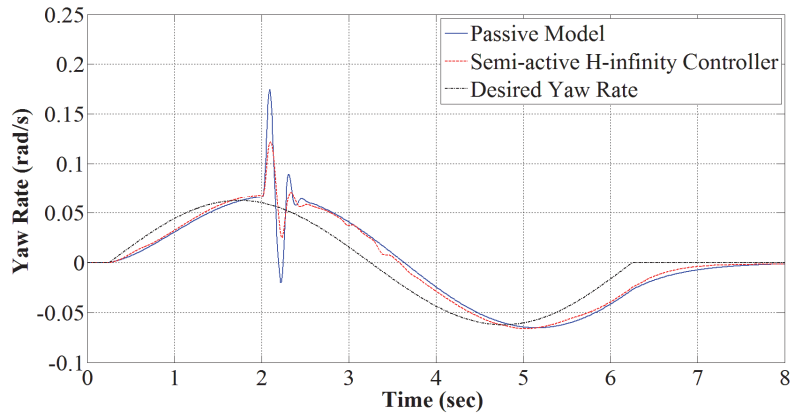
Figure 5. 7 Yaw rate of vehicle in rainy asphalt condition $\mu = 0.5$ for single lane change maneuver
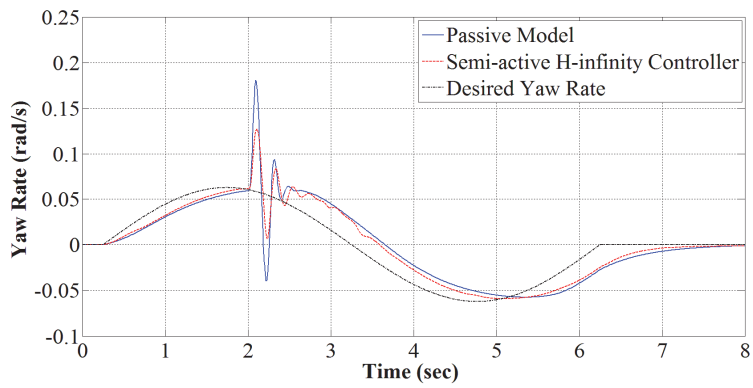
Figure 5. 8 Yaw rate of vehicle in snowy asphalt condition $\mu = 0.3$ for single lane change maneuver
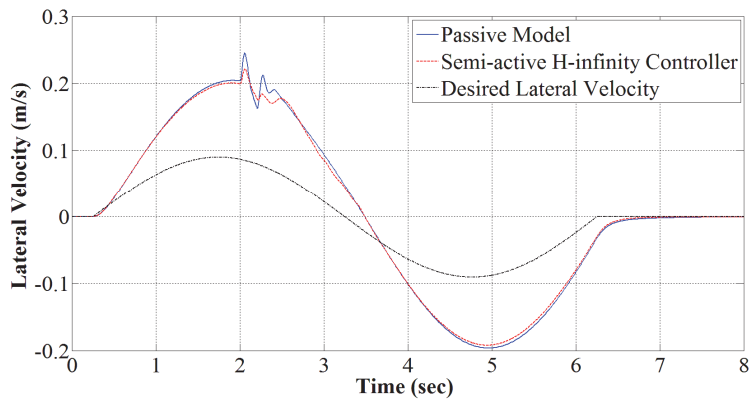
Figure 5. 9 Lateral velocity of vehicle in dry asphalt condition $\mu = 0.7$ for single lane change maneuver
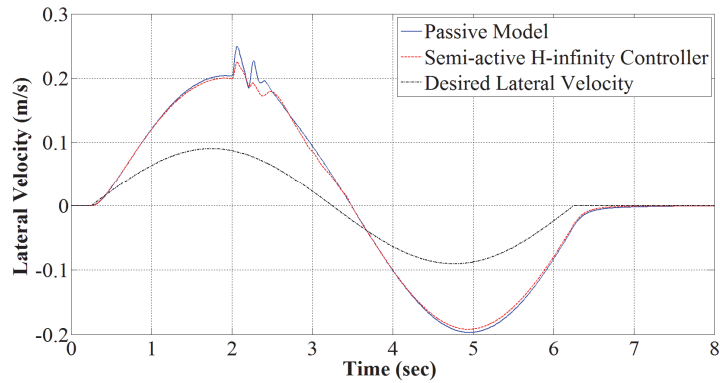
Figure 5. 10 Lateral velocity of vehicle in rainy asphalt condition $\mu = 0.5$ for single lane change maneuver
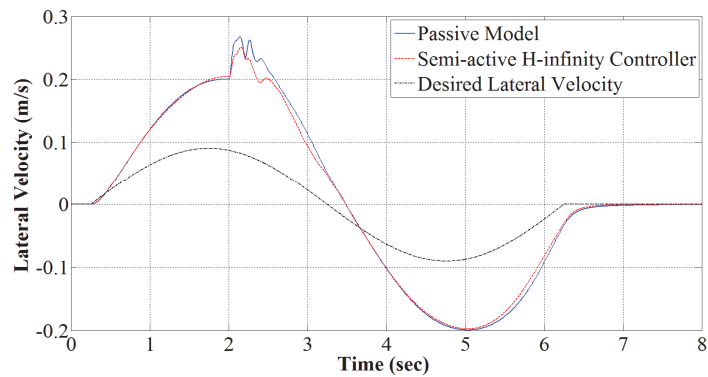
Figure 5. 11 Lateral velocity of vehicle in snowy asphalt condition $\mu = 0.3$ for single lane change maneuver

Figures 5.6 to 5.11 show that the robust controller reduces the effect of road disturbance by about 50%. Moreover, the controller follows the trend of the desired yaw rate and lateral velocity. The lateral force depends on road friction factor. Therefore, the performance of the controller under snowy condition is better than that under rainy and dry conditions. In other words, the effect of the disturbance under snowy condition is smaller than that in dry and rainy conditions. The simulation results for the lateral velocity and yaw rates show the effect of the road input in

95

handling system where the yaw and lateral motions are the most important DOF in handling dynamics. Consequently, Figures 5.6 to 5.11 confirm the interaction of the ride and handling system and the significance of using the integrated vehicle model.

5.5.2.   Braking Control Action

The braking control forces for the single lane change considering three different road conditions are shown in Figures 5.12 to 5.14. The variable braking force assigned by the controller reduces the traveling speed by about 10 %. The desired controller action is to ensure the stability of the vehicle considering small change in the traveling speed. In other words, the braking action should not fully stop the vehicle.
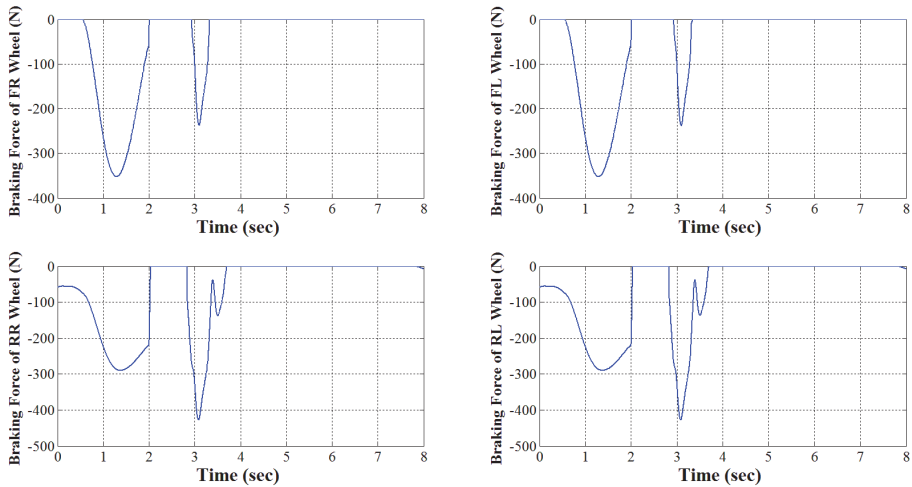
Figure 5. 12 Braking force acting on each wheel in dry asphalt condition $\mu = 0.7$ for single lane change maneuver
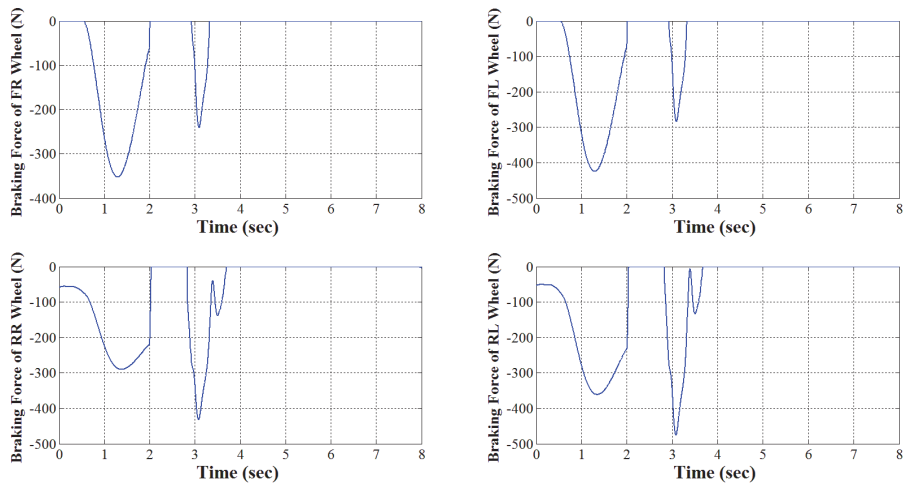
Figure 5. 13 Braking force acting on each wheel in rainy asphalt condition $\mu = 0.5$ for single lane change maneuver
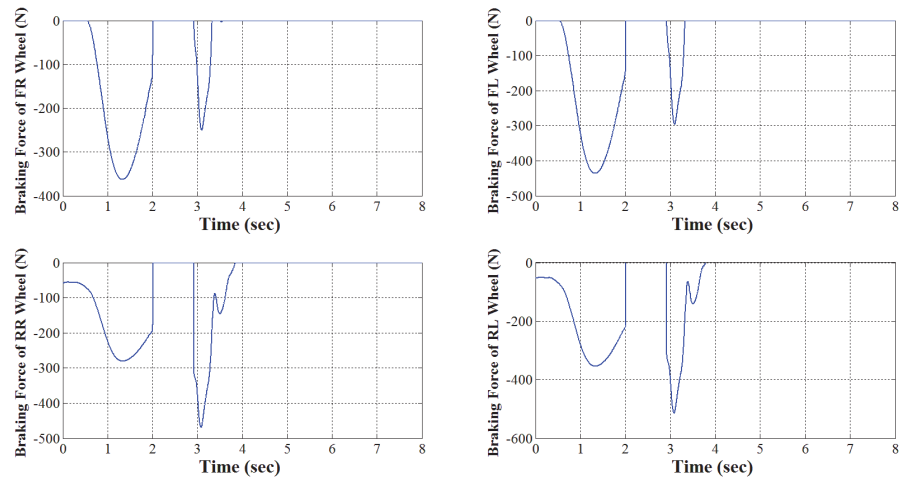
Figure 5. 14 Braking force acting on each wheel in snowy asphalt condition $\mu = 0.3$ for single lane change maneuver

Figurers 5.12 to 5.14 show that the braking forces are not applied when the road input excites the suspension system. The braking model defined in equation (4.31) represents this condition for the bounce velocity of the vehicle. The slight braking action reduces the traveling speed from 15

(m/s) to approximately 13.5 (m/s) which is required by the braking control algorithm to keep the stability of the vehicle with slight change in the traveling speed.

5.6. Vehicle Ride Quality for Combination of Ride and Steering Inputs

The performance of the designed semi-active suspension system is studied by simulating the acceleration and velocity of the vehicle body in vertical, roll and pitch motions. The comparison between the controlled and passive responses of the vehicle body motions presents the robustness of the system in absorbing road disturbances. Moreover, the MR damper control voltage for the defined vehicle maneuver is studied for dry and snowy road conditions.

5.6.1. Simulation Results of Ride System

In order to study the performance of the controller in improving the ride quality of the vehicle, the bounce velocity, roll rate and pitch rate are shown in Figurers 5.15 to 5.20 under two different road conditions: dry and snowy. The response of the suspension system to the road and steering inputs for different road conditions are approximately the same except for the roll motion which is a coupled DOF between ride and handling systems. In other words, the friction factor between road and tire is not a significant factor in the dynamics of the suspension system.
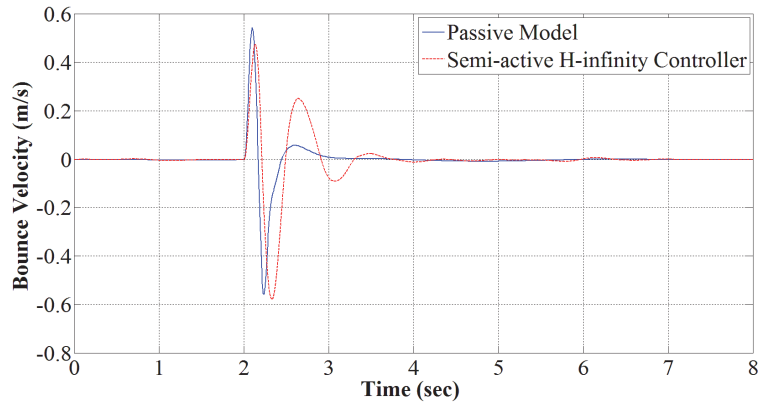
Figure 5. 15 Bounce velocity of vehicle body in dry asphalt condition $\mu = 0.7$
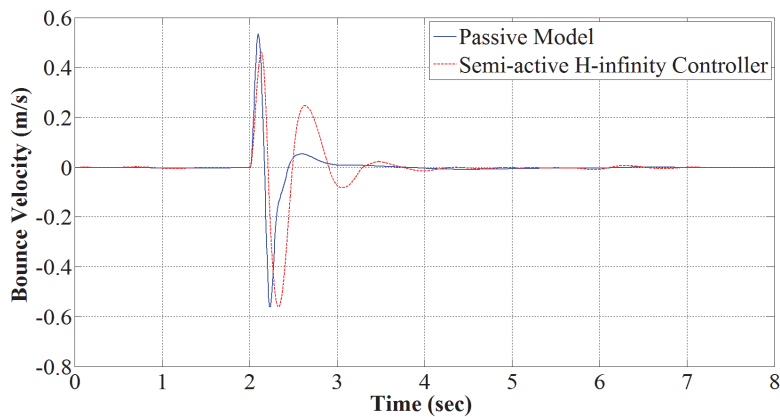
Figure 5. 16 Bounce velocity of vehicle body in snowy asphalt condition $\mu = 0.3$

The bounce velocities of the passive and semi-active system are presented in Figurers 5.15 and 5.16. The semi-active control system with MR damper has less overshoot than passive model. However, the settling time in semi-active system is not improved due to the storage energy effect in hysteresis of MR damper which is shown in Figure 4.6. The comparison between bounce velocities of the vehicle under different road conditions shows that the road and tire friction factor is not a significant parameter in the dynamics of the suspension system.
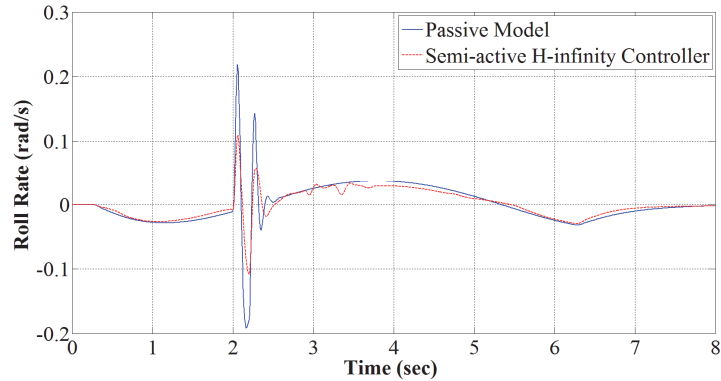
Figure 5. 17 Roll rate of vehicle body in dry asphalt condition $\mu = 0.7$
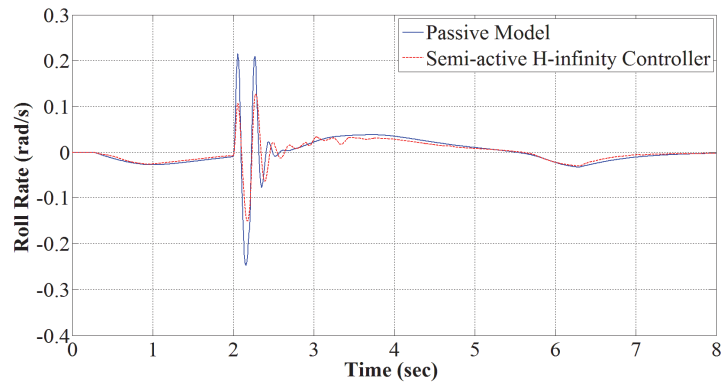
Figure 5. 18 Roll rate of vehicle body in snowy asphalt condition $\mu = 0.3$

Using semi-active suspension, the roll rate is reduced approximately by about 50 % in comparison with the passive system as shown in Figures 5.17 and 5.18. Those figures confirm the significance of H∞ control system in minimizing the roll rate as one of the most important DOFs which has significant coupling with ride and handling systems. The roll motion in the snowy condition is larger than that under the dry asphalt condition which means that the lower friction factor makes larger yaw and lateral motions. Therefore, the roll motion would be increased under snowy condition due to the coupling of the roll motion with yaw and lateral

motion as presented in the modeling section. Figures 5.17 and 5.18 show that the controller keeps the roll rate in the same range in both dry and snowy asphalt conditions which confirms the robustness of H∞ controller under varying road friction factor and bump input as source of disturbances.
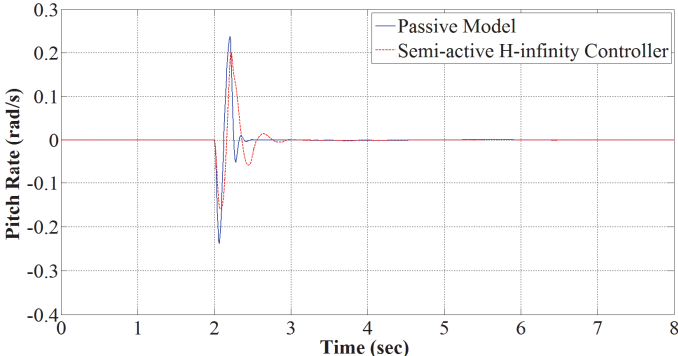
Figure 5. 19 Pitch rate of vehicle body in dry asphalt condition $\mu = 0.7$
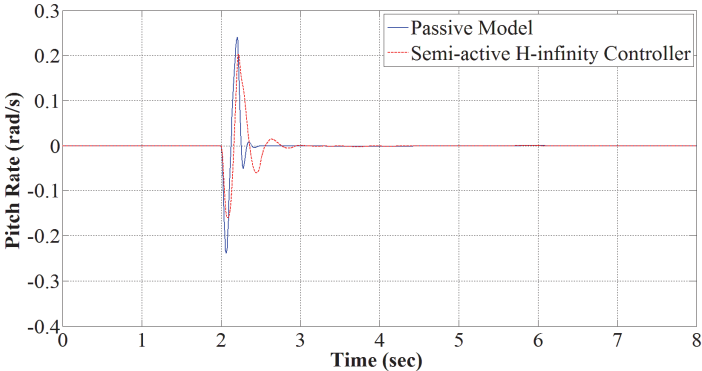
Figure 5. 20 Pitch rate of vehicle body in snowy asphalt condition $\mu = 0.3$

The pitch rate of the vehicle body is presented in Figures 5.19 and 5.20 for two different road conditions. Based on the simulated results, the semi-active control approach reduces the pitch

rate approximately by about 30%. In addition, Figures 5.19 and 5.20 show that the friction factor due to the dry and snowy asphalt is not significant in pitch motion.

In order to study the performance of the controller in absorbing the transmitted acceleration to the vehicle body, the acceleration responses of control model and passive system to the defined vehicle manoeuvre are presented in Figures 5.21 to 5.26. The body roll and pitch accelerations considering dry and snowy weather conditions are simulated to study the effect of variation road condition (tire cornering stiffness) in dynamic behaviour of ride system.
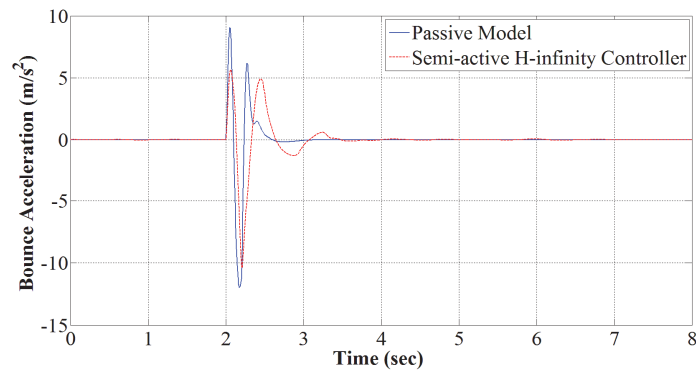
Figure 5. 21 Vertical acceleration of vehicle body in dry asphalt condition $\mu = 0.7$
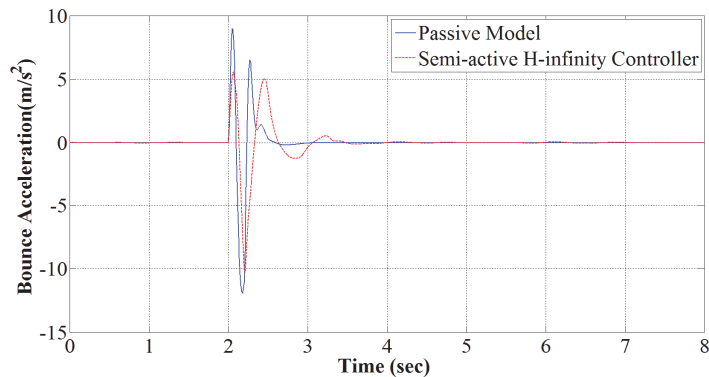
Figure 5. 22 Vertical acceleration of vehicle body in dry snowy condition $\mu = 0.3$

Figures 5.21 and 5.22 show that the bounce acceleration of the vehicle body is reduced significantly by implementing the robust control approach using MR damper. The percentage reduction in acceleration magnitudes is approximately 40 % in peak value. These figures present the friction factor between road and tires which does not make a significant change in the dynamic response of the vehicle bounce accelerations. It should be noted that due to the storage energy in MR damper the settling time is not improved as explained for the velocity response.
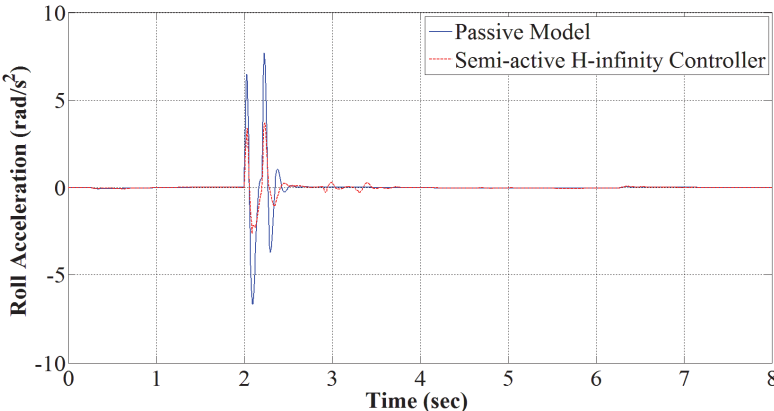
Figure 5. 23 Roll acceleration of vehicle body in dry asphalt condition $\mu = 0.7$
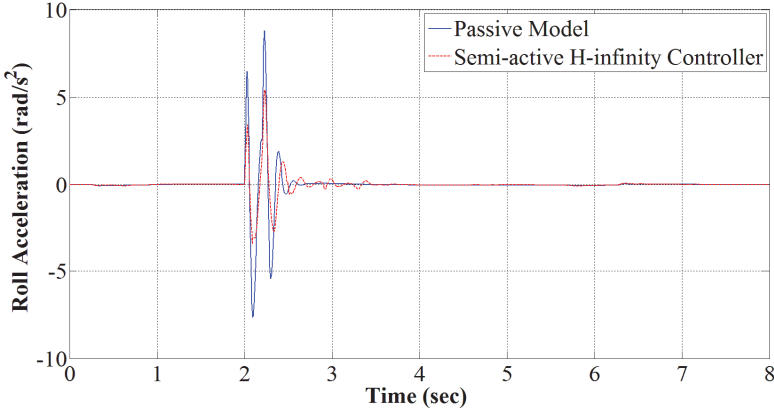
Figure 5. 24 Roll acceleration of vehicle body in dry snowy condition $\mu = 0.3$

The performance of the robust controller in absorbing angular acceleration of roll motion is presented in Figures 5.23 and 5.24 for dry and snowy road conditions. Using the robust controller, the acceleration of roll motion in both dry and snowy weather conditions are decreased more than 50 % in comparing with the passive system. The roll motion is one of the model DOF which is affected by both ride and handling inputs. Figures 5.23 and 5.24 show that the acceleration of the roll motion is increased by about 10 % when the vehicle path is defined in snowy weather condition.
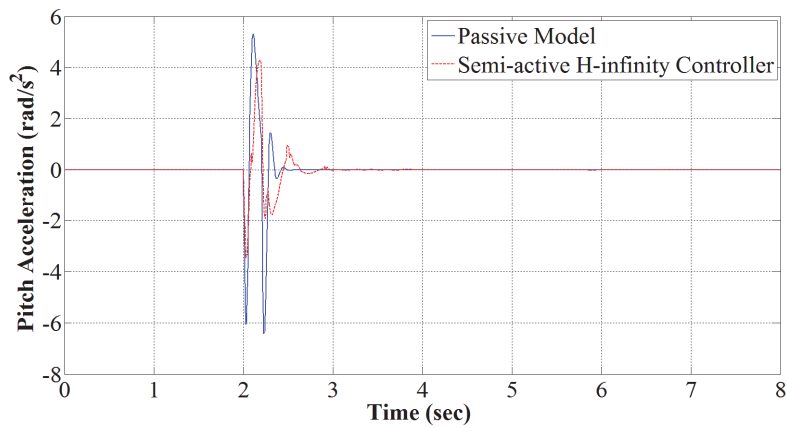
Figure 5. 25 Pitch acceleration of vehicle body in dry asphalt condition $\mu = 0.7$
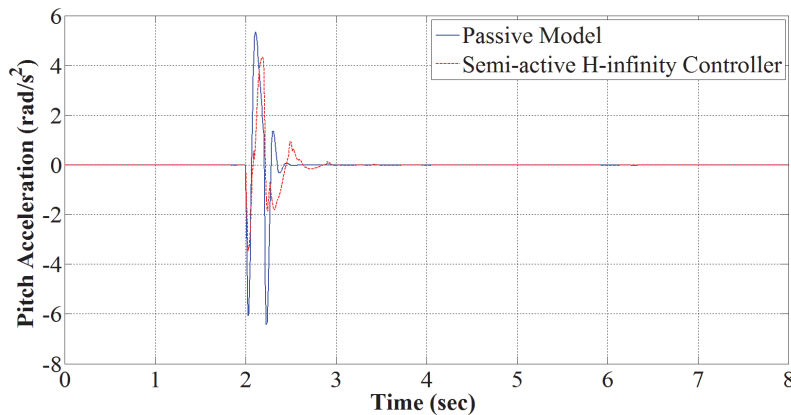
Figure 5. 26 Pitch acceleration of vehicle body in dry snowy condition $\mu = 0.3$

The angular acceleration of the pitch motion in both dry and snowy road conditions is the same. Figures 5.25 and 5.26 show that the designed control approach reduces the angular acceleration of pitch motion by about 40 %. The large magnitude of vehicle body acceleration is due to large applied bump input in Figure 5.2 and high traveling speed 54 (Km/h) which makes high frequency input and lager magnitude for the acceleration of the vehicle body. The reason for choosing this bump input is to make severe manoeuvre (in nonlinear region) to evaluate the ride and handling performance.

5.6.2.   MR Damper Control Inputs

The MR damper is a semi-active control device which has the input as voltage. Whereas, the input of the robust controller is an active force which should be converted to the voltage as semi active control input. The MR damper inverse model acts as MR damper control voltage, and makes a bridge between robust controller and control plant.
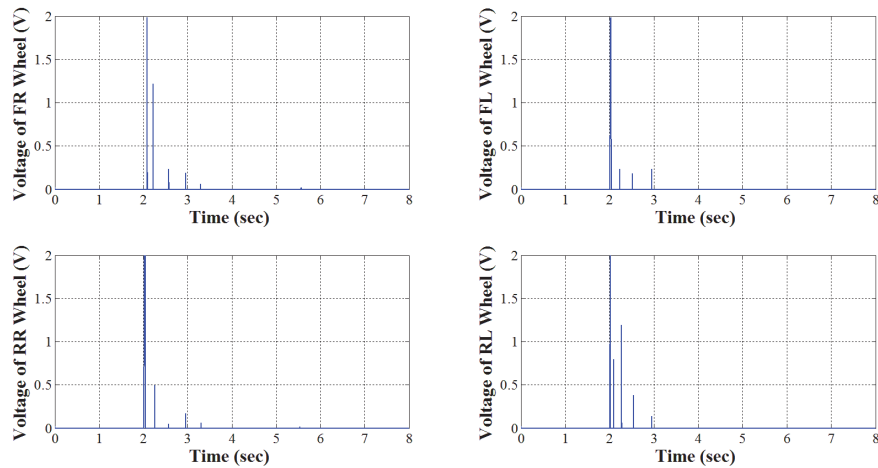
Figure 5. 27 Voltage of MR dampers in dry asphalt condition $\mu = 0.7$
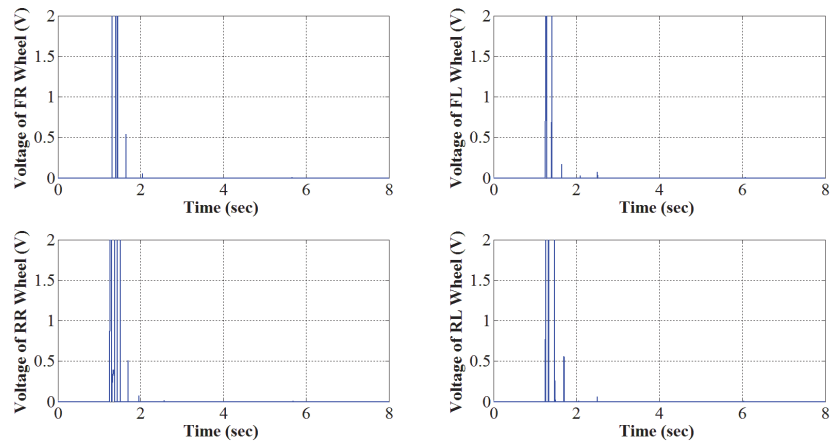
Figure 5. 28 Voltage of MR dampers in snowy asphalt condition $\mu = 0.3$

Figures 5.27 and 5.28 show that the assigned input voltages of the MR dampers by the MR damper controller and H∞ control algorithm. The MR damper voltage is limited between 0 and 2 volts based on the numerical value used for the MR damper model. The results show that the maximum voltage is applied when the car passes the bump. The MR damper does not respond to the steering input.

5.7. Quantitative Study of Designed Control Strategies

In order to summarize and compare the performance and robustness of the designed control algorithm, the results of the passive and semi-active systems are presented quantitatively. The maximum difference between the first peak overshoot of the passive and semi-active systems for presented DOFs are shown in Table 5.1.

106

Table 5. 1 Quantitative comparison between semi-active and passive systems

DOF	Overshoot difference μ= 0.3	Overshoot difference μ= 0.5	Overshoot difference μ= 0.7
Yaw rate	29.57 %	29.51 %	29.45 %
Lateral velocity	10.09 %	10.01 %	9.82 %
Bounce rate	13.33 %	-	13.23 %
Roll rate	50.43 %	-	50.05 %
Pitch rate	33.18 %	-	33.19 %
Bounce acceleration	37.95 %	-	37.65 %
Roll acceleration	47.75 %	-	47.6 %
Pitch acceleration	45.12 %	-	44.98 %

The results presented in Table 5.1 confirm the performance of the designed nonlinear robust controller in improving ride and handling quality. Based on the presented results, the robust controller has better performance in snowy road than that in the road under rainy and dry conditions. The reason is that the snowy road condition has low friction coefficient which make smaller lateral and longitudinal tire forces as disturbance input for the system than rainy and dry road conditions. Moreover, the controller has the most significant effect in reducing roll motion which can be used for roll-over prevention as well as improving ride quality.

5.8. Summary

The vehicle model and nonlinear robust controller are simulated in Matlab/simulink using numerical values corresponding to a passenger car. The results show that the differential braking

system is affected by ride input and can minimize the effect of road disturbance to ensure the stability of the vehicle. However, the effect of steering input for single lane change is not significant in ride system. The simulation results also confirm that the road condition is one of the main factors in affecting the stability of the vehicle. The simulation results under the defined maneuver in three different road conditions: dry, rainy and snowy considering bump input demonstrate the robustness of nonlinear controller and the improved ride quality and stability of the vehicle.

CHAPTER 6   Conclusions and

Recommendations for Future Studies

6.1. Dissertation Summary

In this thesis, the dynamic behavior of a passenger car including the interaction and coupling of ride and handling systems is modelled to improve the ride and handling qualities in severe vehicle turning including road disturbances (bump/pothole). In the first Chapter, the concepts of dynamic modeling of vehicle suspensions and vehicle handling models are reviewed. The integrated ride and handling models which are derived based on the Newtonian and Bond graphs techniques are discussed. Moreover, the simplification assumptions of the models and limitations presented in the literature are studied. The advantages and disadvantages of the passive, semi-active and active suspension systems presented in literature are reviewed and compared. For improving the handling quality, direct yaw moment control approaches for the vehicle handling systems are discussed. The vehicle dynamic model, control strategies and linearization approaches in literature are reviewed in the first Chapter.

In Chapter two, an integrated ride and handling model based on Boltzmann Hamel equations is proposed to simulate the dynamic behaviour of vehicle considering the coupling of ride and handling systems. The integrated model simulates the dynamic response of the vehicle using fourteen DOFs, where six DOFs are for the vehicle body and two DOFs are for each wheel. The Euler motions, traction and braking and load transfer among the wheels are simulated using the

proposed vehicle model. The integrated vehicle model has been validated by ADAMS/Car model for a standard ISO double lane change maneuver. The comparison between ADAMS/Car simulation and integrated model confirms the accuracy of the proposed vehicle model. The difference between the decoupled ride and handling models and the proposed integrated model has been identified as an indication factor to present the effect of coupling in model for a particular maneuver. The coupling factor is proposed to demonstrate the necessity of using integrated model over decoupled model for a defined maneuver.

In Chapter three, a robust H∞ control approach is designed based on the nonlinear integrated vehicle model using HJI function technique. The desired controller output is to improve ride and handling quality in severe maneuver against the road disturbances. The longitudinal and lateral tire forces, and the displacement and velocities due to the bump or pothole inputs are defined as the sources of disturbance. The designed controller provides the robustness against the variations of the defined disturbances. The control plant is partially linearized using the Jacobian approach. The designed control signal is obtained using the control feedback gains and the measured states which can be implemented in the control hardware.

The differential braking system and MR damper are the control devices to implement the ride and handling control system of a passenger car. The dynamics of differential braking system and MR damper are presented in Chapter four. The parameters of Spencer mathematical model have been identified using hybrid optimization approach which is a combination of SQP and GA based on the experimental data. Moreover, using Spencer modelling approach, a mathematical model is proposed to make MR damper model frequency dependent. The comparison between

110

proposed MR damper model and the experimental data confirms the validity and accuracy of the frequency dependent model in high frequency applications.

The inverse model of MR damper is defined based on the proportional control gain which computes the voltage using control force assigned by the robust controller. The control objectives for ride and handling systems are to minimize the vehicle body bounce, roll and pitch velocities, and to follow the desired lateral velocity and yaw rate. The control references signals are defined to keep vehicle in neutral steering condition.

The proposed integrated ride and handling vehicle model and robust controller are simulated using MATLAB/Simulink. The nonlinear governing equations of the vehicle model and logic of the controller are defined in Simulink using MATLAB Embedded function. The dynamic behaviour of the vehicle is simulated based on the parameters of an intermediate passenger car for a single lane change maneuver considering the bump input on the road. Three different road conditions (dry, rainy and snowy) are simulated to study the robustness of the designed control approach. The simulation results confirm that the designed control approach using differential braking system improves the handling quality of the vehicle in all three road conditions. Also, the velocity and acceleration responses of the vehicle body in bounce roll and pitch motion demonstrate the performance of robust control approach and semi-active suspension system in absorbing approximately 40 % of acceleration magnitude in comparison with the passive system. The designed control system improves the safety and comfort of passenger cars in highways and avoids car accidents due to the unwanted steering caused by road disturbances.

6.2. Conclusions

The simulation studies carried out in this PhD work led to observations and conclusions regarding limitations and performance of the proposed dynamic model and the designed robust controller. The major conclusions and results of this study are summarized as follows:

I.   Considering Euler motions in deriving governing equations of vehicle makes nonlinear terms in the dynamics of system. The nonlinear terms have significant effect, when large amplitude and high frequency road input and severe steering input applied to the model.

II.   The proposed coupling factor indicates the necessity of using the integrated ride and handling model over the decoupled models in different vehicle operational conditions.

III. The designed robust controller based on coupled model guarantees the stability of the system against road disturbances. One of the main advantages of using coupled model in control design is to avoid conflict in ride and handling control devices.

IV.   The proposed frequency dependent MR damper model improves the accuracy of the MR damper force simulation. The experimental study shows that the proposed model has significant effect in high frequency application of MR damper such as semi-active suspension for off road vehicles.

V.   The operational range of the differential braking system depends on friction factor between road and tire, and traveling speed of vehicle. The simulation results show that the performance of robust controller can not be changed in different weather conditions.

6.3. Contributions

This thesis presents the studies on the multi-body dynamics, semi-active suspension system, vehicle handling model and robust control. The summary of the thesis contributions are classified as follows:

I.   A new 14-DOF integrated ride and handling model is proposed based on the Boltzmann Hamel equations. In this model, load transfer among wheels, acceleration, braking and Euler motion are considered. The model has been validated using ADAMS/Car software.

II. A new numerical factor is proposed which is called coupling factor to indicate the effect of considering coupling between the ride and handling in the dynamic simulation of a vehicle for specific maneuver.

III. A nonlinear H∞ controller is designed based on the nonlinear integrated ride and handling vehicle model using HJI function.

IV. The dynamics of differential braking and MR damper are modeled. The controller logic for these control devices is defined.

V.   Based on Spencer MR damper mathematical model and experimental data, a frequency dependent model is proposed. The accuracy and adaptability of the proposed model for low and high frequency regions are studied.

The presented original contributions are published in/ submitted to journals and conferences as follows:

Journal Papers:

1   Ali Fellah Jahromi, Rama B. Bhat and Wen-Fang Xie, "An Integrated Ride and Handling Vehicle Model Using Lagrangian Quasi-coordinate Method," *International Journal of Automotive Technology* (*Springer*), vol. 16, no. 2, April 2015, pp. 239−251.

2   Ali Fellah Jahromi, Rama B. Bhat and Wen-Fang Xie, "Frequency Dependent Spencer Modeling of Magnetorheological Damper Using Hybrid Optimization Approach," *Journal of Shock and Vibration*, Accepted on March 2015.

3   Ali Fellah Jahromi, Wen-Fang Xie and Rama B. Bhat, "Robust Control of Nonlinear Integrated Ride and Handling Model Using Magnetorheological Damper and Differential Braking System," *Journal of Mechanical Science and Technology* (*Springer*), Submitted on September 2014.

Conference Papers:

1   Ali Fellah Jahromi, Rama B. Bhat and Wen-Fang Xie, "Robust Control of Passenger Cars with Semi-active Suspension System Using Magnetorheological Shock Absorber," *In Proc. The Canadian Society for Mechanical Engineering International Congress 2014*, June 1 − 4, 2014, Toronto, Ontario, Canada.

2   Ali Fellah Jahromi, Wen-Fang Xie and Rama B. Bhat, "Nonlinear H-Infinity Control Strategy for Differential Braking System of a Passenger Car," *in Proc. 15th IASTED International Conference on Control and Applications* (*CA 2013*), August 26 − 28, 2013, Honolulu, USA.

3   Ali Fellah Jahromi, Wen Fang Xie and Rama B. Bhat, "Ride Control of Passenger Cars with Semi-active Suspension System Using a Linear Quadratic Regulator and Hybrid Optimization Algorithm," *in Proc. ICAMAME 2012: International Conference on Aerospace, Mechanical, Automotive and Materials Engineering*, July 25 – 26, 2012, Amsterdam, The Netherlands.

The following journal and conference papers are published based on the course projects and cooperation with Prof. Rama B. Bhat, Prof. Wen Fang Xie and their research teams.

Journal Papers:

1   Ali Fellah Jahromi, Ahmed Atia, Rama B. Bhat and Wen-Fang Xie, "Optimizing the Pole Properties in Pole Vaulting by Using Genetic Algorithm Based on Frequency Analysis," *International Journal of Sports Science and Engineering*, vol. 6, no. 1, March 2012, pp. 41 – 55.

2   Mohammad Keshmiri, Ali Fellah Jahromi, Abolfazl Mohebbi and Mohammad Hadi Amoozgar and Wen-Fang Xie, "Modeling and Control of Ball and Beam System Using Model Based and Non-model Based Control Approaches," *International Journal on Smart Sensing and Intelligent Systems*, vol. 5, no. 1, pp. 14 – 35, March 2012.

Conference Papers:

1   Ali Fellah Jahromi, Rama B. Bhat and Wen-Fang Xie, "Forward and Backward Whirling of a Rotor with Gyroscopic Effect," *In Proc. Springer 10th International Conference on*

Vibration Engineering and Technology of Machinery, September 9 – 11, 2014, Manchester, UK.

2 Ajinkya A. Gharapurkar, Ali Fellah Jahromi, Rama B. Bhat and Wen Fang Xie, "Semi-Active Control of Aircraft Landing Gear System Using H-infinity Control Approach," *in Proc. IEEE/ International Conference on Connected Vehicles and Expo*, December 2 – 6, 2013, Las Vegas, USA.

6.4. Recommendations for Future Works

The further studies which can be done based on this thesis in control, modeling and design criteria are listed in the following subsections.

6.4.1.   Gain-scheduling Robust Control Approach

The gain-scheduling H∞ control approach can be utilized as a control technique to linearize the DOFs of handling system. As discussed in Chapter 3, the equilibrium point cannot be defined for yaw, lateral and longitudinal motions. Therefore, using Linear Parameter Varying (LPV) approach these DOFs can be linearized in defined region. The gain-scheduling controller is calculated by interpolation of local control [105], [106], [107]. However, this approach requires advanced mathematical calculations which should be implemented using advanced hardware in industrial application.

6.4.2. Control Devices

In this study, the required braking force is determined as the control input for the system. However, in industrial applications the dynamics of the hydraulic braking system and action of braking pump should also be considered in the dynamic modeling of the braking system. Moreover, the dynamics of frequency dependent MR damper model can be considered in robust control design.

6.4.3. Application in Off-road Vehicles

The proposed integrated vehicle model can be used in modeling the off-road vehicles. The vehicle model simulates the dynamic behaviour of ride and handling systems. The roll motion is a common DOF on ride and handling systems and the proposed model is capable to simulate the dynamic behaviour of this DOF due to road or steering inputs. The roll-over prevention control strategy can be designed for off-road vehicles using active anti-roll bar based on the proposed integrated model.

Bibliography

[1]   W. F. Powers and P. R. Nicastri, "Automotive vehicle control challenges in the 21st century," *Control Engineering Practice 8*, 2000, pp. 605–618.

[2]   R. Rajamani, *Vehicle Dynamics and Control*, New York: Springer, 2006.

[3]   NHTSA, "State traffic safety information," National Highway Traffic Safety Administration: USA, Rep. 1999.

[4]   C. W. Wambold, *et al.* "Influence of Roadway Surface Discontinuities on Safety/Roughness, Holes, and Bumps," Transportation Research Board of the National Academies: USA, Rep. E-C134, 2009.

[5]   B. Mashadi and D.A. Crolla, "Influence of Ride Motions on the Handling Behaviour of a Passenger Vehicle," *Part D: Journal of Automobile Engineering*, vol. 219, 2005, pp. 1047–1058.

[6]   J. Wu, Q. Wang; X. Wei, and H. Tang, "Studies on Improving Vehicle Handling and Lane Keeping Performance of Closed-loop Driver-vehicle System with Integrated Chassis Control," *Mathematics and Computers in Simulation*, vol. 80, 2010, pp. 2297–2308.

[7]   B. Németh; and P. Gáspár "Vehicle Modeling for Integrated Control Design," *Periodica Polytechnica*, vol. 38, 2010, pp. 45–51.

[8]   F. Lai; and Z. Deng, "Control Strategy Study on Active Suspension and Four Wheel Steering Integrated Control System of Vehicle," *Intelligent Vehicles Symposium*, China:IEEE, pp. 695–700, June 2009.

[9]   D. Kamopp, "Active Damping in Road Vehicle Suspension Systems," *Vehicle System Dynamics*, vol. 12, 1983, pp. 291–311.

[10] M. M. Elmadany and Z. Abduljabbar, "On the Ride and Attitude Control of Road Vehicle," *Computer and Structure*, vol. 42, 1992, pp. 245–253.

[11] Y. Sun and G. A. Parker, "A Position Controlled Disc Valve in Vehicle Semi-active Suspension Systems," *Control Engineering Practice*, vol. 1, 1993, pp. 927–935.

[12] H. Du, K.Y. Sze and J. Lam, "Semi-active H∞ Control of Vehicle Suspension with Magneto-rheological Dampers," *Journal of Sound and Vibration*, vol. 283, 2005, pp. 981–996.

[13] G. Priyandoko, M. Mailah and H. Jamaluddin, "Vehicle Active Suspension System Using Skyhook Adaptive Nero Active Force Control," *Mechanical Systems and Signal Processing*, vol. 23, 2009, pp. 855–868.

[14] M. M. Elmadany and Z. Abduljabbar, "Linear Quadratic Gaussian Control of a Quarter-car Suspension," *Vehicle System Dynamics*, vol. 32, 1999, pp. 479–497.

[15] L. V. V. G. Rao and S. Narayanan, "Sky-hook Control of Nonlinear Quarter Car Model Traversing Rough Road Matching Performance of LQR Control," *Journal of Sound and Vibration*, vol. 323, 2009, pp. 515–529.

[16] R. Krtolica and D. Hrovat, "Optimal Active Suspension Control Based on a Half-Car Model: An Analytical Solution," *IEEE Transaction on Automatic Control*, vol. 31, 1992, pp. 528–532.

[17]   Y.M. Sam and J. H. S. B. Osman, "Modeling and Control of the Active Suspension System Using Proportional Integral Sliding Mode Approach," *Asian Journal of Control*, vol. 7, pp. 91–98, 2005.

[18]   M. Yu, *et. al.* "Human Simulated Intelligent Control of Vehicle Suspension System with MR Dampers," *Journal of Sound and Vibration*, vol. 319, 2009, pp. 753–767.

[19]   R. S. Prabakar, C. Sujatha and S. Narayanan, "Optimal Semi-active Preview Control Response of a Half Car Vehicle Model with Magnetorheological Damper," *Journal of Sound and Vibration*, vol. 326, 2009, pp. 400–420.

[20]   C. P. Cheng, C. H. Chao and T. H. S Li, "Design of Observer-based Fuzzy Sliding-mode Control for an Active Suspension System with Full-car Model,", *2010 IEEE International Conference on Systems Man and Cybernetics* (*SMC*), Turkey: IEEE, pp. 1939–1944, 10–13 Oct. 2010.

[21]   A. F. Jahromi; and A. Zabihollah, "Linear Quadratic Regulator and Fuzzy Controller Application in Full-car Model of Suspension System with Magnetorheological Shock Absorber," *Mechatronics and Embedded Systems and Applications* (*MESA*), *2010 IEEE/ASME International Conference*, Turkey: IEEE/ASME, pp. 522–528, 15–17 July 2010.

[22]   A. F. Jahromi, W. F. Xie and R. B. Bhat, "Ride Control of Passenger Cars with Semi-active Suspension System Using a Linear Quadratic Regulator and Hybrid Optimization Algorithm," *ICAMAME 2012: International Conference on Aerospace, Mechanical,*

Automotive and Materials Engineering, The Netherland: WAST, pp. 1083–1089, July 25–26, 2012.

[23]   R. Guclu, "Active Control of Seat Vibrations of a Vehicle Model Using Various Suspension Alternatives," *Turkish Journal of Engineering and Environmental Sciences*, vol. 27, 2003, pp. 361–373.

[24]   E. Esmailzadeh, A. Goodarzi and G.R. Vossoughi, "Optimal Yaw Moment Control Law for Improved Vehicle Handling," *Mechatronics*, vol. 13, 2003, pp. 659–675.

[25]   H. Du, N. Zhang and F. Naghdy, "Velocity-dependent Robust Control for Improving Vehicle Lateral Dynamics," *Transportation Research Part C*, vol. 19, 2011, pp. 454–468.

[26]   H. J. Kim and Y. P. Park, "Investigation of Robust Roll Motion Control Considering Varying Speed and Actuator Dynamics," *Mechatronics*, 2004, vol. 14, pp. 35–54.

[27]   G. Tsampardoukas, C. W. Stammers and E. Guglielmino, "Semi-active Control of a Passenger Vehicle for Improved Ride and Handling," *Part D: Journal of Automobile Engineering*, vol. 222, 2008, pp. 325–352.

[28]   Y. Fan, D. F. Li and D. A. Crolla, "Integrated Vehicle Dynamics Control—state-of-the art review," *In Vehicle Power and Propulsion Conference IEEE,VPPC'08*, pp. 1–6, 2008.

[29]   J. Wang and S. Shen, "Integrated Vehicle Ride and Roll Control via Active Suspensions," *Vehicle System Dynamics*, vol. 46, 2008, pp. 495–508.

[30] J. D. Setiawan, M.Safarudin and A. Singh, "Modeling, Simulation and Validation of 14 DOF Full Vehicle Model," *Instrumentation, Communications, Information Technology, and Biomedical Engineering* (*ICICI-BME*), pp. 1-6, 23–25 Nov. 2009.

[31] T. K. Bera, K. Bhattacharya and A. K. Samantaray, "Evaluation of Antilock Braking System with an Integrated Model of Full Vehicle System Dynamics," *Simulation Modelling Practice and Theory*, vol. 19, 2011, pp. 2131–2159.

[32] M. S. Fallah, R. B. Bhat and W. F. Xie, "Optimized Control of Semi-active Suspension Systems Using H∞ Robust Control Theory and Current Signal Estimation," *IEEE/ASME Transactions on Mechatronics*, vol. 16, 2011, pp. 1–12.

[33] S. S. Sedeh, R. S. Sedeh and K. Navi, "Using Car Semi-active Suspension System to Decrease Undesirable Effects of Road Excitation on Human Health," *Proceeding of BIOCOMP*, pp. 242–250, 2006.

[34] B.F. Spencer Jr., *et al.*, "Phenomenological Model of a Magnetorheological Damper," ASCE Journal of Engineering Mechanics, vol. 123, no. 3, 1997, pp. 230-238.

[35] D.A. Brooks, "Design and Development of Flow Based Electro-rheological Devices," *International Journal of Modern Physics*, vol. B 6, no. 15–16, 1992, pp. 2705–2730.

[36] F. Mohammadi and R. Sedaghati, "Dynamic Mechanical Properties of an Electrorheological Fluid under Large-amplitude Oscillatory Shear Strain," *Journal of Intelligent Material Systems and Structures*, vol. 23, no. 10, 2012, pp. 1093-1105.

[37] S.M. Savaresi, S. Bittanti and M. Montiglio, "Identification of Semi-physical and Black-Box non-linear Models: the Case of MR-dampers for Vehicles Control," *Automatica*, vol. 41, no. 1, 2005, pp. 113-127.

[38] I. H. Shames, and F. A. Cozzarelli, *Elastic and Inelastic Stress Analysis*, New Jersey: Prentice-Hall, Englewood Cliffs, 1992.

[39] D. R. Gamota, and F. E. Filisko, "Dynamic Mechanical Studies of Electrorheological Materials: Moderate Frequencies," *Journal of Rheology*, vol. 35, 1991, pp. 399–425.

[40] Y. K. Wen, "Method of Random Vibration of Hysteretic Systems," *ASCE Journal of Engineering Mechanics Division*, vol. 102, No. EM2, 1976, pp. 249–263.

[41] F. Donado, "Viscosity Enhancement in Dilute Magnetorheological Fluids through Magnetic Perturbation," *Revista Mexicana de Fisica*, vol. 57, 2011, pp. 426–434.

[42] N.M. Kwok, et al., "Bouc–Wen model parameter identification for a MR fluid damper using computationally efficient GA," *ISA transactions*, vol. 46, no. 2, 2007, pp. 167-179.

[43] P. Yih; and J. C. Gerdes "Steer-by-wire for Vehicle State Estimation and Control," *Proceedings of AVEC*, pp. 785–790, 2004.

[44] P. Setlur, *et al.* "Nonlinear Tracking Controller Design for Steer-by-Wire Automotive Systems," *Proceeding of the American Control Conference*, pp. 280–285, 8–10 May, 2002.

[45]   M. Doumiati, *et al.*, "Vehicle Yaw Control Via Coordinated Use of Steering/Braking Systems," *Proceeding of the 18th IFAC World Congress*, pp. 644–649, 28 August – 2 September, 2011.

[46]   S. Amberkar, *et al.*, "A Control System Methodology for Steer by Wire Systems," *SAE Technical Paper*, no. 2004-01-1106, 2004.

[47]   P. Dominke and G. Ruck, "Electric Power Steering-the First Step on the Way to Steer by Wire," *SAE Technical Paper*, no. 1999-01-0401, 1999.

[48]   R.P. Osborn; and T. Shim, "Independent Control of All-Wheel-Drive Torque Distribution," *Vehicle System Dynamics*, vol. 44, 2006, pp. 529–546.

[49]   F. Tahami, S. Farhangi, and R. Kazemi, "A Fuzzy Logic Direct Yaw-Moment Control System for All-wheel-drive Electric Vehicles," *Vehicle System Dynamics*, vol. 41, 2004, pp. 203–221.

[50]   R. Latif, *et al.*, "Vehicle Modeling and Performance Evaluation Using Active Torque Distribution," *SAE Technical Paper*, no. 2014-01-0103, 2014.

[51]   S. Zhang, T. Zhang and S. Zhou, "Vehicle Stability Control Strategy Based on Active Torque Distribution and Differential Braking," *International Conference on Measuring Technology and Mechatronics Automation, ICMTMA '09*, pp. 922–925, April 11–12, 2009.

[52] K. Yi1; T. Chung; J. Kim; and S. Yi1, "An Investigation into Differential Braking Strategies for Vehicle Stability Control," *Part D: Journal of Automobile Engineering*, vol. 217, 2003, pp. 1081–0193.

[53] H. Nakazato, K. Iwata and Y. Yoshioka, "A New System for Independently Controlling Braking Force Between Inner and Outer Rear Wheels," *SAE Technical Paper*, no. 890835, 1989.

[54] B.C. Chen and H. Peng, "Differential-Braking-Based Rollover Prevention for Sport Utility Vehicles with Human-in-the-loop Evaluations," *Vehicle System Dynamics*, vol. 36, 2001, pp. 359–389.

[55] A. F. Jahromi, W. F. Xie and R. B. Bhat, "Nonlinear H-Infinity Control Strategy for Differential Braking System of a Passenger Car," *in Proc. 15th IASTED International Conference on Control and Applications* (*CA 2013*), pp. 98–103, August 26–28, 2013.

[56] Y. Zeyada, *et al.*, "A Combined Active-Steering Differential-Braking Yaw Rate Control Strategy for Emergency Maneuvers," *SAE Technical Paper*, no. 980230, 1998.

[57] K. Gulez and R. Guclu, "CBA-neural Network Control of a Nonlinear Full Vehicle Model," *Simulation Modeling Practice and Theory*, vol. 16, 2008, pp. 1163–1176.

[58] İ. Eski and Ş. Yıldırım, "Vibration Control of Vehicle Active Suspension System Using a New Robust Neural Network Control System," *Simulation Modelling Practice and Theory*, vol. 17, no. 5, 2009, pp. 778–793.

[59] R.Guclu and K. Gulez, "Neural network control of seat vibrations of a non-linear full vehicle model using PMSM," *Mathematical and Computer Modelling*, vol. 47, 2008, pp. 1356–1371.

[60] D. Hanafi, "PID Controller Design for Semi-active Car Suspension Based on Model from Intelligent System Identification," *2010 Second International Conference on Computer Engineering and Applications* (*ICCEA*), vol. 2, pp. 60–63, March 19–21, 2010.

[61] K. Hudha, *et al.*, "Semi Active Roll Control Suspension (SARCS) System on a New Modified Half Car Model," *SAE Technical Paper*, no. 2003-01-2274, 2003.

[62] M. H. A. Talib and I.Z. M. Darns, "Self-tuning PID Controller for Active Suspension System with Hydraulic Actuator," *2013 IEEE Symposium on Computers and Informatics* (*ISCI*), pp. 86–91, April 7–9, 2013.

[63] A. Tandel, *et al.*, "Modeling, Analysis and PID Controller Implementation on Double Wishbone Suspension Using SimMechanics and Simulink," *Procedia Engineering*, vol. 97, 2014, pp. 1274–1281.

[64] S. M. Fayyad, "Constructing Control System for Active Suspension System," *Contemporary Engineering Sciences*, vol. 5, no. 4, 2012, pp. 189–200.

[65] H. Bolandhemmata, C.M. Clark, and F. Golnaraghi, "Development of a Systematic and Practical Methodology for the Design of Vehicles Semi-active Suspension Control System," *Vehicle System Dynamics*, vol. 48, 2010, pp. 567–585.

[66] Y. Chen, *et al.*, "Hybrid Fuzzy Skyhook Surface Control Using Multi-Objective Microgenetic Algorithm for Semi-Active Vehicle Suspension System Ride Comfort Stability Analysis," *Journal of Dynamic Systems, Measurement, and Control*, vol. 134, no. 4, 2012, pp. 041003–14.

[67] Y. Chen, "Skyhook Surface Sliding Mode Control on Semi-Active Vehicle Suspension System for Ride Comfort Enhancement," *Engineering*, vol. 1, no. 1, pp. 23–32.

[68] M. Ahmadian "On the Development of Fuzzy Skyhook Control for Semiactive Magneto-rheological Systems," *Proceedings of SPIE, Smart Structure and Material: Damping and Isolation*, vol. 5760, 2005, pp. 268–282.

[69] J. Swevers, *et al.*, "A Model-free Control Structure for the On-line Tuning of the Semi-active Suspension of a Passenger Car," *Mechanical Systems and Signal Processing*, vol. 21, 2007, pp. 1422–1436.

[70] Ubaidillah, K. Hudha, H, Jamaluddin, "Simulation and Experimental Evaluation on a Skyhook Policy-based Fuzzy Logic Control for Semi-active Suspension System," *International Journal of Structural Engineering*, vol. 2, no. 3, 2011, pp. 234–272.

[71] G.D. Buckner, K.T. Schuetze and J.H. Beno, "Active Vehicle Suspension Control Using Intelligent Feedback Linearization," *Proceedings of the American Control Conference*, pp. 4014–4018, June 28–30, 2000.

[72]   J.W. Shi, X.W. Li and J.W. Zhang, "Feedback Linearization and Sliding Mode Control for Active Hydropneumatic Suspension of a Special-purpose Vehicle," *Part D: Journal of Automobile Engineering*, vol. 222, 2010, pp. 41–53.

[73]   O.T.C. Nyandoro, *et al.*, "State Feedback Based Linear Slip Control Formulation for Vehicular Antilock Braking System," *Proceedings of the World Congress on Engineering*, July 6–8, 2011.

[74]   J.O. Pedro and O.A. Dahunsi, "Neural Network-based Feedback Linearization Control of a Servo-hydraulic Vehicle Suspension System," *International Journal of Applied Mathematics and Computer Science*, vol. 21, no. 1, 2011, pp. 137–147.

[75]   Y. Hirano, *et al.*, "Development of an Integrated System of 4WS and 4WD by H∞ Control," *SAE Technical Paper*, no. 93–0267, 1993.

[76]   H. M. Lv, N. Chen and P. Li, "Multi-objective H∞ Optimal Control for Four-wheel Steering Vehicle Based on Yaw Rate Tracking," *Part D: Journal of Automobile Engineering*, vol. 218, no. 10, 2004, pp. 1117–1123.

[77]   L. X. Guo and L. P. Zhang, "Robust H∞ Control of Active Vehicle Suspension under Non-Stationary Running," *Journal of Sound and Vibration*, vol. 331, no. 26, 2012, pp. 5824–5837.

[78]   C. Lauwerys, J. Swevers and P. Sas, "Robust Linear Control of an Active Suspension on a Quarter Car Test-rig," *Control Engineering Practice*, vol. 13, no. 5, 2005, pp. 577–586.

[79]   R.D. Quinn, "Equations of Motion for Structures in Terms of Quasicoordinates," *Journal of Applied Mechanics*, vol. 57, 1990, pp. 745–749.

[80]   J. M. Cameron and W. J. Book, "Modeling Mechanisms with Nonholonomic Joints Using the Boltzmann-Hamel Equations," *International Journal of Robotics Research*, vol. 16, 1997, pp. 47–59.

[81]   L. Meirovitch, *Methods of analytical dynamics*, New York: McGraw Hill, 1970.

[82]   L. Meirovitch and I. Tuzcu, "Integrated Approach to the Dynamics and Control of Maneuvering Flexible Aircraft," National Aeronautics and Space Administration: Virginia, Rep. NASA/CR-2003-211748, 2003.

[83]   I. Tuzcu1 and L. Meirovitch, "Control of Flying Flexible Aircraft Using Control Surfaces and Dispersed Piezoelectric Actuators," *Smart Materials and Structures*, vol. 15, 2006, pp. 893–903.

[84]   ISO 3888-1:1999(E). Passenger Cars-test Track for a Severe Lane-change Manoeuver-Part 1: Double lane-change.

[85]   G. Zames, "Feedback and Optimal Sensitivity: Model Reference Transformations, Multiplicative Seminorms, and Approximate Inverses," *IEEE Transactions on Automatic Control*, vol. 26, no. 2, 1981, pp. 301–320.

[86]   H. Kwakernaak, "Robust Control and H∞-optimization—Tutorial Paper," *Automatica* vol. 29, no. 2, 1993, pp. 255–273.

[87] M. Green, "H Controller Synthesis by J-lossless Coprime Factorization," *SIAM Journal on Control and Optimization*, vol. 30, no. 3, 1992, pp. 522–547.

[88] D. F. Coutinho, A. Trofino and M. Fu. "Nonlinear H-infinity control: An LMI approach," *Proceeding of IFAC World Congress*, 2002.

[89] J. J. E. Slotine and W. Li, *Applied nonlinear control*, New Jersey: Prentice-Hall, 1991.

[90] A. Packard, Poola and Horowitz, *Dynamic Systems and Feedback*, 2002.

[91] A. Isidori and A. Astolfi, "Disturbance Attenuation and H∞ Control via Measurement Feedback in Nonlinear Systems," *IEEE Transactions on Automatic Control,* vol. 37, 1992, pp. 1283–1293.

[92] W. M. Lu and J. C. Doyle, "H∞ Control of Nonlinear Systems: A Class of Controllers," California: California Institute of Technology, 1993.

[93] C. H. Jin, H. S. Li and L. Z. Song, "An LMI Approach to H∞ Control for Affine Nonlinear System," *Proceeding IEEE 2011 International Conference on Electronics and Optoelectronics*, vol. 2, pp. V2–26–V2-29, 2011.

[94] N. P. Sabes, "Linear Algebraic Equations, SVD, and the Pseudo-Invers," San Francisco, Oct. 2001.

[95] A. A. Gharapurkar, A. F. Jahromi, R. B. Bhat and W. F. Xie, "Semi-active control of aircraft landing gear system using H-infinity control approach," *IEEE International*

Conference on Connected Vehicles and Expo (*ICCVE*), pp. 679–686, December 2-6. 2013.

[96] W. H. Liao and C. Y. Lai, "Harmonic Analysis of a Magnetorheological Damper for Vibration Control," *Smart Materials and Structures*, vol. 11, pp. 288–296, 2002.

[97] P. T. Boggs, "Sequential Quadratic Programming," *Acta Numerica*, 1996.

[98] J. H. Holland, *Adaption in Natural and Artificial Systems*, Massachusetts: MIT Press/Bradford Books Edition, 1992.

[99] J. S. Arora, *Introduction to optimum design*, 2th ed. California: Elsevier Academic Press, 2004.

[100] A. Hadadian, R. Sedaghati and E. Esmailzadeh, "Design Optimization of Magnetorheological Fluid Valves Using Response Surface Method," *Journal of Intelligent Material Systems and Structures*, 2014, vol. 25, no. 11, 2013, pp. 1352–1371.

[101] M. Bagheri, A. A. Jafari and M. Sadeghifar "Multi-objective Optimization of Ring Stiffened Cylindrical Shells Using a Genetic Algorithm," *Journal of Sound and Vibration*, vol. 330, no. 3, 2011, pp. 374–384.

[102] C. Y. Lai, and W. H. Liao, "Vibration Control of a Suspension System via a Magnetorheological Fluid Damper," *Journal of Vibration and Control*, vol. 8, 2002, pp. 527–547.

[103] X. Yang Z. Wang and W. Peng, "Coordinate of AFS and DYC for Vehicle Handling and Stability Based on Optimal Guaranteed Cost Theory," *Vehicle System Dynamic*, vol. 47, 2007, pp. 57–79.

[104] W. H. Liao and C. Y. Lai, "Harmonic Analysis of a Magnetorheological Damper for Vibration Control," *Smart Materials and Structures*, vol. 11, 2002, pp. 288–296.

[105] I. Fialho and G. J. Balas, "Road Adaptive Active Suspension Design using Linear Parameter-Varying gain-scheduling," *IEEE Transactions on Control System Technology*, vol. 10, no. 1, 2002, pp. 43–54.

[106] A. L. Do, O. Sename and L. Dugard. "An LPV control approach for semi-active suspension control with actuator constraints," *In American Control Conference* (*ACC*), *IEEE*, pp. 4653–4658, 2010.

[107] O. Sename, *et al.*, "Some LPV Approaches for Semi-active Suspension Control," *In American Control Conference* (*ACC*), *IEEE*, pp. 1567–1572. 2012.

Appendix I.   Rotation Sequence of Coordinate Systems

Figures A.1-2, show that the assumption of the rotation sequence of the coordinate system can be used to derive transformation matrices for translational and rotational speeds.

(a)   (b)   (c)
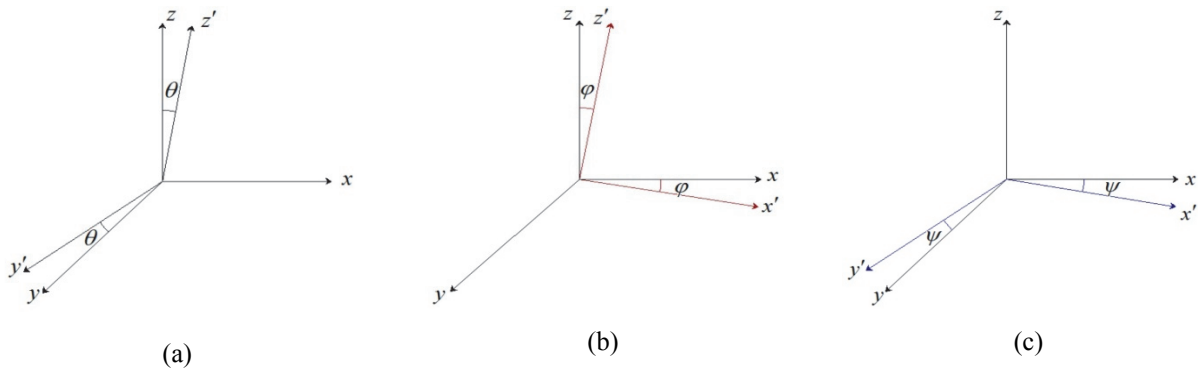
Fig. A.1 (a), (b) and (c) are rotations about x (roll), y (pitch) and z (yaw) axis, respectively
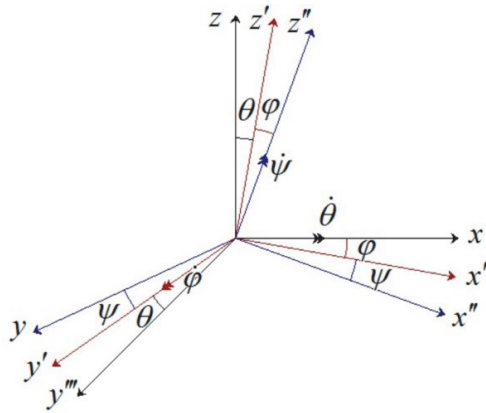

Fig. 1 Angular velocities images in rotation of the coordinate system (xyz)

Appendix II. Dynamics Equation of Integrated Ride and Handling Model

The Dynamic equations of the developed vehicle model presented as follows:

$$\ddot{X} = \left(\frac{-1}{m_t}\right)\begin{pmatrix}\sum_{j=1}^{2}m_j(\ddot{Y}(\psi+2\dot{\psi}v_{yhf})+\sum_{j=3}^{4}m_j(\ddot{Y}\psi+2\dot{\psi}v_{yhr})\\[4pt] -m_5\begin{pmatrix}\ddot{\varphi}h_f-\ddot{\theta}\psi h_s+\ddot{Z}\varphi-\ddot{Y}\psi+\dot{\varphi}\left(\dot{Z}-\varphi v_{xr}+\varphi\psi v_{yr}-\dot{\varphi}\varphi h_f\right)\\ +(\dot{\psi}-\dot{\varphi}\theta)\left(\dot{Z}\theta+v_{yr}(\theta\varphi\psi-1)-h_s(\dot{\theta}\dot{\psi}\varphi)-v_{xr}(\psi+\theta\varphi)\right)\\ +(\dot{\varphi}-\dot{\psi}\varphi)\left(\dot{Z}-v_{xr}(\varphi-\theta\psi)+v_{yr}(\theta+\varphi\psi)\right)+\dot{\theta}^2\theta h_s\psi\end{pmatrix}+\varphi\sum_{j=1}^{4}K_jv_j+C_j\dot{v}_j\\[4pt] -\sum_{j=1}^{4}(F_{xj}+F_{bj})+\psi\left(\sum_{j=1}^{4}F_{yj}+\delta(F_{x1}+F_{b1}+F_{x2}+F_{b2})\right)+\varphi\sum_{j=1}^{4}F_j+\delta(F_{y1}+F_{y2})\end{pmatrix} \quad\text{(II.1)}$$

$$\ddot{Y}=\left(\frac{1}{\sum_{j=1}^{4}m_j-m_5(\theta\varphi\psi-1)}\right)$$
$$\begin{pmatrix}-m_5\begin{pmatrix}\ddot{Z}\theta-(\ddot{\varphi}h_f+\ddot{X})(\psi+\varphi\theta)+(\dot{\theta}+\dot{\psi}\varphi)\left(\dot{Z}-v_{xr}(\varphi-\theta\psi)+v_{yr}(\theta+\varphi\psi)\right)\\ -\dot{\varphi}\left(\theta v_{xr}-\theta\psi v_{yr}+\dot{Z}\theta\varphi-\dot{\varphi}\varphi h_f(\psi+\varphi\theta)\right)+\ddot{\theta}h_s(\theta\varphi\psi-1)\end{pmatrix}\\[4pt] -m_5\begin{pmatrix}+\dot{\theta}\left(\dot{Z}+v_{yr}(\theta+\varphi\psi)-v_{xr}(\varphi-\theta\psi)-\dot{\theta}\theta h_s(\theta\varphi\psi-1)\right)\\ -(\dot{\psi}-\dot{\varphi}\theta)\left(\dot{X}+\dot{Z}\varphi+\dot{\varphi}h_f-v_{yr}\psi+h_f(\dot{\varphi}-\dot{\psi}\varphi)\right)+\dot{\psi}\left(v_{xr}(\theta\varphi\psi-1)+v_{yr}(\psi+\varphi\theta)\right)\end{pmatrix}\\[4pt] +(\psi+\varphi\theta)\left(\sum_{j=1}^{4}(F_{xj}+F_{bj})-\delta(F_{y1}+F_{y2})\right)-(\theta\varphi\psi-1)\left(\sum_{j=1}^{4}F_{yj}+\delta(F_{x1}+F_{b1}+F_{x2}+F_{b2})\right)+\theta\sum_{j=1}^{4}F_j\\[4pt] +\theta\sum_{j=1}^{4}K_jv_j+C_j\dot{v}_j+\sum_{j=1}^{2}m_j(\ddot{X}(\psi+\delta)+2v_{xhf})+\sum_{j=3}^{4}m_j(\ddot{X}+2v_{xhr})\end{pmatrix} \quad\text{(II.2)}$$

$$\ddot{Z}=\left(\frac{-1}{m_5}\right)\begin{pmatrix}m_5\begin{pmatrix}\dot{\varphi}\left(v_{xr}+\dot{Z}\varphi-v_{yr}\psi-\dot{\varphi}\varphi h_f(\varphi-\theta\psi)\right)+\ddot{X}(\varphi-\theta\psi)-\ddot{Y}(\theta+\varphi\psi)\\ +\dot{\theta}\left(\dot{Z}\theta-v_{xr}(\psi+\varphi\theta)+v_{yr}(\theta\varphi\psi-1)+\dot{\theta}\theta h_s(\theta+\varphi\psi)\right)\\ -\dot{\psi}\left(v_{xr}(\theta+\varphi\psi)+v_{yr}(\varphi-\theta\psi)\right)-\ddot{\varphi}h_f(\varphi-\theta\psi)-\ddot{\theta}h_s(\theta+\varphi\psi)\\ +(\dot{\theta}+\varphi\dot{\psi})\left(\dot{Z}\theta+v_{yr}(\theta\varphi\psi-1)-h_s(\dot{\theta}+\dot{\psi}\varphi)-v_{xr}(\psi+\varphi\theta)\right)\\ +(\dot{\varphi}-\dot{\psi}\varphi)\left(v_{xr}+\dot{Z}\varphi+h_f(\dot{\varphi}-\dot{\psi}\varphi)-v_{yr}\psi\right)\end{pmatrix}+\sum_{j=1}^{4}K_jv_j+C_j\dot{v}_j\\[4pt] -(\theta+\varphi\psi)\left(\sum_{j=1}^{4}F_{yj}+\delta(F_{x1}+F_{b1}+F_{x2}+F_{b2})\right)+\sum_{j=1}^{4}F_{Cj}+(\varphi-\theta\psi)\left(\sum_{j=1}^{4}(F_{xj}+F_{bj})-\delta(F_{y1}+F_{y2})\right)\end{pmatrix} \quad\text{(II.3)}$$

$$\ddot{\theta} = \left(\frac{-1}{m_5 h_s^2 + I_x}\right) \begin{pmatrix} (\dot\psi - \dot\varphi\theta)\left(I_y(\dot\varphi - \dot\psi\varphi) + m_5 h_f\left(v_{xr} + \dot{Z}\varphi + h_f(\dot\varphi - \dot\psi\varphi) - v_{yr}\psi\right)\right) \\[4pt] -(\dot\theta + \dot\psi\varphi)\left(h_s m_5\theta\left(\dot{Z}\theta - v_{xr}(\psi + \varphi\theta) + v_{yr}(\theta\varphi\psi - 1) - h_s(\dot\theta + \dot\psi\varphi)\right) - m_5\theta h_s^2(\dot\theta + \dot\psi\varphi)\right) \\[4pt] -I_z(\dot\varphi - \dot\psi\varphi)(\dot\psi - \dot\varphi\theta) + h_s m_5\theta + m_5\left(\dot{Z}\theta - v_{xr}(\psi + \varphi\theta) + v_{yr}(\theta\varphi\psi - 1)\right) \\[4pt] \times\left(\dot{Z} - v_{xr}(\varphi - \theta\psi) + v_{yr}(\theta + \varphi\psi)\right) - (m_5 h_s^2 + I_x)(\ddot\psi\varphi + \dot\varphi\dot\psi) + \sum_{j=1}^{4} I_\omega\dot\psi\omega_j \\[4pt] +\left(h_s m_5\theta(\dot\theta + \dot\psi\varphi) - m_5\left(\dot{Z} - v_{xr}(\varphi - \theta\psi) + v_{yr}(\theta + \varphi\psi)\right)\right) \\[4pt] \times\left(\dot{Z}\theta + v_{yr}(\theta\varphi\psi - 1) - h_s(\dot\theta + \dot\psi\varphi) - v_{xr}(\psi + \varphi\theta)\right) + K_{\theta f}\dfrac{\theta + (Z_1 - Z_2)}{h_r + h_l} \\[4pt] +K_{\theta r}\dfrac{\theta + (Z_3 - Z_4)}{h_r + h_l} + C_{\theta f}\dfrac{\dot\theta + (\dot{Z}_1 - \dot{Z}_2)}{h_r + h_l} + C_{\theta r}\dfrac{\dot\theta + (\dot{Z}_3 - \dot{Z}_4)}{h_r + h_l} + h_r(K_1 v_1 + K_3 v_3) \\[4pt] -h_l(K_2 v_2 + K_4 v_4) + h_r(C_1\dot{v}_1 + C_3\dot{v}_3) - h_l(C_2\dot{v}_2 + C_4\dot{v}_4) - h_l(F_{C2} + F_{C4}) + h_r(F_{C1} + F_{C3}) \end{pmatrix} \tag{II.4}$$

$$\ddot{\varphi} = \left(\frac{-1}{m_5 h_f^2 + I_y}\right)$$

$$\begin{pmatrix} (\dot\psi\varphi - \dot\varphi)\left(h_f m_5\varphi\left(v_{xr} + \dot{Z}\varphi + h_f(\dot\varphi - \dot\psi\varphi) - v_{yr}\psi\right) + m_5\varphi h_f^2(\dot\varphi - \dot\psi\varphi)\right) \\[4pt] +(m_5 h_f^2 + I_y)\left(\dot\theta(\dot\varphi\theta - \dot\psi\varphi\theta) + \ddot\psi\varphi + \dot\varphi\dot\psi\right) + I_z(\dot\theta + \dot\psi\varphi)(\dot\psi - \dot\varphi\theta) \\[4pt] +(\dot\psi - \dot\varphi\theta)\left(I_x(\dot\theta + \dot\psi\varphi) - h_s m_5\left(\dot{Z}\theta - v_{xr}(\theta + \varphi\psi) + v_{yr}(\theta\varphi\psi - 1) - h_s(\dot\theta + \dot\psi\varphi)\right)\right) \\[4pt] +m_5\left(\dot{Z} - v_{xr}(\varphi - \theta\psi) + v_{yr}(\theta + \varphi\psi)\right)\left(2v_{xr} + 2\dot{Z}\varphi - 2v_{yr}\psi + h_f(\dot\varphi - \dot\psi\varphi)\right) \\[4pt] \left.\begin{pmatrix} l_r(K_3 v_3 + K_4 v_4) - l_f(K_1 v_1 + K_2 v_2) + l_r(C_3\dot{v}_3 + C_4\dot{v}_4) - l_f(C_1\dot{v}_1 + C_2\dot{v}_2) \\[2pt] -h_f m_5\varphi + h_f m_5\varphi(\dot\varphi - \dot\psi\varphi)\left(v_{xr} - \dot{Z}\varphi - h_f(\dot\varphi - \dot\psi\varphi) + v_{yr}\psi\right) \\[2pt] -l_f(F_{C1} + F_{C2}) + l_r(F_{C3} + F_{C4}) + \theta\left(h_r(F_{x1} + F_{b1} + F_{x3} + F_{b3}) - h_l(F_{x2} + F_{b2} + F_{x4} + F_{b4})\right) \\[2pt] +\theta\left(\delta(l_f(F_{x1} + F_{b1} + F_{x2} + F_{b2}) + F_{y2}h_l - F_{y1}h_r) + l_f(F_{y1} + F_{y2}) - l_r(F_{y3} + F_{y4})\right) \end{pmatrix}\right/(\theta\varphi - 1) \\[6pt] \left.\begin{pmatrix} K_{\theta f}\dfrac{\theta + (Z_1 - Z_2)}{h_r + h_l} + K_{\theta r}\dfrac{\theta + (Z_3 - Z_4)}{h_r + h_l} + C_{\theta f}\dfrac{\dot\theta + (\dot{Z}_1 - \dot{Z}_2)}{h_r + h_l} + C_{\theta r}\dfrac{\dot\theta + (\dot{Z}_3 - \dot{Z}_4)}{h_r + h_l} \\[2pt] h_r(K_1 v_1 + K_3 v_3) - h_l(K_2 v_2 + K_4 v_4) + h_r(C_1\dot{v}_1 + C_3\dot{v}_3) - h_l(C_2\dot{v}_2 + C_4\dot{v}_4) \\[2pt] +h_s m_5\theta(\dot\theta + \dot\psi\varphi)\left(\dot{Z}\theta - v_{xr}(\psi + \varphi\theta) + v_{yr}(\theta\varphi\psi - 1) - h_s(\dot\theta + \dot\psi\varphi)\right) \\[2pt] -h_l(F_{C2} + F_{C4}) + h_r(F_{C1} + F_{C3}) \end{pmatrix}\right/\left(\dfrac{\theta\varphi}{(\theta\varphi - 1)}\right) \end{pmatrix} \tag{II.5}$$

$$\ddot{\psi} = \left(\frac{-\varphi}{I_z(\varphi\theta - 1)} \right)$$

$$
\begin{pmatrix}
-l_f(K_1v_1 + K_2v_2) + l_r(K_3v_4 + K_4v_4) - l_f(C_1\dot{v}_1 + C_2\dot{v}_2) + l_r(C_3\dot{v}_4 + C_4\dot{v}_4) - h_l(K_2v_2 + K_4v_4) \\
+h_r(K_1v_1 + K_3v_3) - h_l(C_2\dot{v}_2 + C_4\dot{v}_4) + h_r(C_1\dot{v}_1 + C_3\dot{v}_3) + K_{\theta f}\dfrac{\theta + (Z_1 - Z_2)}{h_r + h_l} + K_{\theta r}\dfrac{\theta + (Z_3 - Z_4)}{h_r + h_l} \\
+C_{\theta f}\dfrac{\dot{\theta} + (\dot{Z}_1 - \dot{Z}_2)}{h_r + h_l} + C_{\theta r}\dfrac{\dot{\theta} + (\dot{Z}_3 - \dot{Z}_4)}{h_r + h_l} + h_f m_5\varphi(\dot{\varphi} - \dot{\psi}\varphi)\left(v_{xr} + \dot{Z}\varphi + h_f(\dot{\varphi} - \dot{\psi}\varphi) - v_{yr}\psi\right) \\
-h_f m_5\varphi + h_f m_5\theta(\dot{\theta} + \dot{\psi}\varphi)\left(\dot{Z}\theta - v_{xr}(\psi + \varphi\theta) + v_{yr}(\theta\varphi\psi - 1) - h_s(\dot{\theta} + \dot{\psi}\varphi)\right) \\
\left.
\begin{pmatrix}
I_z\left(\ddot{\varphi}\theta + \dot{\theta}(\dot{\varphi} + \dot{\psi}\theta) + \dot{\varphi}\dot{\psi}\varphi\right) \\
+(\dot{\theta} + \dot{\psi}\varphi)\left(I_y(\dot{\varphi} - \dot{\psi}\varphi) + h_f m_5\left(v_{xr} + \dot{Z}\varphi + h_f(\dot{\varphi} - \dot{\psi}\varphi) - v_{yr}\psi\right)\right) \\
+(\dot{\varphi} - \dot{\psi}\theta)\left(I_x(\dot{\theta} + \dot{\psi}\varphi) - h_s m_5\left(\dot{Z}\theta - v_{xr}(\psi + \varphi\theta) + v_{yr}(\theta\varphi\psi - 1) - h_s(\dot{\theta} + \dot{\psi}\varphi)\right)\right)
\end{pmatrix} \right/ \left(\dfrac{\varphi\theta - 1}{\varphi}\right) \\
-h_l(F_{C2} + F_{C4}) + h_r(F_{C1} + F_{C3}) - l_r(F_{C3} + F_{C4}) + l_f(F_{C1} + F_{C2}) \\
+\begin{pmatrix} h_r(F_{x1} + F_{b1} + F_{x3} + F_{b3}) - h_l\left(F_{x2} + F_{b2} + F_{x4} + F_{b4}\right) + \delta(F_{y2}h_l - F_{y1}h_r) \\ +l_f(F_{y1} + F_{y2}) - l_r(F_{y3} + F_{y4}) + \delta l_f(F_{x1} + F_{b1} + F_{x2} + F_{b2}) \end{pmatrix} \middle/ \varphi
\end{pmatrix}
$$

(II.6)

$$\ddot{Z}_1 = \left(\frac{-1}{m_1}\right)\left(K_{t1}(Z_1 - Z_{i1}) + C_{t1}(\dot{Z}_1 - \dot{Z}_{i1}) - K_1v_1 - C_1\dot{v}_1 + K_{\theta f}\frac{\theta + (Z_1 - Z_2)}{h_r + h_l} + C_{\theta f}\frac{\dot{\theta} + (\dot{Z}_1 - \dot{Z}_2)}{h_r + h_l} - F_{C1}\right)$$

(II.7)

$$\ddot{Z}_2 = \left(\frac{-1}{m_2}\right)\left(K_{t2}(Z_2 - Z_{i2}) + C_{t2}(\dot{Z}_2 - \dot{Z}_{i2}) - K_2v_2 - C_2\dot{v}_2 + K_{\theta f}\frac{\theta + (Z_1 - Z_2)}{h_r + h_l} + C_{\theta f}\frac{\dot{\theta} + (\dot{Z}_1 - \dot{Z}_2)}{h_r + h_l} - F_{C2}\right)$$

(II.8)

$$\ddot{Z}_3 = \left(\frac{-1}{m_3}\right)\left(K_{t3}(Z_3 - Z_{i3}) + C_{t3}(\dot{Z}_3 - \dot{Z}_{i3}) - K_3v_3 - C_3\dot{v}_3 + K_{\theta r}\frac{\theta + (Z_3 - Z_4)}{h_r + h_l} + C_{\theta r}\frac{\dot{\theta} + (\dot{Z}_3 - \dot{Z}_4)}{h_r + h_l} - F_{C3}\right)$$

(II.9)

$$\ddot{Z}_4 = \left(\frac{-1}{m_4}\right)\left(K_{t4}(Z_4 - Z_{i4}) + C_{t4}(\dot{Z}_4 - \dot{Z}_{i4}) - K_4v_4 - C_4\dot{v}_4 + K_{\theta r}\frac{\theta + (Z_3 - Z_4)}{h_r + h_l} + C_{\theta r}\frac{\dot{\theta} + (\dot{Z}_3 - \dot{Z}_4)}{h_r + h_l} - F_{C4}\right)$$

(II.10)

$$\ddot{\alpha}_j = \left(\frac{-F_{xj}R - F_{bj}R_b}{I_\omega}\right) \quad _{j=1-4}$$

(II.11)

where:

$$v_{xr} = \dot{X} + h_f\varphi$$

(II.12)

136

$$v_{xhf} = \dot{X} - \dot{Y}(\psi + \delta) \qquad\qquad\qquad\qquad\qquad\qquad\qquad \text{(II.13)}$$

$$v_{xhr} = \dot{X} - \dot{Y}\psi \qquad\qquad\qquad\qquad\qquad\qquad\qquad\qquad \text{(II.14)}$$

$$v_{yr} = \dot{Y} + h_s\theta \qquad\qquad\qquad\qquad\qquad\qquad\qquad\qquad \text{(II.15)}$$

$$v_{yhf} = \dot{Y} + \dot{X}(\psi + \delta) \qquad\qquad\qquad\qquad\qquad\qquad\qquad \text{(II.16)}$$

$$v_{yhr} = \dot{Y} + \dot{X}\psi \qquad\qquad\qquad\qquad\qquad\qquad\qquad\qquad \text{(II.17)}$$

Appendix III.   Numerical Value of Vehicle Model

The numerical values of the vehicle parameters are presented in the following table:

Table III. 1 Numerical values of the vehicle parameters

Symbol	Quantity	Value
m_5	Mass of car body	995 (kg)
m_{1-4}	Mass one of the wheels	25 (kg)
I_y	Body mass moment of inertia about roll axis	500 (kg.m^2)
I_z	Body mass moment of inertia about yaw axis	600 (kg.m^2)
I_ω	Wheel mass moment of inertia about yaw axis	80 (kg.m^2)
I_x	Body mass moment of inertia about pitch axis	200 (kg.m^2)
K_{1-2}	Stiffness of the car springs on front axle	12500 (N/m)
K_{3-4}	Stiffness of the car springs on front axle	12500 (N/m)
$K_{\theta f-r}$	Stiffness of front and rear anti roll bars	2500 (N/m)
$C_{\theta f-r}$	Equivalent viscous damping of front and rear anti roll bar	150 (Ns/m)
K_{t1-4}	Stiffness of the tires	125000 (N/m)
K_{x1-4}	Cornering stiffness of tires in longitudinal axis	30000 (N/m)
K_{y1-2}	Cornering stiffness of front tires in lateral axis	79000 (N/m)
K_{y3-4}	Cornering stiffness of rear tires in lateral axis	95000 (N/m)
C_{1-4}	Equivalent viscous damping	2500 (Ns/m)
C_{t1-4}	Damping coefficient of tires	560 (Ns/m)
l_f	The distance between the front wheels and vehicle center of gravity	1.224 (m)
l_r	The distance between the rear wheels and vehicle center of gravity	1.327 (m)
h_{f-r}	Half of track base	0.76 (m)
h_s	The distance between the roll center and body center of gravity	0.055 (m)
h_f	The distance between the pitch center and body center of gravity	0.25 (m)
μ	Road friction factor	0.8
R	Wheel radius	0.3164 (m)
R_b	Brake disc radius	0.1778 (m)

Appendix IV.   Matlab Simulink Block Diagram

Figure 5.1 shows the outer layer of Matlab/ Simulink file for the vehicle model and the controller. Each subsystem and Matlab embedded function are shown by different color to be traceable. This simulink block diagram is built based on controller algorithm in Chapter 3 (Figure 3.1). The controller operates based on output feedbacks as shown in simulink block diagram. However "goto" and "from" simulink blocks are used instead of connection line to avoid complexity in simulink block diagram. Moreover the same blocks are used to define vehicle parameters for all subsystems.
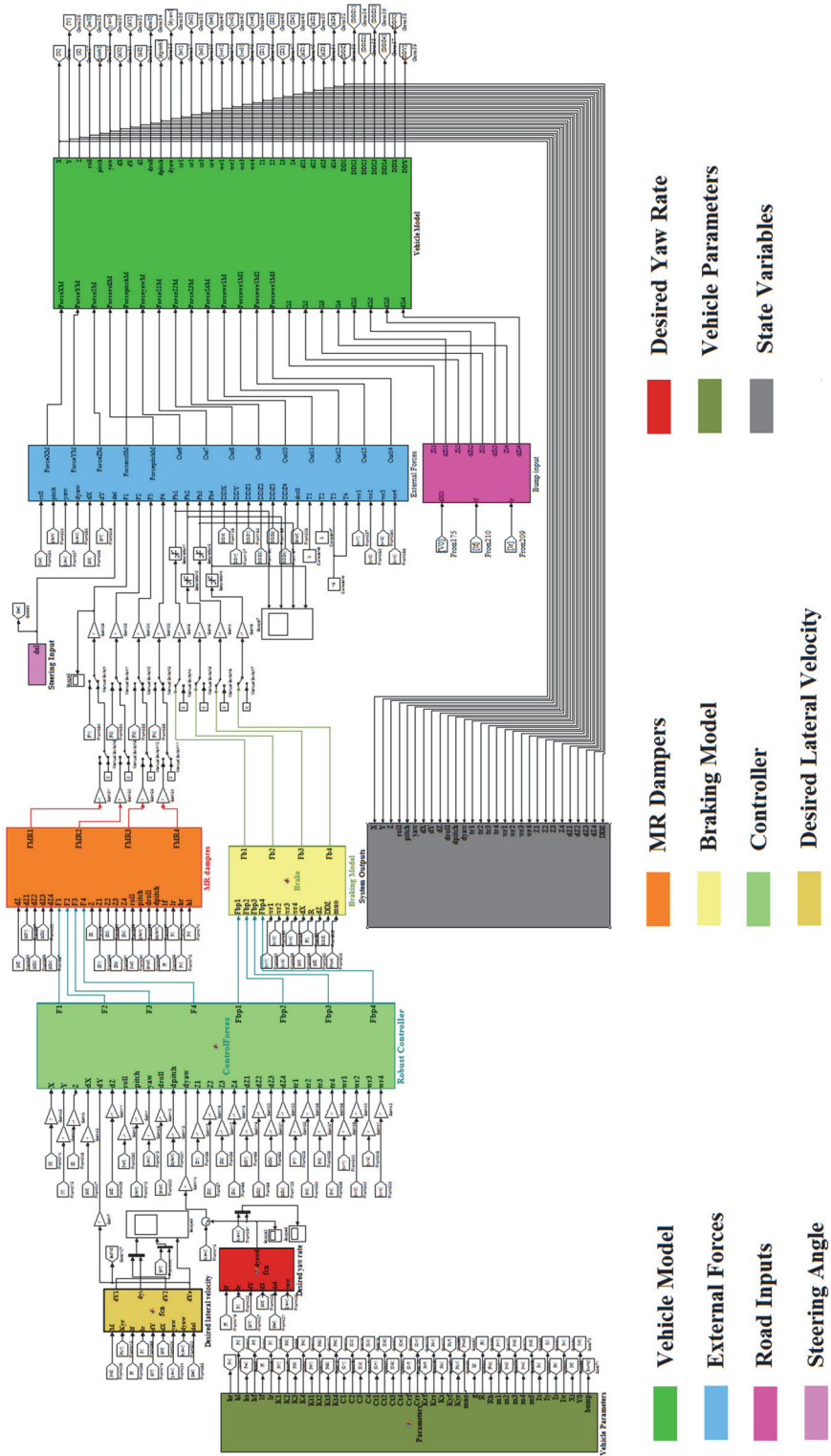
Figure 1V. Simulated vehicle and robust controller in MATLAB simulink